Investigation of the GCP Structure of Three-Higgs-Doublet Models and a General Method to Derive Boundedness Constraints for Multi-Higgs Potentials

Master's Thesis

Marcel Köpke

January 14, 2018

Under the supervision of

Prof. Dr. M. M. Mühlleitner

at the Institute of Theoretical Physics (KIT)

First reviewer: Prof. Dr. M. M. Mühlleitner
Second reviewer: Prof. Dr. D. Zeppenfeld

Statement of Authorship

Deutsch

Ich versichere wahrheitsgemäß, dass ich die Arbeit selbstständig verfasst und keine anderen als die angegebenen Quellen und Hilfsmittel benutzt habe, die wörtlich oder inhaltlich übernommenen Stellen als solche kenntlich gemacht und die Satzung der Universität Karlsruhe (TH) / des KIT zur Sicherung guter wissenschaftlicher Praxis in der jeweils gültigen Fassung[1] beachtet habe.

Marcel Köpke, Karlsruhe, den 22. Februar 2018

English

I hereby confirm truthfully, that I wrote this thesis on my own, that I did not use any references and aids other than the ones which are specified, that I marked the literally and contentually adopted passages and that I followed the statue of good scientific practice of the University of Karlsruhe (TH) / the KIT in the respective valid version[2].

Marcel Köpke, Karlsruhe, February 22, 2018

[1] Nach `http://www.kit.edu/studieren/amtlicheBekanntmachungen.php`; 2008, "81. Studien- und Prüfungsordnung der Universität Karlsruhe (TH) für den Masterstudiengang Physik" - abgerufen am 22. Februar 2018.

[2] See `http://www.kit.edu/studieren/amtlicheBekanntmachungen.php`; 2008, "81. Studien- und Prüfungsordnung der Universität Karlsruhe (TH) für den Masterstudiengang Physik" - last checked February 22, 2018.

Abstract

In this thesis the theoretical analysis of an inert three-Higgs-doublet model with a generalized CP symmetry is presented. The phenomenological consequences of astrophysical observables and theoretical constraints are discussed. In particular, perturbative unitarity constraints and the thermal evolution of the relic density of possible dark matter candidates are investigated to check the phenomenological significance of Higgs potential parameters. In addition, a completely new method to derive necessary and sufficient conditions for boundedness of Higgs potentials has been developed and is presented here. It is the first and to date only algorithm that can be applied to any multi-Higgs model. References to a working implementation are provided in the text.

Acknowledgements

I thank my supervisor Prof. Dr. M. Margarete Mühlleitner for the opportunity to work in this interesting field of research. I also want to thank her for the steady support during the course of the thesis and especially during the time of writing. Then there is another great supporter, Dr. Igor P. Ivanov, whom I have met personally for the first time in summer 2017 at the Instituto Superior Técnico in Lisbon, Portugal. It was at that first meeting, that he pointed me towards the problem of Higgs potential boundedness of the model he had developed and which is investigated in this thesis. I also want to thank him for the warm welcome in Portugal and the scientific and personal conversations that I have always enjoyed. Next, I want to thank Sven Caspart from the Institute of Algebra and Geometry (KIT) for his time that he generously spent with a stranger to introduce him to the very concepts of Algebraic Geometry and the vast selection of programs in this field. However, a program is only as good as the programmer who has fixed its bugs. Without the cross-checks of Dr. Dorota Sokolowska, I would probably still be fixing the MicrOmegas implementation and without Dr. Florian Staub the one of SARAH and SPheno. Speaking of cross-checks, at the very beginning of my thesis, Dr. David López-Val provided me without hesitation the means to compare my calculation of Feynman rules to the ones generated by MadGraph. This saved me a great deal of time. He was also involved in proofreading the thesis, for which I want to thank Fritz Waitz, Jakob Schwichtenberg, Maximilian Stadelmaier and my wife Rike Köpke as well. Lastly, I thank my parents for their continuous support during my studies.

Contents

List of Figures

List of Tables

Part I

Thesis

Chapter 1

Introduction

Beyond the Standard Model (BSM) physics is an intriguing field of research. There are several approaches to extend the prediction of the Standard Model and account for the hierarchy problem, Higgs potential instability, inflation, the strong CP problem, observations like the gravitational influence of dark matter, CP violation, matter-antimatter asymmetry and many more hints at new physics. The most prominent frameworks are probably supersymmetry and grand unified theories but also advancements with axions, independent gauge symmetries, technicolor, extra dimensions, etc. can be mentioned. A list that cannot possibly be exhausted here. Most of these models exhibit a vast and diverse particle spectrum which, unfortunately, lacks confirmation from colliders and other experiments so far. The great majority of current BSM studies has one thing in common though: an extended Higgs sector.

Multi-Higgs models are a well known resource for BSM phenomenology. Two-Higgs-doublet models with and without extra singlets were and are still examined thoroughly. However, with an increasing number of particles the number of free parameters rises rapidly. Symmetry constrained Higgs potentials are therefore a convenient choice to circumvent the practical and conceptual problems of this fact. Probably the most natural discrete symmetry to impose on a Higgs potential is the combination of charge conjugation and parity CP. Almost all observations and Standard Model interactions, except for weak interactions, show no violation of this symmetry.

In this thesis a three-Higgs-doublet model with a generalized CP symmetry (GCP) and no other accidental symmetries is investigated. It was first proposed by Ivanov and Silva [1] and possesses in total 11 new parameters compared to the Standard Model. This is more than twice as much as in the inert two-Higgs-doublet model [2, 3]. Therefore, great effort has been spent on the identification of phenomenologically significant parameters. To do this, the doubled inert two-Higgs-doublet model is introduced. It is very

similar to both, the inert two-Higgs-doublet model and the former three-Higgs-doublet model. It has a reduced parameter set and an ordinary CP symmetry only. Hence, it is a phenomenological stepping stone towards the understanding of the full model. As a result, the GCP structure of the Higgs potential plays an important role because most of the additional parameters can be linked to the existence of this GCP symmetry.

Various constraints and observables can be used to identify differences or similarities of the models. Unfortunately, there are currently no necessary and sufficient conditions for boundedness, equivalently stability, of the Higgs potentials under investigation. A completely new method to derive these conditions for any multi-Higgs model has been developed during the course of this thesis and is presented here as well.

The thesis can be split into three parts. Firstly, the theoretical introduction consisting of Chapter 2 and Chapter 3. Chapter 2 explains the concept of GCP symmetries while Chapter 3 introduces the two three-Higgs-doublet models. Secondly, in Chapter 4 the phenomenological comparison is done. The dark matter relic density as well as aspects of perturbative unitarity constraints are discussed. In principle they are able to probe quartic coupling parameters, which constitute the majority of the additional free parameters and the GCP structure. Thirdly, in Chapter 5 a general method to derive boundedness constraints is presented.

In addition, Appendix B describes two Mathematica packages, BFB [4] and PUC [5], that have been written for this thesis. They are publicly available. BFB implements the algorithm deduced in Chapter 5. PUC can be used to calculate unitarity constraints for the three-Higgs-doublet models discussed above. It is easily extendable to different Higgs potentials as well.

Chapter 2

Generalized CP Transformations

Symmetries play an important role for the analysis of extended Higgs sectors. Especially discrete symmetries have become of great interest since they allow the introduction of stable dark matter candidates and limit the parameter space drastically. An example is the $\mathbb{Z}_2$ symmetric two-Higgs-doublet model which has been extensively studied [6, 7].

The most prominent discrete symmetries in quantum field theory are those of charge conjugation C, space inversion P and time reversal T. It was Eugene Paul Wigner who showed that all symmetries that act on Hilbert space vectors and preserve their length, that is they preserve probabilities, are either unitary or anti-unitary operators. The first two, C and P, can be represented by unitary operators, while T is anti-unitary. The product CP is unitary, too. Needless to say it is a linear operator. This fact will become important shortly.

There is a certain freedom in the definition of CP when one deals with several fields with identical gauge quantum numbers and masses. This ambiguity will result in the definition of generalized CP symmetries (GCP). The distinctive feature is

$$(\mathrm{GCP})^2 \neq \mathbb{1} \ . \tag{2.1}$$

For ordinary CP transformations one would expect to get the identity when applying it twice. In literature there is a slightly different notion of GCP transformations. Any form of CP that differs from the normal one is said to be a GCP even if it has no physical consequences, e.g. can be connected to the normal form by a basis change.

2.1 Basis Change of Higgs Doublets

The discussion in this section follows the one in [7]. The usual definition of CP applied to a Higgs doublet ϕ is:

$$\mathrm{CP}[\phi(t,\vec{x})] = \phi^*(t,-\vec{x}) \ . \tag{2.2}$$

The arguments of the fields before and after the transformation will be omitted in the following.

Take two doublets ϕ_1 and ϕ_2, perform a basis change and define new fields ϕ_1', ϕ_2' by

$$\begin{aligned} \phi_1 &= \frac{1}{\sqrt{2}}\Big(\phi_1' + e^{i\pi/4}\ \phi_2'\Big) \\ \phi_2 &= \frac{1}{\sqrt{2}}\Big(-e^{-i\pi/4}\ \phi_1' + \phi_2'\Big) \ . \end{aligned} \tag{2.3}$$

This is generally allowed because both doublet fields have the same gauge quantum numbers. Now perform a CP transformation:

$$\begin{aligned} \mathrm{CP}[\phi_1] &= \frac{1}{\sqrt{2}}\Big(\mathrm{CP}[\phi_1'] + e^{i\pi/4}\ \mathrm{CP}[\phi_2']\Big) \\ \mathrm{CP}[\phi_2] &= \frac{1}{\sqrt{2}}\Big(-e^{-i\pi/4}\ \mathrm{CP}[\phi_1'] + \mathrm{CP}[\phi_2']\Big) \ . \end{aligned} \tag{2.4}$$

Note that the linearity of CP has been used, that is the coefficients have not been conjugated. According to Eq. (2.2) the explicit form for the original fields ϕ_i is $\mathrm{CP}[\phi_i] = \phi_i^*$, hence

$$\begin{aligned} \mathrm{CP}[\phi_1] &= \frac{1}{\sqrt{2}}\Big((\phi_1')^* + e^{-i\pi/4}\ (\phi_2')^*\Big) \\ \mathrm{CP}[\phi_2] &= \frac{1}{\sqrt{2}}\Big(-e^{i\pi/4}\ (\phi_1')^* + (\phi_2')^*\Big) \ . \end{aligned} \tag{2.5}$$

By combining Eq. (2.3) and (2.4) the resulting linear system of equations yields

$$\begin{aligned} \mathrm{CP}[\phi_1'] &= \frac{1+i}{2}(\phi_1')^* - \frac{i}{\sqrt{2}}(\phi_2')^* \\ \mathrm{CP}[\phi_2'] &= -\frac{i}{\sqrt{2}}(\phi_1')^* + \frac{1-i}{2}(\phi_2')^* \ . \end{aligned} \tag{2.6}$$

As one can see, this has not the simple form of Eq. (2.2). In general one may write

$$\mathrm{CP}[\phi_a] = \sum_{b=1}^{n} X_{ab}\phi_b^* \ , \tag{2.7}$$

where n is the number of Higgs doublets.

For the previous example with $n = 2$, one has for the original fields ϕ_i that $X_{ab} = \delta_{ab}$ the Kronecker delta while for ϕ'_i it is

$$X = \begin{pmatrix} \frac{1+i}{2} & -\frac{i}{\sqrt{2}} \\ -\frac{i}{\sqrt{2}} & \frac{1-i}{2} \end{pmatrix} . \tag{2.8}$$

In principle, X_{ab} can represent any invertible matrix that preserves probabilities, that is $X \in \mathrm{U}(n)$. One may expect that the complicated form of Eq. (2.8) is just due to a badly chosen basis of the Higgs doublets ϕ'_i and that one can always revert back to the more simple form of Eq. (2.2). This is, however, not the case for general unitary matrices. The implications of this fact are described in the next section.

2.2 Classification

One can apply the CP transformation defined by Eq. (2.8) twice,

$$\begin{aligned} \mathrm{CP}[\mathrm{CP}[\phi'_a]] &= \sum_{b=1}^{2} \sum_{c=1}^{2} X_{ab} \cdot X^*_{bc} \cdot \phi'_c \\ &= \sum_{c=1}^{2} \left[\begin{pmatrix} \frac{1+i}{2} & -\frac{i}{\sqrt{2}} \\ -\frac{i}{\sqrt{2}} & \frac{1-i}{2} \end{pmatrix} \cdot \begin{pmatrix} \frac{1-i}{2} & \frac{i}{\sqrt{2}} \\ \frac{i}{\sqrt{2}} & \frac{1+i}{2} \end{pmatrix} \right]_{ac} \cdot \phi'_c \\ &= \sum_{c=1}^{2} \left[\begin{pmatrix} 1 & 0 \\ 0 & 1 \end{pmatrix} \right]_{ac} \cdot \phi'_c = \phi'_a \ , \end{aligned} \tag{2.9}$$

to get the identity transformation. This is not unusual, because the original form of Eq. (2.2) has that property, too. The explicit form of a transformation may be altered under a basis change but the physical action (here: no action when applied twice) does not get altered.

This is a general property: A rotation of the Higgs basis is given by

$$\phi'_a = \sum_{b=1}^{n} U_{ab} \phi_b \tag{2.10}$$

with n the number of Higgs doublets and $U \in \mathrm{U}(n)$. By this transformation,

the generalized CP transformation of Eq. (2.7) becomes

$$\begin{aligned}\mathrm{CP}[\phi'_a] &= \mathrm{CP}\left[\sum_{b=1}^{n} U_{ab}\phi_b\right] = \sum_{b=1}^{n} U_{ab}\mathrm{CP}[\phi_b] \\ &= \sum_{b=1}^{n}\sum_{c=1}^{n} U_{ab}X_{bc}\phi_c^* = \sum_{b=1}^{n}\sum_{c=1}^{n} U_{ab}X_{bc}\left(\sum_{d=1}^{n} U_{cd}^{\dagger}\ \phi'_d\right)^* \\ &= \sum_{d=1}^{n}\sum_{b=1}^{n}\sum_{c=1}^{n} U_{ab}X_{bc}U_{cd}^{\top}\ (\phi'_d)^*\end{aligned} \tag{2.11}$$

such that the transformed matrix X' in the new basis is given by

$$X' := UXU^{\top}\ . \tag{2.12}$$

From Eq. (2.9) one can deduce that applying CP twice is equivalent to a basis rotation with the matrix

$$W := X \cdot X^* \in \mathrm{U}(n)\ . \tag{2.13}$$

Suppose that there is a number $m \in \mathbb{N}$ such that

$$(X \cdot X^*)^m = \mathbb{1}\ , \tag{2.14}$$

i.e. applying CP in total $2m$ times gives the identity. Then it also holds that

$$\begin{aligned}(X' \cdot X'^*)^m &= (UXU^{\top} \cdot U^*X^*U^{\dagger})^m \\ &= (UX\ (\ U^{\dagger}U\ )^*\ X^*U^{\dagger})^m \\ &= (UX \cdot X^*U^{\dagger})^m \\ &= U\ (X \cdot X^*)^m\ U^{\dagger} = \mathbb{1}\ .\end{aligned} \tag{2.15}$$

The minimal number N of applications of CP that give back the identity is a basis invariant. One classifies different CP transformations by this number, e.g. CP2, CP4, CP8 are transformations which have to be applied 2, 4, 8 times to give the identity.

In fact, for a CPN this minimal number N has to be a power of two in order to get a physically different transformation. Consider CP6 which essentially has a $\mathbb{Z}_6$ structure. It can be factorized into $\mathbb{Z}_2 \times \mathbb{Z}_3$. So one can write any CP6 symmetry as the direct product

$$\mathrm{CP2} \times \mathbb{Z}_3\ . \tag{2.16}$$

This shows that CP6 is not a new CP transformation, but the independent combination of a CP2 and some discrete symmetry. Such discrete symmetries can always be factored out if the prime number factorization of N includes different prime numbers than 2. If there is such a factorization, then the CP symmetry of the theory is actually this smaller CPN', because the additional discrete symmetries are completely independent. One can combine them with CP but this will not change any physical implication. Hence, for physically different GCP transformations N has to be a power of two.

CP2 is up to a basis change the ordinary transformation formulated in Eq. (2.2). It was shown in [8] that for every matrix $X \in \mathrm{U}(n)$ there exists a basis transformation $U \in \mathrm{U}(n)$ such that $X' = UXU^\top$ is block diagonal with $\mathrm{SO}(2)$ and identity submatrices. Hence, if $X \cdot X^* = \mathbb{1}$ then $X' \cdot X'^* = X' \cdot X' = \mathbb{1}$, because X' is real. This implies up to some basis transformation $X' = \mathbb{1}$, which is the ordinary CP transformation.

2.3 CP4

In contrast to CP2, the CP4 transformation is an actual GCP because it is not possible to bring it into the from $X' = \mathbb{1}$ through some basis change.

For a single Higgs doublet there are only CP2 transformations because $X \in \mathrm{U}(1)$ such that $X = e^{i\alpha}$ and $X \cdot X^* = e^{i\alpha} \cdot e^{-i\alpha} = 1$.

Two Higgs doublets have only one possible form of CP4. One can see this as follows: According to [8], for $X \in \mathrm{U}(2)$ there exists a basis change $U \in \mathrm{U}(2)$ such that

$$X' = UXU^\top = \begin{pmatrix} \cos\theta & \sin\theta \\ -\sin\theta & \cos\theta \end{pmatrix} \ . \tag{2.17}$$

Furthermore, the angle θ is given by the twice degenerate eigenvalue $4\cos^2\theta$ of

$$(X + X^\top)(X + X^\top)^* \tag{2.18}$$

such that $\theta \in [0, \pi/2]$. Every $\mathrm{U}(2)$ matrix X can be expressed as

$$X = e^{i\alpha} \cdot (x_0 \ \mathbb{1} + i \ \vec{x} \cdot \vec{\sigma}) \ , \tag{2.19}$$

where $\alpha, x_0, x_1, x_2, x_3 \in \mathbb{R}$, $\sqrt{x_0^2 + x_1^2 + x_2^2 + x_3^2} = 1$ and $\vec{\sigma}$ is the 3-vector of Pauli matrices. The term in brackets is a unit quaternion, which can span all $\mathrm{SU}(2)$ transformations. The phase factor $e^{i\alpha}$ is an element of $\mathrm{U}(1)$. So the whole expression is a $\mathrm{U}(2)$ transformation. The twice degenerate eigenvalue of (2.18) is therefore

$$4(x_0^2 + x_1^2 + x_3^2) = 4(1 - x_2^2) = 4\cos^2\theta \ . \tag{2.20}$$

For a CP4 transformation $\theta = \pi/2$, which gives $x_0 = x_1 = x_3 = 0$ and $x_2 = \pm 1$. So a CP4 matrix has the form

$$X = \pm i \cdot e^{i\alpha} \cdot \begin{pmatrix} 0 & -i \\ i & 0 \end{pmatrix} = e^{i\alpha'} \cdot \begin{pmatrix} 0 & -1 \\ 1 & 0 \end{pmatrix} \ . \tag{2.21}$$

All phase factors like ± 1 and i have been incorporated in $\alpha' \in \mathbb{R}$. The global phase α' is not measurable. This corresponds to the usual fact that CP transformations are defined only up to a phase factor.

In the case of three Higgs doublets there exists a transformation such that

$$X' = \begin{pmatrix} 1 & 0 & 0 \\ 0 & \cos\theta & \sin\theta \\ 0 & -\sin\theta & \cos\theta \end{pmatrix} \ . \tag{2.22}$$

Matrix addition, multiplication, transposition and conjugation does not mix the submatrices of a block diagonal matrix. The eigenvalues of (2.18) are invariant under a Higgs basis change. So the discussion for a single Higgs doublet and two Higgs doublets can be applied to the above submatrices separately. Thus, a general form for a CP4 matrix is

$$X = \begin{pmatrix} e^{i\beta'} & 0 & 0 \\ 0 & 0 & -e^{i\alpha'} \\ 0 & e^{i\alpha'} & 0 \end{pmatrix} \ , \tag{2.23}$$

where α' and β' come from the U(2) and U(1) subpart respectively. Both of them are spurious though, because they can be eliminated by the basis transformation

$$\begin{pmatrix} e^{-i\beta'/2} & 0 & 0 \\ 0 & e^{-i\alpha'/2} & 0 \\ 0 & 0 & e^{-i\alpha'/2} \end{pmatrix} \ . \tag{2.24}$$

Hence, they can be chosen to have arbitrary values without changing the physical content of the theory. For instance, in the three-Higgs-doublet model introduced in [1] and discussed in Section 3.2 the phases were chosen to be $\alpha' = -\pi/2$ and $\beta' = 0$.

If there are four Higgs doublets there are actually two different CP4 transformations

$$X' = \begin{pmatrix} \cos\theta_1 & \sin\theta_1 & 0 & 0 \\ -\sin\theta_1 & \cos\theta_1 & 0 & 0 \\ 0 & 0 & \cos\theta_2 & \sin\theta_2 \\ 0 & 0 & -\sin\theta_2 & \cos\theta_2 \end{pmatrix} \tag{2.25}$$

with either $\theta_1 = 0$ and $\theta_2 = \pi/2$ or $\theta_1 = \theta_2 = \pi/2$. They are not connected through a Higgs basis transformation and are thus different. However, any other CP4 transformation can be obtained by an appropriate basis change.

As one can see, starting at four Higgs doublets there is another characteristic for GCP classification. Only one SO(2) submatrix has to be a rotation by the angle $\theta = \frac{2\pi}{N}$ where N is the number of applications which give the identity. The other submatrices can have different angles $\frac{2\pi}{M}$ such that M divides N.

2.4 Constructing GCP invariant Potentials

A general Higgs potential with doublets ϕ_a can be written as

$$V = Y_{ab}(\phi_a^\dagger \phi_b) + \frac{1}{2} Z_{ab,cd}(\phi_a^\dagger \phi_b)(\phi_c^\dagger \phi_d) \tag{2.26}$$

with parameters $Y_{ab}, Z_{ab,cd} \in \mathbb{C}$ and $Y_{ab}^* = Y_{ba}$, $Z_{ab,cd}^* = Z_{ba,dc}$ because the overall potential is real valued.

A basis transformation $U \in \mathrm{U}(n)$ with $\phi'_a = U_{ab}\phi_b$ changes the parameters according to

$$\begin{aligned} Y'_{ab} &= U_{ai} Y_{ij} U_{jb}^\dagger \\ Z_{ab,cd} &= U_{ai} U_{ck} Z_{ij,kl} U_{jb}^\dagger U_{ld}^\dagger \ . \end{aligned} \tag{2.27}$$

Similarly, a GCP transformation $X \in \mathrm{U}(n)$ with $\mathrm{CP}[\phi_a] = X_{ab}\phi_b^*$ will yield

$$\begin{aligned} \mathrm{CP}[Y_{ab}] &= X_{ai} Y_{ij}^* X_{jb}^\dagger \\ \mathrm{CP}[Z_{ab,cd}] &= X_{ai} X_{ck} Z_{ij,kl}^* X_{jb}^\dagger X_{ld}^\dagger \ . \end{aligned} \tag{2.28}$$

For a CP2 transformation with $X_{ab} = \delta_{ab}$, the Kronecker delta, these are the familiar identities $\mathrm{CP}[Y_{ab}] = Y_{ab}^*$ and $\mathrm{CP}[Z_{ab,cd}] = Z_{ab,cd}^*$. Hence, for a CP2 invariant Higgs potential, there exists a basis such that all parameters are real. Inversely, if all parameters are real, then CP2 is a symmetry of that Higgs potential.

Consider a two-Higgs-doublet model with CP4 symmetry. According to Section 2.3, there exists a basis such that

$$X = \begin{pmatrix} 0 & -1 \\ 1 & 0 \end{pmatrix} \ . \tag{2.29}$$

The invariance conditions for Y are then

$$\begin{aligned} Y_{11}^* &= Y_{22} \\ Y_{12}^* &= -Y_{21} \ . \end{aligned} \tag{2.30}$$

Because the Higgs potential V is real valued, one also has

$$\begin{aligned} Y_{11}^* &= Y_{11} \\ Y_{12}^* &= Y_{21} \ , \end{aligned} \tag{2.31}$$

which in combination gives that $Y_{11} = Y_{22}$, $Y_{12} = Y_{21} = 0$ and $Y_{11}, Y_{22} \in \mathbb{R}$. An equivalent discussion for Z shows that for the quartic coupling parameters

$$Z_{11,12} = Z_{11,21} = Z_{22,12} = Z_{22,21} = 0 \tag{2.32}$$

and

$$Z_{11,11}, Z_{22,22}, Z_{11,22}, Z_{12,21} \in \mathbb{R} \ . \tag{2.33}$$

Except for $Z_{12,12} = Z_{21,21}^* = r \cdot e^{i\varphi}$, all parameters are real. The basis transformation

$$U = \begin{pmatrix} e^{-i\varphi/4} & 0 \\ 0 & e^{i\varphi/4} \end{pmatrix} \tag{2.34}$$

makes the last two parameters also real without altering any of the others. Therefore, a CP4 invariant Higgs potential is also CP2 invariant. A similar discussion can be found in [9].

Furthermore, there are no non-zero parameters with an uneven number of indices in either 1 or 2. Hence, the potential is also symmetric under

$$D_1 : \begin{cases} \phi_1 \to \phi_2 \\ \phi_2 \to \phi_1 \end{cases} \tag{2.35}$$

and

$$D_2 : \begin{cases} \phi_1 \to \phi_1 \\ \phi_2 \to -\phi_2 \end{cases} \ . \tag{2.36}$$

All of them, CP2, D_1 and D_2, are called accidental symmetries, because they emerged from the imposition of invariance conditions of a different symmetry (here: CP4). It is interesting to note that the successive application

$$\mathrm{CP2} \circ D_1 \circ D_2 \tag{2.37}$$

is the same as a single application of CP4. Therefore, CP4 is not an actual physical symmetry of two-Higgs-doublet models but rather a combination of CP2 and some discrete symmetries. In a sense, the (parameter) space of two Higgs doublets is too small for the action of a GCP. This is somewhat

analogous to the argument of factorization in Section 2.2. The CP4 is split up into a smaller CP2 symmetry and some independent discrete symmetries.

There exists no two-Higgs-doublet model that is solely CP4 invariant. Such models are only possible when incorporating at least three doublets. One of these models was proposed in [1] and will be further investigated in Chapter 3.

Chapter 3

Three-Higgs-Doublet Models

In this chapter the three-Higgs-doublet models (3HDMs) that will be investigated in Chapter 4 are introduced. The inert two-Higgs-doublet model (IDM) [3, 2] is presented here as a know reference for phenomenology studies, too. It will set the standard for notation. The actually studied models in Chapter 4 will be the three-Higgs-doublet model of Section 3.2 and the very similar doubled inert doublet model of Section 3.3.

3.1 IDM

The IDM is a two-Higgs-doublet model (2HDM). The potential is given by

$$\begin{aligned} V = &-m_{11}^2(\phi_1^\dagger\phi_1) - m_{22}^2(\phi_2^\dagger\phi_2) + \lambda_1(\phi_1^\dagger\phi_1)^2 + \lambda_2(\phi_2^\dagger\phi_2)^2 \\ &+ \lambda_3(\phi_1^\dagger\phi_1)(\phi_2^\dagger\phi_2) + \lambda_4(\phi_1^\dagger\phi_2)(\phi_2^\dagger\phi_1) + \frac{\lambda_5}{2}\left[(\phi_2^\dagger\phi_1)^2 + (\phi_1^\dagger\phi_2)^2\right] \end{aligned} \tag{3.1}$$

with doublets ϕ_1 and ϕ_2 and all parameters real.

If one mass eigenstate of the neutral Higgs bosons acquires Standard-Model-like couplings by aligning with the vacuum expectation values (VEVs) of the doublets, this limit is called alignment limit [10]. Here, the VEVs of the doublets in the alignment limit are

$$\langle\phi_1\rangle = \begin{pmatrix} 0 \\ \frac{v}{\sqrt{2}} \end{pmatrix} \text{ and } \langle\phi_2\rangle = \begin{pmatrix} 0 \\ 0 \end{pmatrix} \ . \tag{3.2}$$

The minimum conditions of the Higgs potential yield

$$v = \sqrt{\frac{m_{11}^2}{\lambda_1}} = 246.22\,\text{GeV} \ . \tag{3.3}$$

Because the IDM is an inert model, the Yukawa sector is especially simple. The first Higgs doublet ϕ_1 couples to all fermions. The second doublet ϕ_2 is inert and does not couple to fermions at all. By construction, the first doublet ϕ_1 is completely Standard-Model-like and we define

$$\phi_1 := \begin{pmatrix} G^+ \\ \frac{1}{\sqrt{2}}(v + h_{\mathrm{SM}} + iG_0) \end{pmatrix} . \tag{3.4}$$

It incorporates the charged and neutral Goldstone bosons $G^\pm$ and G_0 and the 125 GeV Standard Model (SM) Higgs boson h_{SM} with mass term

$$m^2_{h_{\mathrm{SM}}} = 2m^2_{11} = 2\lambda_1 v^2 . \tag{3.5}$$

The second doublet is written in terms of the charged field H_2^+ and the two neutral fields h and a,

$$\phi_2 := \begin{pmatrix} H_2^+ \\ \frac{1}{\sqrt{2}}(h + ia) \end{pmatrix} . \tag{3.6}$$

The masses of the neutral and charged Higgs fields read

$$\begin{aligned} m^2_h &= \frac{m^2_{11}}{2\lambda_1} \cdot \lambda_{345} - m^2_{22} \\ m^2_a &= \frac{m^2_{11}}{2\lambda_1} \cdot \bar{\lambda}_{345} - m^2_{22} \\ m^2_{H_2^\pm} &= \frac{m^2_{11}}{2\lambda_1} \cdot \lambda_3 - m^2_{22} \end{aligned} \tag{3.7}$$

with

$$\begin{aligned} \lambda_{345} &= \lambda_3 + \lambda_4 + \lambda_5 \\ \bar{\lambda}_{345} &= \lambda_3 + \lambda_4 - \lambda_5 . \end{aligned} \tag{3.8}$$

By restricting λ_5 to negative values, there is one light scalar h and a heavy pseudoscalar a. One could also choose positive values at this point but this would only change the mass ordering of the neutral scalars, which does not affect any observable. The choice of negative values for λ_5 is a convention.

The model is CP2 but not CP4 invariant. There is also a $\mathbb{Z}_2$ symmetry induced by

$$\begin{aligned} \phi_1 &\to \phi_1 \\ \phi_2 &\to -\phi_2 . \end{aligned} \tag{3.9}$$

This symmetry stabilizes the light scalar h and promotes it to a dark matter (DM) candidate. The trilinear and quartic couplings of the light scalar h to the SM Higgs boson h_{SM} are proportional to λ_{345} while the couplings of the heavy scalar a to it are proportional to $\bar{\lambda}_{345}$. Because of the mass ordering with $\lambda_5 < 0$, the couplings of the heavy scalar are enhanced compared to the ones of the light scalar.

3.2 DM CP4 3HDM

The inert three-Higgs-doublet model with dark matter candidates arising from a CP4 symmetry (DM CP4 3HDM) was first proposed by Ivanov and Silva [1]. Its potential is given by

$$V = V_0 + V_1 \tag{3.10}$$

with

$$\begin{aligned} V_0 = &-m_{11}^2(\phi_1^\dagger\phi_1) - m_{22}^2\left[(\phi_2^\dagger\phi_2) + (\phi_3^\dagger\phi_3)\right] + \lambda_1(\phi_1^\dagger\phi_1)^2 \\ &+ \lambda_2\left[(\phi_2^\dagger\phi_2)^2 + (\phi_3^\dagger\phi_3)^2\right] + \lambda_3(\phi_1^\dagger\phi_1)\left[(\phi_2^\dagger\phi_2) + (\phi_3^\dagger\phi_3)\right] \\ &+ \lambda_4\left[(\phi_1^\dagger\phi_2)(\phi_2^\dagger\phi_1) + (\phi_1^\dagger\phi_3)(\phi_3^\dagger\phi_1)\right] + \lambda_3'(\phi_2^\dagger\phi_2)(\phi_3^\dagger\phi_3) \\ &+ \lambda_4'(\phi_2^\dagger\phi_3)(\phi_3^\dagger\phi_2) \end{aligned} \tag{3.11}$$

and

$$\begin{aligned} V_1 = &\frac{\lambda_6}{2}\left[(\phi_2^\dagger\phi_1)^2 - (\phi_1^\dagger\phi_3)^2\right] + \lambda_8(\phi_2^\dagger\phi_3)^2 \\ &+ \lambda_9(\phi_2^\dagger\phi_3)\left[(\phi_2^\dagger\phi_2) - (\phi_3^\dagger\phi_3)\right] + h.c. \end{aligned} \tag{3.12}$$

Here, ϕ_1, ϕ_2 and ϕ_3 are Higgs doublets. All parameters are real except for $\lambda_8, \lambda_9 \in \mathbb{C}$.

In the alignment limit, the VEV configuration of the three Higgs doublets is given by

$$\langle\phi_1\rangle = \begin{pmatrix} 0 \\ \frac{v}{\sqrt{2}} \end{pmatrix} \text{ and } \langle\phi_2\rangle = \langle\phi_3\rangle = \begin{pmatrix} 0 \\ 0 \end{pmatrix} . \tag{3.13}$$

Applying the minimum conditions to the Higgs potential yields

$$v = \sqrt{\frac{m_{11}^2}{\lambda_1}} = 246.22\,\mathrm{GeV} . \tag{3.14}$$

Again, the Yukawa sector is especially simple because the DM CP4 3HDM is an inert model. The first Higgs doublet ϕ_1 couples to all fermions while the other two doublets ϕ_2 and ϕ_3 are inert and do not couple to fermions at all.

Hence, one can identify ϕ_1 with the doublet of the SM and write

$$\phi_1 := \begin{pmatrix} G^+ \\ \frac{1}{\sqrt{2}}(v + h_{\mathrm{SM}} + iG_0) \end{pmatrix} . \tag{3.15}$$

It incorporates the charged and neutral Goldstone bosons $G^\pm$ and G_0, and the 125 GeV SM Higgs boson h_{SM} with mass term

$$m^2_{h_{\mathrm{SM}}} = 2m^2_{11} = 2\lambda_1 v^2 . \tag{3.16}$$

The second and third doublet are written in terms of charged Higgs bosons H_2^+, H_3^+ and neutral fields H, a and h, A respectively:

$$\phi_2 := \begin{pmatrix} H_2^+ \\ \frac{1}{\sqrt{2}}(H + ia) \end{pmatrix} \text{ and } \phi_3 := \begin{pmatrix} H_3^+ \\ \frac{1}{\sqrt{2}}(h + iA) \end{pmatrix} \tag{3.17}$$

The mass spectrum becomes

$$\begin{aligned} m^2_a = m^2_h &= \frac{m^2_{11}}{2\lambda_1} \cdot \bar{\lambda}_{346} - m^2_{22} \\ m^2_A = m^2_H &= \frac{m^2_{11}}{2\lambda_1} \cdot \lambda_{346} - m^2_{22} \\ m^2_{H_2^\pm} = m^2_{H_3^\pm} &= \frac{m^2_{11}}{2\lambda_1} \cdot \lambda_3 - m^2_{22} \end{aligned} \tag{3.18}$$

with

$$\begin{aligned} \lambda_{346} &= \lambda_3 + \lambda_4 + \lambda_6 \\ \bar{\lambda}_{346} &= \lambda_3 + \lambda_4 - \lambda_6 . \end{aligned} \tag{3.19}$$

By restricting λ_6 to positive values, there are two mass degenerate light scalars a and h and two mass degenerate heavy scalars A and H. Again, this is just convention.

Compared to the IDM of Section 3.1 there are some noteworthy differences: First of all, there is another doublet ϕ_3 and additional interaction terms between ϕ_2 and ϕ_3. They are proportional to λ_3', λ_4', λ_8 and λ_9. Secondly, except for the term proportional to λ_6 all the other interactions are the same as in the IDM. For each coupling to ϕ_2 the same coupling to ϕ_3 has been added. Thirdly, the parameter λ_6 is essentially the same parameter as

λ_5 in the IDM. However, ϕ_2 couples exactly IDM-like while ϕ_3 couples with $-\lambda_5$.

Furthermore, this model has a CP4 symmetry generated by

$$X = \begin{pmatrix} 1 & 0 & 0 \\ 0 & 0 & i \\ 0 & -i & 0 \end{pmatrix} \ . \tag{3.20}$$

It corresponds to the choice of phases $\alpha' = -\pi/2$ and $\beta' = 0$ in Eq. (2.23) of Section 2.3. There are no other accidental symmetries, like additional global symmetries or certain discrete symmetries other than $X \cdot X^*$, under which the potential is invariant. In fact, it is the only 3HDM potential that has this property and it is the minimal multi-Higgs-doublet model that is CP4 invariant.

The neutral scalars a, h, A, H are not CP eigenstates. They transform as

$$\begin{aligned} \mathrm{CP}[a] &= h \\ \mathrm{CP}[h] &= -a \\ \mathrm{CP}[A] &= -H \\ \mathrm{CP}[H] &= A \ . \end{aligned} \tag{3.21}$$

There are, however, certain linear combinations that are eigenstates:

$$\begin{aligned} \varphi &:= \frac{1}{\sqrt{2}}(h + ia) \\ \mathrm{CP}[\varphi] &= i\varphi \end{aligned} \tag{3.22}$$

and

$$\begin{aligned} \Phi &:= \frac{1}{\sqrt{2}}(H - iA) \\ \mathrm{CP}[\Phi] &= i\Phi \ . \end{aligned} \tag{3.23}$$

Because they are composed of mass degenerate and neutral fields, they are complex, neutral fields which are also mass eigenstates. One can associate a CP quantum number q modulo 4 with them, i.e. $q = 1$. The conjugate fields have the quantum number $q = 3$,

$$\begin{aligned} \mathrm{CP}[\varphi^\dagger] &= -i\varphi^\dagger \\ \mathrm{CP}[\Phi^\dagger] &= -i\Phi^\dagger \ , \end{aligned} \tag{3.24}$$

while the SM Higgs boson has $q = 0$,

$$\mathrm{CP}[h_{\mathrm{SM}}] = h_{\mathrm{SM}} \ . \tag{3.25}$$

The charged scalars transform as

$$\begin{aligned} \mathrm{CP}[H_2^+] &= iH_3^- \\ \mathrm{CP}[H_2^-] &= -iH_3^+ \\ \mathrm{CP}[H_3^+] &= -iH_2^- \\ \mathrm{CP}[H_3^-] &= iH_2^+ \ . \end{aligned} \tag{3.26}$$

For them there is no linear combination $S^+ := aH_2^+ + bH_3^+$ of fields with equal gauge quantum numbers such that there is any sensible definition of CP in terms of field conjugates only, i.e. $\mathrm{CP}[S^+] \neq e^{i\gamma}(S^+)^\dagger$.

Because CP4 is a symmetry of the Lagrangian and by definition all SM CP eigenstates have either $q = 0$ or $q = 2$, there is no decay channel for the lightest scalars φ and $\varphi^\dagger$ with quantum numbers $q = 1$ and $q = 3$. They are stable. Hence, they constitute good DM candidates. The trilinear and quartic couplings of the light scalars φ and $\varphi^\dagger$ to the SM Higgs boson h_{SM} are proportional to $\bar{\lambda}_{346}$ while the couplings of the heavy scalars Φ and $\Phi^\dagger$ to it are proportional to λ_{346}. They are given in Appendix A.1. Because of the mass ordering with $\lambda_6 > 0$, the couplings of the heavy scalars are enhanced compared to the ones of the light scalars just as it is in the IDM. The phenomenological consequences of the DM properties will be described in Chapter 4.

3.3 DIDM

The doubled inert doublet model (DIDM) is a 3HDM. The potential is given by

$$\begin{aligned} V = &-m_{11}^2(\phi_1^\dagger\phi_1) - m_{22}^2\left[(\phi_2^\dagger\phi_2) + (\phi_3^\dagger\phi_3)\right] + \lambda_1(\phi_1^\dagger\phi_1)^2 \\ &+ \lambda_2\left[(\phi_2^\dagger\phi_2)^2 + (\phi_3^\dagger\phi_3)^2\right] + \lambda_3(\phi_1^\dagger\phi_1)\left[(\phi_2^\dagger\phi_2) + (\phi_3^\dagger\phi_3)\right] \\ &+ \lambda_4\left[(\phi_1^\dagger\phi_2)(\phi_2^\dagger\phi_1) + (\phi_1^\dagger\phi_3)(\phi_3^\dagger\phi_1)\right] \\ &- \frac{\lambda_6}{2}\left[(\phi_2^\dagger\phi_1)^2 + (\phi_1^\dagger\phi_2)^2 + (\phi_3^\dagger\phi_1)^2 + (\phi_1^\dagger\phi_3)^2\right] \end{aligned} \tag{3.27}$$

with the doublets ϕ_1, ϕ_2 and ϕ_3 and all parameters real.

The DIDM is almost equivalent to the IDM. The parameter λ_6 corresponds to $-\lambda_5$ in the IDM. In fact, the third doublet ϕ_3 is a copy of the second one ϕ_2, since there are no interaction terms that distinguish between them. However, the vertex structure resembles more the one of the DM CP4 3HDM due to the additional doublet. Compared to the DM CP4 3HDM only

the additional interaction terms proportional to λ_3', λ_4', λ_8 and λ_9, which encode the CP4 symmetry properties, and the minus factor for the λ_6 term of ϕ_3 are missing. In Chapter 4 the DIDM will be used as a direct comparison model for the DM CP4 3HDM.

The doublet VEVs in the alignment limit are given by

$$\langle\phi_1\rangle = \begin{pmatrix} 0 \\ \frac{v}{\sqrt{2}} \end{pmatrix} \text{ and } \langle\phi_2\rangle = \langle\phi_3\rangle = \begin{pmatrix} 0 \\ 0 \end{pmatrix} . \tag{3.28}$$

Evaluating the minimum conditions of the potential yields

$$v = \sqrt{\frac{m_{11}^2}{\lambda_1}} = 246.22\,\text{GeV} . \tag{3.29}$$

As before, the Yukawa structure is simple. Only the first doublet ϕ_1 couples to all fermions, while the second and third doublets ϕ_2 and ϕ_3 are inert and do not couple to fermions at all.

The first doublet ϕ_1 is completely SM-like and we define

$$\phi_1 := \begin{pmatrix} G^+ \\ \frac{1}{\sqrt{2}}(v + h_{\text{SM}} + iG_0) \end{pmatrix} . \tag{3.30}$$

It incorporates the charged and neutral Goldstone bosons $G^\pm$ and G_0, and the 125 GeV SM Higgs boson h_{SM} with mass term

$$m_{h_{\text{SM}}}^2 = 2m_{11}^2 = 2\lambda_1 v^2 . \tag{3.31}$$

For the second and third doublet written in terms of charged Higgs bosons H_2^+, H_3^+ and neutral scalars h_2, a_2 and h_3, a_3 respectively,

$$\phi_2 := \begin{pmatrix} H_2^+ \\ \frac{1}{\sqrt{2}}(h_2 + ia_2) \end{pmatrix} \text{ and } \phi_3 := \begin{pmatrix} H_3^+ \\ \frac{1}{\sqrt{2}}(h_3 + ia_3) \end{pmatrix} , \tag{3.32}$$

the mass spectrum becomes

$$\begin{aligned} m_{h_2}^2 = m_{h_3}^2 &= \frac{m_{11}^2}{2\lambda_1} \cdot \bar{\lambda}_{346} - m_{22}^2 \\ m_{a_2}^2 = m_{a_3}^2 &= \frac{m_{11}^2}{2\lambda_1} \cdot \lambda_{346} - m_{22}^2 \\ m_{H_2^\pm}^2 = m_{H_3^\pm}^2 &= \frac{m_{11}^2}{2\lambda_1} \cdot \lambda_3 - m_{22}^2 \end{aligned} \tag{3.33}$$

with

$$\begin{aligned} \lambda_{346} &= \lambda_3 + \lambda_4 + \lambda_6 \\ \bar{\lambda}_{346} &= \lambda_3 + \lambda_4 - \lambda_6 . \end{aligned} \tag{3.34}$$

By restricting λ_6 to positive values, there are two mass degenerate light scalars h_2 and h_3 and two mass degenerate heavy scalars a_2 and a_3. Again, this is just convention.

The DIDM is CP4 invariant with

$$X = \begin{pmatrix} 1 & 0 & 0 \\ 0 & 0 & -1 \\ 0 & 1 & 0 \end{pmatrix} , \tag{3.35}$$

which corresponds to the choice of phases $\alpha' = \beta' = 0$ in Eq. (2.23) of Section 2.3. However, this symmetry is just apparent. Similar to the discussion in Section 2.4 there are two discrete symmetries

$$D_1 : \begin{cases} \phi_1 \to \phi_1 \\ \phi_2 \to \phi_3 \\ \phi_3 \to \phi_2 \end{cases} \tag{3.36}$$

and

$$D_2 : \begin{cases} \phi_1 \to \phi_1 \\ \phi_2 \to \phi_2 \\ \phi_3 \to -\phi_3 \end{cases} \tag{3.37}$$

under which the potential is invariant. The IDM is also CP2 invariant just like the IDM. Again, the successive application of

$$\mathrm{CP2} \circ D_1 \circ D_2 \tag{3.38}$$

is the same as a single application of CP4. Therefore, CP4 is not an actual physical symmetry of this model. The parameter space is too small and CP4 is split up into CP2 and some independent discrete symmetries.

In the DM CP4 3HDM it was the CP4 that stabilized the DM candidates. Here, however, these additional discrete symmetries D_1 and D_2 stabilize the light scalars h_2 and h_3 such that they are good DM candidates. Their trilinear and quartic couplings to the SM Higgs boson h_{SM} are proportional to $\bar{\lambda}_{346}$ while the couplings of the heavy scalars a_2 and a_3 to it are proportional to λ_{346}. They are given in Appendix A.2. Because of the mass ordering with $\lambda_6 > 0$, the couplings of the heavy scalars are enhanced compared to the ones of the light scalars just as it is in the IDM and the DM CP4 3HDM.

Chapter 4

Phenomenology

This chapter describes the phenomenological comparison of the 3HDMs introduced in Chapter 3: DM CP4 3HDM and DIDM. In particular, checks for the dark matter relic density and theoretical constraints are presented.

The goal is to see whether or not the observables and theoretical constraints will be influenced by the Higgs potential parameters $\lambda_3', \lambda_4', \lambda_8, \lambda_9$, which encode the information about the CP4 symmetry in the DM CP4 3HDM.

4.1 Tools

For the relic density scans the toolchain in Figure 4.1 was implemented. First, the Higgs potential and Yukawa couplings are given as inputs to SARAH [11, 12]. Then one can export CalcHEP [13] model files, which will contain all vertex factors etc. Also, SARAH can automatically generated SPheno [14, 15] code that can be compiled. This binary then performs the SM matching of parameters like masses and coupling constants. The SM input values are taken from the latest release of the Particle Data Group [16]. Furthermore, minimum conditions for the Higgs potential are evaluated numerically. The CalcHEP model files and SM matched input parameters are then given to MicrOmegas [17] to calculate the relic density. To conduct the actual scan SSP [18] was used. Among other features, it has the ability to define Higgs potential parameter ranges for the scans. Each point is passed to SPheno to supplement the SM input values.

The calculation of perturbative unitarity constraints in Section 4.3 was done with PUC [5]. For further reference see Appendix B.1.

Unfortunately, the package BFB [4] is not yet able to calculate boundedness constraints that are necessary and sufficient for 3HDMs in a reasonable

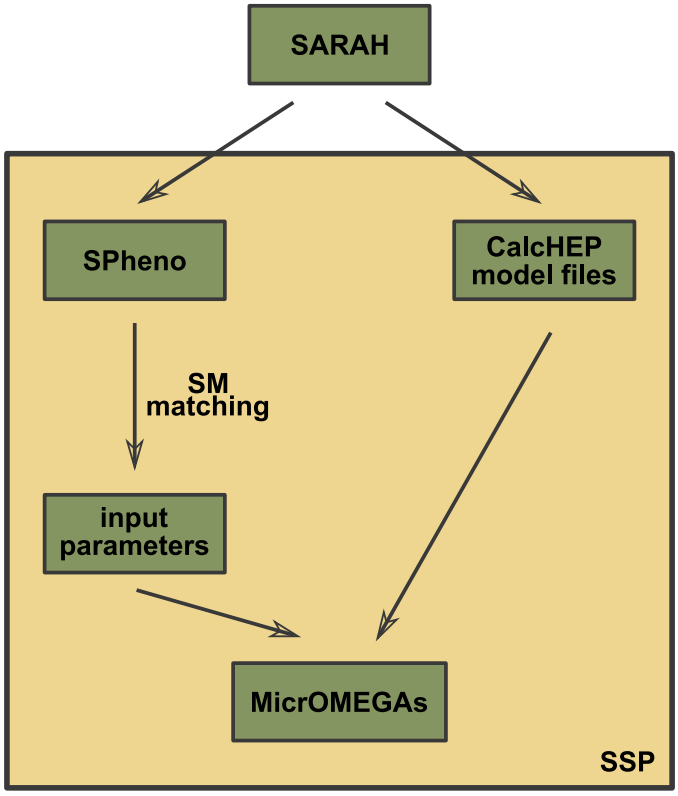

Figure 4.1: Flowchart for the relic density scan.

runtime. This task will be completed in the future (see also Section 5.6 and Appendix B.2). There are sufficient conditions for boundedness of the DM CP4 3HDM [19]. For the DIDM, sufficient boundedness conditions can be derived in relation to the IDM, because the third doublet in the DIDM is a copy of the second one. This allows a splitting of the quartic interactions of the potential in two parts. One for the second doublet and one for the third doublet, which will contain identical terms with respect to the second doublet. If the IDM conditions [20, 21, 22] are met, both parts will be positive separately such that the overall potential is bounded, too. This is not necessary though since they only have to be positive in total. For this analysis, however, sufficient conditions will not suffice and are therefore not considered. A general method to calculate necessary and sufficient conditions will be developed in Chapter 5.

Table 4.1: Input parameter set for the relic density scans.

parameter:	g_{DM}	m_{light}	m_{heavy}
description:	dark matter coupling to SM Higgs	mass of light (neutral) scalars	mass of heavy (neutral) scalars
dependence:	$\lambda_3 + \lambda_4 - \lambda_6$	$\sqrt{\frac{m_{11}^2}{2\lambda_1} \cdot \bar{\lambda}_{346} - m_{22}^2}$	$\sqrt{\frac{m_{11}^2}{2\lambda_1} \cdot \lambda_{346} - m_{22}^2}$
parameter:	m_{charged}	λ_2	λ_3'
description:	mass of charged scalars	real quartic coupling parameter	real quartic coupling parameter
dependence:	$\sqrt{\frac{m_{11}^2}{2\lambda_1} \cdot \lambda_3 - m_{22}^2}$	–	–
parameter:	λ_4'	λ_8	λ_9
description:	real quartic coupling parameter	complex quartic coupling parameter	complex quartic coupling parameter
dependence:	–	–	–

4.2 Relic Density Scans

4.2.1 Parameter Setup

For the relic density scans the input parameter set in Table 4.1 is used. The remaining two parameters m_{11} and λ_1 are given via the SM Higgs boson mass of Eq. (3.16) or (3.31) and the minimum conditions of Eq. (3.14) or (3.29) in connection with the Fermi constant G_F:

$$\begin{aligned} & m_{h_{\mathrm{SM}}} = 125.09\,\mathrm{GeV} \\ & \rightarrow m_{11} = \frac{m_{h_{\mathrm{SM}}}}{\sqrt{2}} = 88.45\,\mathrm{GeV} \end{aligned} \tag{4.1}$$

and

$$\begin{aligned} & G_F = 1.166\,378\,76 \times 10^{-5}\,\mathrm{GeV}^{-2} \\ & \rightarrow \lambda_1 = \frac{m_{11}^2}{v^2} = \sqrt{2}\; m_{11}^2\; G_F = 0.129\,054\;. \end{aligned} \tag{4.2}$$

The last 4 parameters λ_3', λ_4', λ_8 and λ_9 are not present in the DIDM.

4.2.2 Mass Ordering

To label the mass orderings of the scalars, their masses m_{light}, m_{heavy}, m_{charged} and $m_{h_{\mathrm{SM}}}$ will be abbreviated by l, h, c and s, respectively. For instance we

have

$$\text{lshc} \quad :\Leftrightarrow \quad m_{\text{light}} < m_{h_{\text{SM}}} < m_{\text{heavy}} < m_{\text{charged}} \ . \tag{4.3}$$

There are essentially 8 different mass orderings one can think of. By convention, there will be no ordering like hl. Furthermore, DM candidates should have no net charge as this is not observed in astrophysical experiments. Hence, cl is also not allowed. Orderings like ch and hc are both valid though. So in general an ordering will consist of one of the two strings lhc or lch.

The SM Higgs boson mass can then be inserted at the end, in the beginning, after l or between h and c. We call these 4 possibilities type I, type II, type III or type IV orderings respectively. Thus, in total there are $4 \times 2 = 8$ (two for each type) different mass orderings.

4.2.3 Scans

In this section relic density scans over the DM candidate mass m_{light} in the range from 10 GeV to 500 GeV are presented. The goal is to demonstrate that the relic density does not depend on the parameters λ_2, λ_3', λ_4', λ_8 and λ_9. Furthermore, the complete equality of the DM CP4 3HDM and the DIDM will be shown.

To do this, a generic value of

$$g_{\text{DM}} = 0.1 \tag{4.4}$$

is used throughout all the scans. There are two sets of parameters (a) and (b), which differ by the choice of quartic coupling parameters λ_2, λ_3', λ_4', λ_8 and λ_9:

- Parameter set (a)

$$\lambda_2 = \lambda_3' = \lambda_4' = \lambda_8 = \lambda_9 = 0 \tag{4.5}$$

- Parameter set (b)

$$\begin{aligned} \lambda_2 &= 200.0 \\ \lambda_3' &= -700.0 \\ \lambda_4' &= 500.0 \\ \lambda_8 &= -1000.0 + i \cdot 100.0 \\ \lambda_9 &= 350.0 - i \cdot 200.0 \end{aligned} \tag{4.6}$$

One can see that parameter set (b) incorporates positive and negative numbers with big magnitude. Obviously, they will not be allowed by perturbative unitarity constraints. However, set (b) has been chosen such that

1. any dependence on the quartic coupling parameters will show up (in comparison to set (a)) and

2. there happens no accidental cancellation within any vertex factor involving the quartic coupling parameters.

It is used for demonstration purposes only.

The IDM relic density is independent of λ_2 and so is the relic density in the DIDM, because the third doublet is merely a copy of the second one. This fact was explicitly tested but will not be presented in the following for reasons of brevity. After all, the DIDM was constructed to be IDM-like. Hence, all DIDM scans will essentially be parameter set (a) scans with $\lambda_2 = 0$.

The remaining parameters, the masses, are categorized by their mass ordering to show mass regions with different kinematic constraints on decay particles or intermediate states. The scans will be conducted on all possible mass orderings within the scalar sector such that all kinematically allowed decay and coannihilation channels that may influence the thermal evolution of the relic density are included. The mass values are given in the respective sections below.

Additional constraints like perturbative unitarity or boundedness of the Higgs potential as well as collider observables and the most recent measurements of the DM relic density will not be considered in the following sections. These observations and constraints are not important for the main point of the analysis, which is the found independence of the relic density from the quartic coupling parameters λ_2, λ_3', λ_4', λ_8 and λ_9.

Type I: lhcs

The mass region labeled by lhcs corresponds to a mass ordering with

$$m_{\text{light}} < m_{\text{heavy}} < m_{\text{charged}} < m_{h_{\text{SM}}} \ . \tag{4.7}$$

It is a type I ordering. The DM candidate mass scan was performed over the range

$$m_{\text{light}} \in [10\,\text{GeV}, 80\,\text{GeV}] \ . \tag{4.8}$$

The other masses are set to

$$\begin{aligned} m_{\text{heavy}} &= 81.0\,\text{GeV} \\ m_{\text{charged}} &= 90.0\,\text{GeV} \\ m_{h_{\text{SM}}} &= 125.09\,\text{GeV} \end{aligned} \tag{4.9}$$

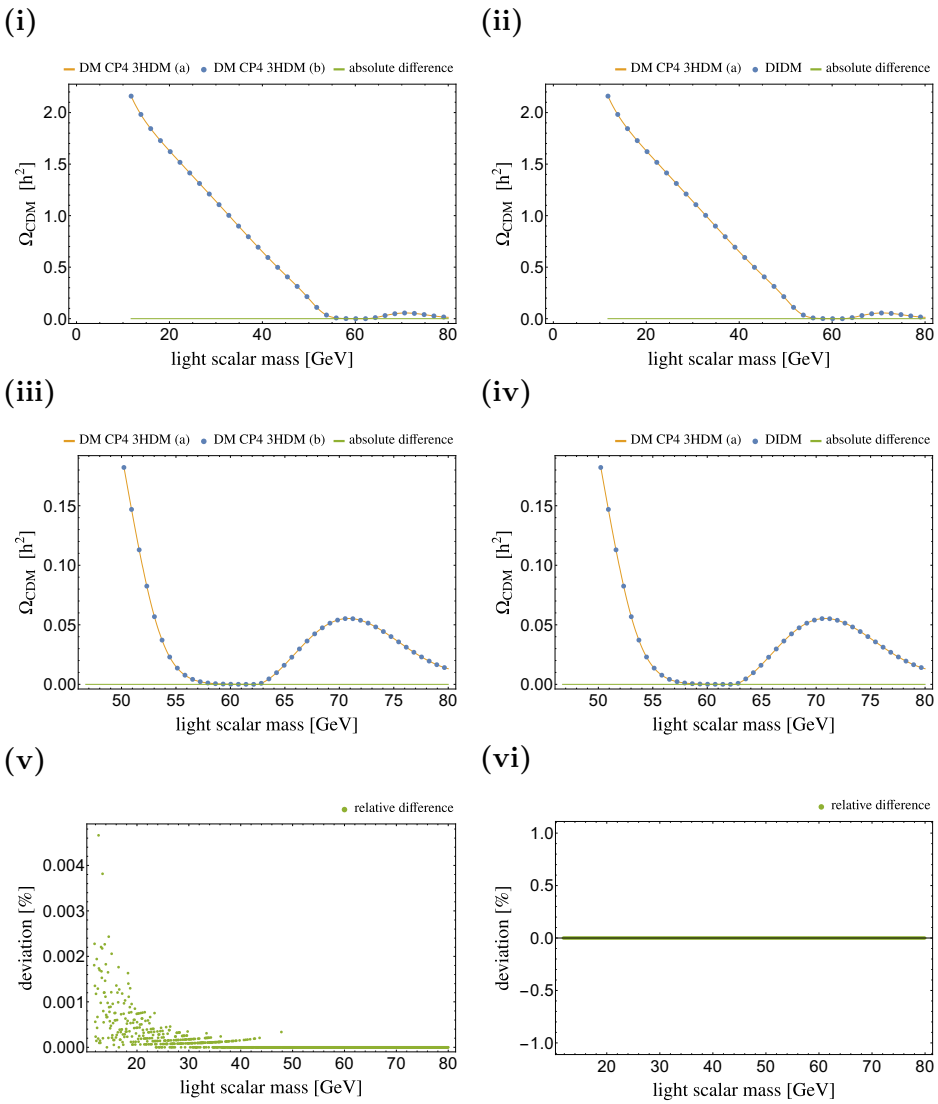

Figure 4.2: Comparison of the DM CP4 3HDM (a), DM CP4 3HDM (b) and the DIDM for the mass ordering lhcs. (i)-(ii): full scan range. (iii)-(iv): zoomed scan range. (v): relative difference of DM CP4 3HDM (a) and DM CP4 3HDM (b). (vi): relative difference of DM CP4 3HDM (a) and DIDM.

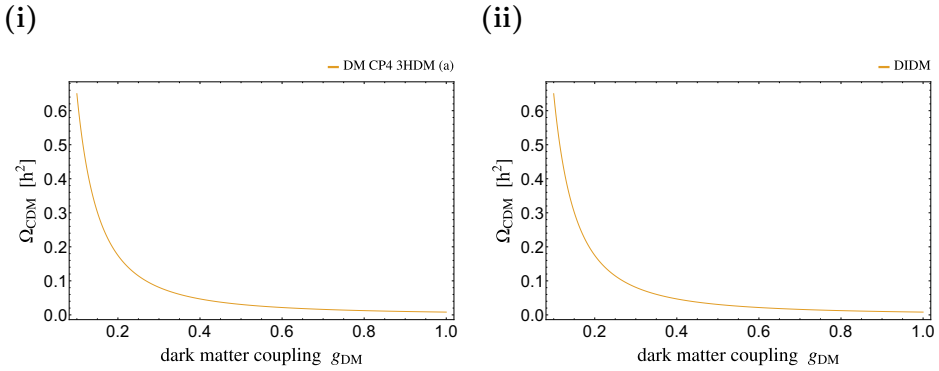

Figure 4.3: Relic density scan over g_{DM} of (i) the DM CP4 3HDM (a) and (ii) the DIDM for the mass ordering lhcs.

to comply with the mass ordering.

Figure 4.2 shows the comparison of the parameter sets (a) and (b) for the DM CP4 3HDM and the comparison to the DIDM. The lines are an interpolation of the scan values. The blue points are a selection of every 10th (zoomed range) or 30th (full range) point to increase legibility. The green points indicate the relative difference

$$\frac{|\Omega_{\text{CDM},1} - \Omega_{\text{CDM},2}|}{\Omega_{\text{CDM},1}} \cdot 100\,\% \tag{4.10}$$

of both parameter sets or models relative to the one that is mentioned first in the plots.

One can see that there is no difference between the DM CP4 3HDM and the DIDM in this mass region. DM CP4 3HDM (a) and DM CP4 3HDM (b) show a slight deviation of $\leq 0.005\,\%$. This can be attributed to numerical instability. For instance, the mass matrix is diagonalized numerically by SPheno. The vertex factors are expressed in terms of the elements of the mixing matrix. Even though all factors with quartic coupling parameters λ_2, λ_3', λ_4', λ_8 and λ_9 should cancel exactly in the masses, they might not do so numerically. Hence, some vertex factors will have a small but erroneous dependence on these quartic coupling parameters, resulting in a slightly different thermal evolution of both parameter sets. Furthermore, the deviations do not show a continuous dependence but are almost randomly scattered within the parameter space. This hints at numerical instabilities, too. To demonstrate the deviations of the relic density on a coupling parameter that has an actual influence, Figure 4.3 shows a set (a) scan over g_{DM} in the range

$$g_{\text{DM}} \in [0.1, 1.0] \tag{4.11}$$

with mass parameters

$$\begin{aligned} m_{\text{light}} &= 40.0\,\text{GeV} \\ m_{\text{heavy}} &= 81.0\,\text{GeV} \\ m_{\text{charged}} &= 90.0\,\text{GeV} \\ m_{h_{\text{SM}}} &= 125.09\,\text{GeV}\ . \end{aligned} \tag{4.12}$$

Again, the DM CP4 3HDM and the DIDM show complete agreement. Moreover, the behavior is continuous and the change in the relic density is much larger compared to the difference of the parameter sets (a) and (b), even though g_{DM} changes only by an order of magnitude. In conclusion, the deviations are only due to numerical fluctuations.

Type I: lchs

The mass region labeled by lchs corresponds to a mass ordering with

$$m_{\text{light}} < m_{\text{charged}} < m_{\text{heavy}} < m_{h_{\text{SM}}}\ . \tag{4.13}$$

It is a type I ordering. The DM candidate mass scan was done over the range

$$m_{\text{light}} \in [10\,\text{GeV}, 80\,\text{GeV}]\ . \tag{4.14}$$

The other masses are set to

$$\begin{aligned} m_{\text{heavy}} &= 90.0\,\text{GeV} \\ m_{\text{charged}} &= 81.0\,\text{GeV} \\ m_{h_{\text{SM}}} &= 125.09\,\text{GeV} \end{aligned} \tag{4.15}$$

to comply with the mass ordering.

Figure 4.4 shows the comparison of the parameter sets (a) and (b) for the DM CP4 3HDM and the comparison to the DIDM. All of them show close to perfect agreement. The deviations between the DM CP4 3HDM (a) and (b) are slightly higher compared to the lhcs mass ordering but still $\leq 0.006\,\%$ and randomly distributed. Again, this is due to numerical fluctuations.

Compared to the mass ordering lhcs, the masses of the heavy and charged scalars were flipped. The direct comparison between lhcs and lchs in Figure 4.5 shows that there is a slight difference when m_{light} approaches $80.0\,\text{GeV}$, that is when the mass splitting gets small. Up to $18\,\%$ higher relic density values are achieved when the next-to-lightest (non-SM-like) scalar is neutral and not charged. However, there are also smaller values.

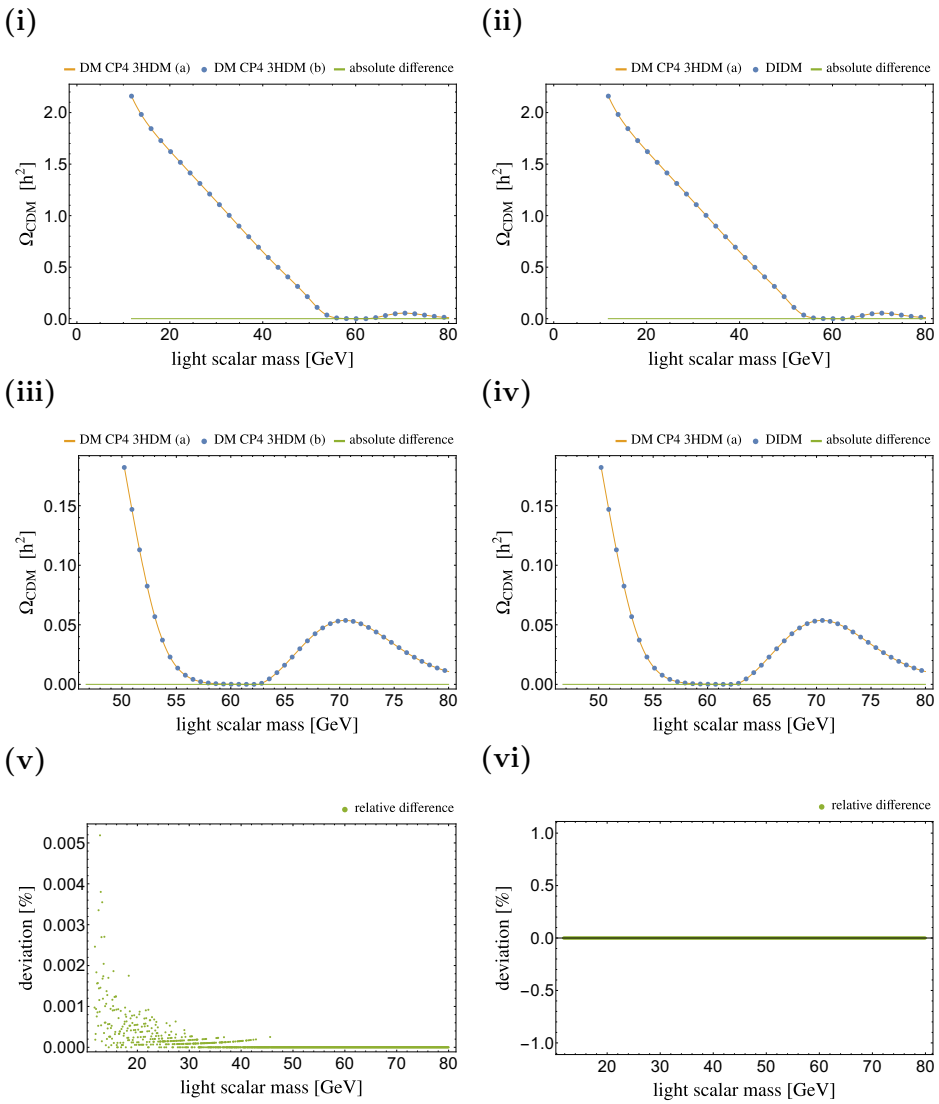

Figure 4.4: Comparison of the DM CP4 3HDM (a), DM CP4 3HDM (b) and the DIDM for the mass ordering lchs. (i)-(ii): full scan range. (iii)-(iv): zoomed scan range. (v): relative difference of DM CP4 3HDM (a) and DM CP4 3HDM (b). (vi): relative difference of DM CP4 3HDM (a) and DIDM.

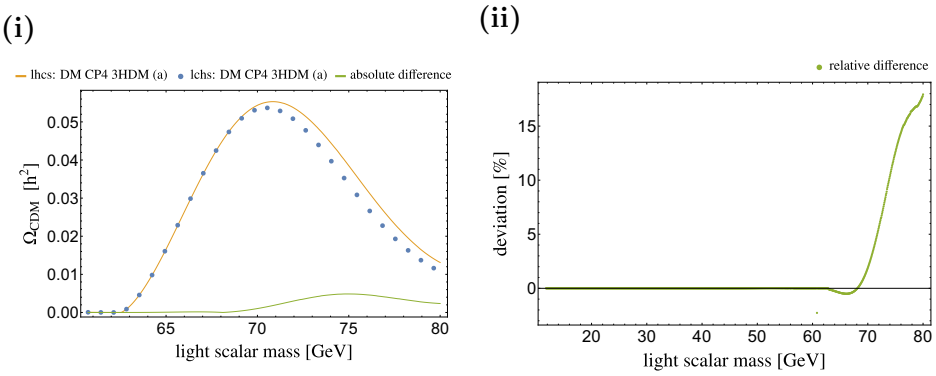

Figure 4.5: Comparison of the mass orderings lhcs and lchs for the DM CP4 3HDM (a). (i) zoomed scan range. (ii) relative difference of lhcs and lchs.

Type II: slhc

The mass region labeled by slhc corresponds to a mass ordering with

$$m_{h_{\mathrm{SM}}} < m_{\mathrm{light}} < m_{\mathrm{heavy}} < m_{\mathrm{charged}} \ . \tag{4.16}$$

It is a type II ordering. The DM candidate mass was scanned over the range

$$m_{\mathrm{light}} \in [130\,\mathrm{GeV}, 500\,\mathrm{GeV}] \ . \tag{4.17}$$

The other masses are set to

$$\begin{aligned} m_{\mathrm{heavy}} &= 501.0\,\mathrm{GeV} \\ m_{\mathrm{charged}} &= 800.0\,\mathrm{GeV} \\ m_{h_{\mathrm{SM}}} &= 125.09\,\mathrm{GeV} \end{aligned} \tag{4.18}$$

to comply with the mass ordering.

Figure 4.6 shows the comparison of the parameter sets (a) and (b) for the DM CP4 3HDM and the comparison to the DIDM. The deviations between the DM CP4 3HDM (a) and (b) are $\leq 0.9\,\%$ and between the DM CP4 3HDM and the DIDM are $\leq 1.0\,\%$. They are not systematic and occur somewhere between 275 GeV and 375 GeV. This not a distinguished mass range because no special fractions or multiples of the masses of the other particles fall into it. The deviations are again just numerical fluctuations.

Type II: slch

The mass region labeled by slch corresponds to a mass ordering with

$$m_{h_{\mathrm{SM}}} < m_{\mathrm{light}} < m_{\mathrm{charged}} < m_{\mathrm{heavy}} \ . \tag{4.19}$$

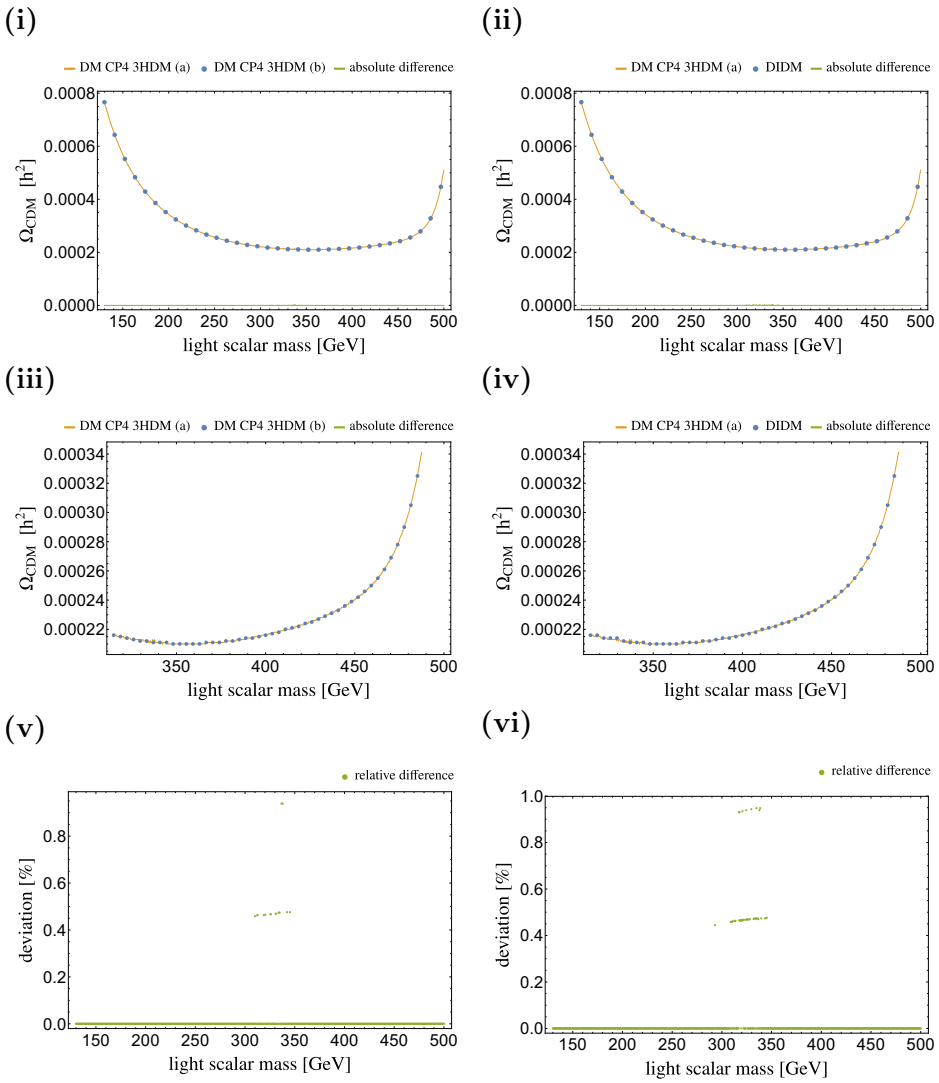

Figure 4.6: Comparison of the DM CP4 3HDM (a), DM CP4 3HDM (b) and the DIDM for the mass ordering slhc. (i)-(ii): full scan range. (iii)-(iv): zoomed scan range. (v): relative difference of DM CP4 3HDM (a) and DM CP4 3HDM (b). (vi): relative difference of DM CP4 3HDM (a) and DIDM.

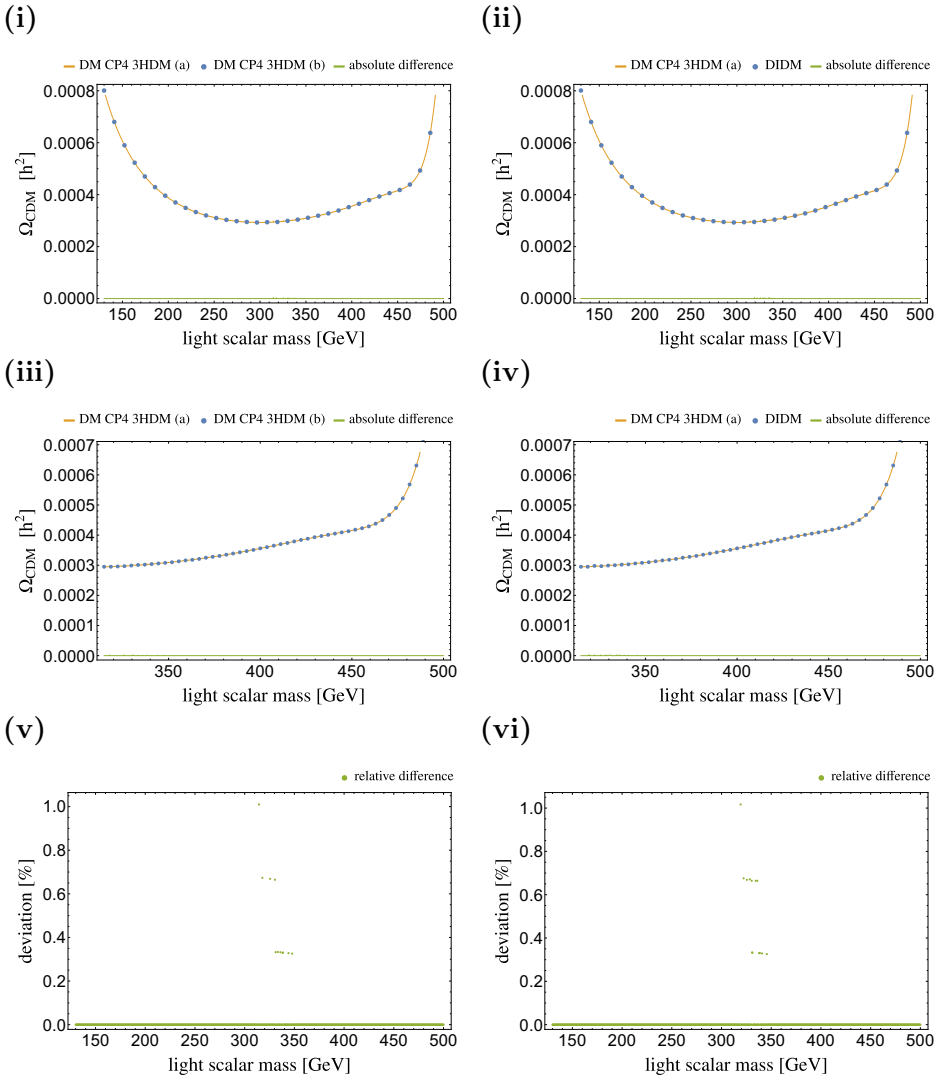

Figure 4.7: Comparison of the DM CP4 3HDM (a), DM CP4 3HDM (b) and the DIDM for the mass ordering slch. (i)-(ii): full scan range. (iii)-(iv): zoomed scan range. (v): relative difference of DM CP4 3HDM (a) and DM CP4 3HDM (b). (vi): relative difference of DM CP4 3HDM (a) and DIDM.

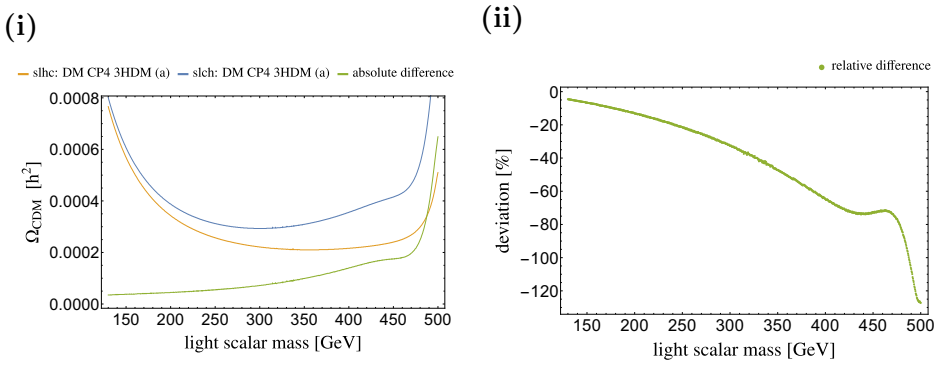

Figure 4.8: Comparison of the mass orderings slhc and slch for the DM CP4 3HDM (a). (i) full scan range. (ii) relative difference of slhc and slch.

It is a type II ordering. The DM candidate mass scan was performed over the range

$$m_{\text{light}} \in [130\,\text{GeV}, 500\,\text{GeV}] \ . \tag{4.20}$$

The other masses are set to

$$\begin{aligned} m_{\text{heavy}} &= 800.0\,\text{GeV} \\ m_{\text{charged}} &= 501.0\,\text{GeV} \\ m_{h_{\text{SM}}} &= 125.09\,\text{GeV} \end{aligned} \tag{4.21}$$

to comply with the mass ordering.

Figure 4.7 shows the comparison of the parameter sets (a) and (b) for the DM CP4 3HDM and the comparison to the DIDM. All models show good agreement among all tested parameter sets. The deviations of $\leq 0.9\,\%$ and $\leq 1.0\,\%$ of the DM CP4 3HDM (a) towards the DM CP4 3HDM (b) and the DIDM respectively are again random such that they can be attributed to numerical fluctuations.

Compared to the mass ordering slhc, the masses of the heavy and charged scalars were flipped. The direct comparison between slhc and slch in Figure 4.8 shows that the relic density values of slch are enhanced compared to those of slhc. The relic density is larger when the next-to-lightest (non-SM-like) scalar is charged and not neutral. The values can be more than twice as large for small mass splittings.

Type III: lshc

The mass region labeled by lshc corresponds to a mass ordering with

$$m_{\text{light}} < m_{h_{\text{SM}}} < m_{\text{heavy}} < m_{\text{charged}} \ . \tag{4.22}$$

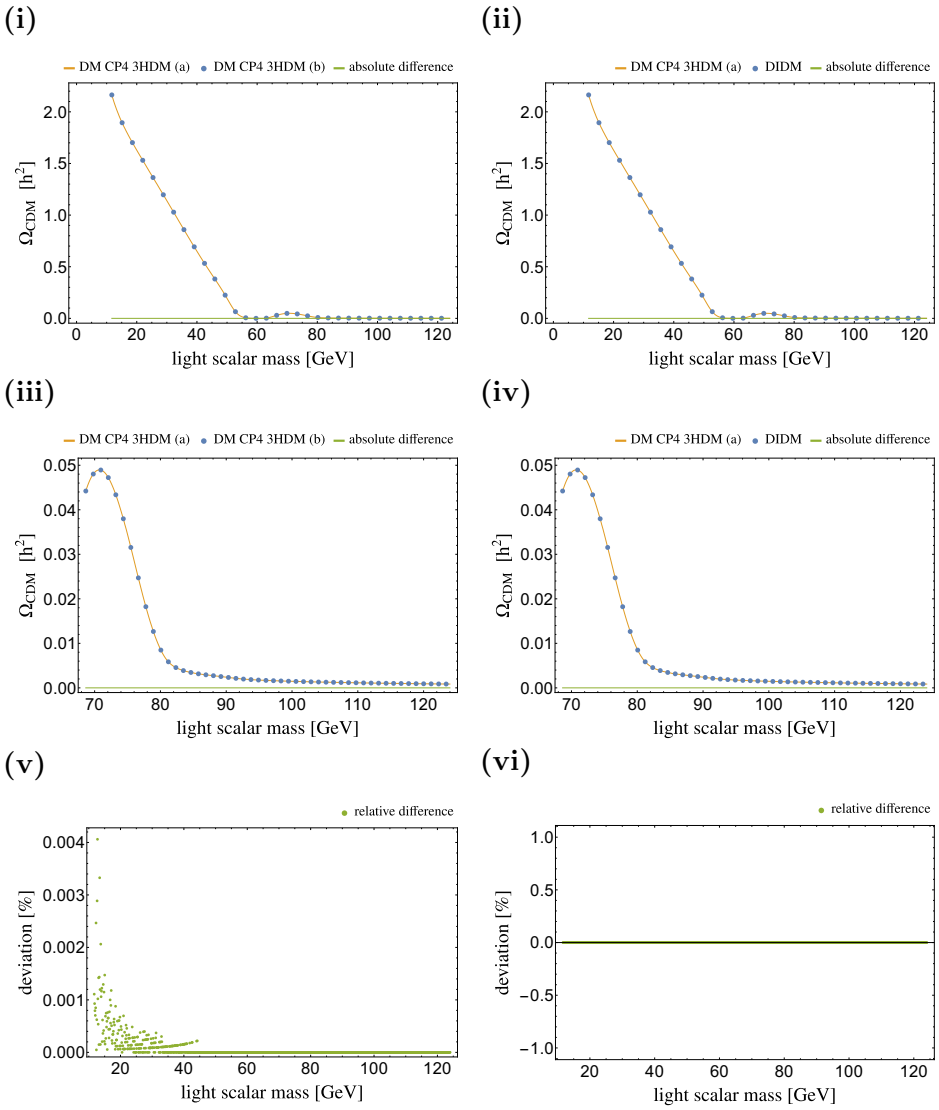

Figure 4.9: Comparison of the DM CP4 3HDM (a), DM CP4 3HDM (b) and the DIDM for the mass ordering lshc. (i)-(ii): full scan range. (iii)-(iv): zoomed scan range. (v): relative difference of DM CP4 3HDM (a) and DM CP4 3HDM (b). (vi): relative difference of DM CP4 3HDM (a) and DIDM.

It is a type III ordering. The DM candidate mass scan was done over the range

$$m_{\text{light}} \in [10\,\text{GeV}, 124\,\text{GeV}] \ . \tag{4.23}$$

The other masses are set to

$$\begin{aligned} m_{\text{heavy}} &= 501.0\,\text{GeV} \\ m_{\text{charged}} &= 800.0\,\text{GeV} \\ m_{h_{\text{SM}}} &= 125.09\,\text{GeV} \end{aligned} \tag{4.24}$$

to comply with the mass ordering.

Figure 4.9 shows the comparison of the parameter sets (a) and (b) for the DM CP4 3HDM and the comparison to the DIDM. The DM CP4 3HDM and the DIDM show complete agreement. The deviations of $\leq 0.005\,\%$ between the DM CP4 3HDM (a) and (b) are randomly distributed. Similar to the preceding discussions, they can be attributed to numerical fluctuations. Hence, all models and parameter sets are equivalent in this mass region, too.

Type III: lsch

The mass region labeled by lsch corresponds to a mass ordering with

$$m_{\text{light}} < m_{h_{\text{SM}}} < m_{\text{charged}} < m_{\text{heavy}} \ . \tag{4.25}$$

It is a type III ordering. The DM candidate mass was scanned over the range

$$m_{\text{light}} \in [10\,\text{GeV}, 124\,\text{GeV}] \ . \tag{4.26}$$

The other masses are set to

$$\begin{aligned} m_{\text{heavy}} &= 800.0\,\text{GeV} \\ m_{\text{charged}} &= 501.0\,\text{GeV} \\ m_{h_{\text{SM}}} &= 125.09\,\text{GeV} \end{aligned} \tag{4.27}$$

to comply with the mass ordering.

Figure 4.10 shows the comparison of the parameter sets (a) and (b) for the DM CP4 3HDM and the comparison to the DIDM. Again, the relic density values of the DM CP4 3HDM and the DIDM fully agree. Between the DM CP4 3HDM (a) and (b) there are deviations $\leq 0.005\,\%$. These are, however, not systematic and therefore just numerical fluctuations.

Compared to the mass ordering lshc, the masses of the heavy and charged scalars were flipped. The direct comparison between lshc and lsch in Figure 4.11 shows that the relic density values of lsch are enhanced compared to

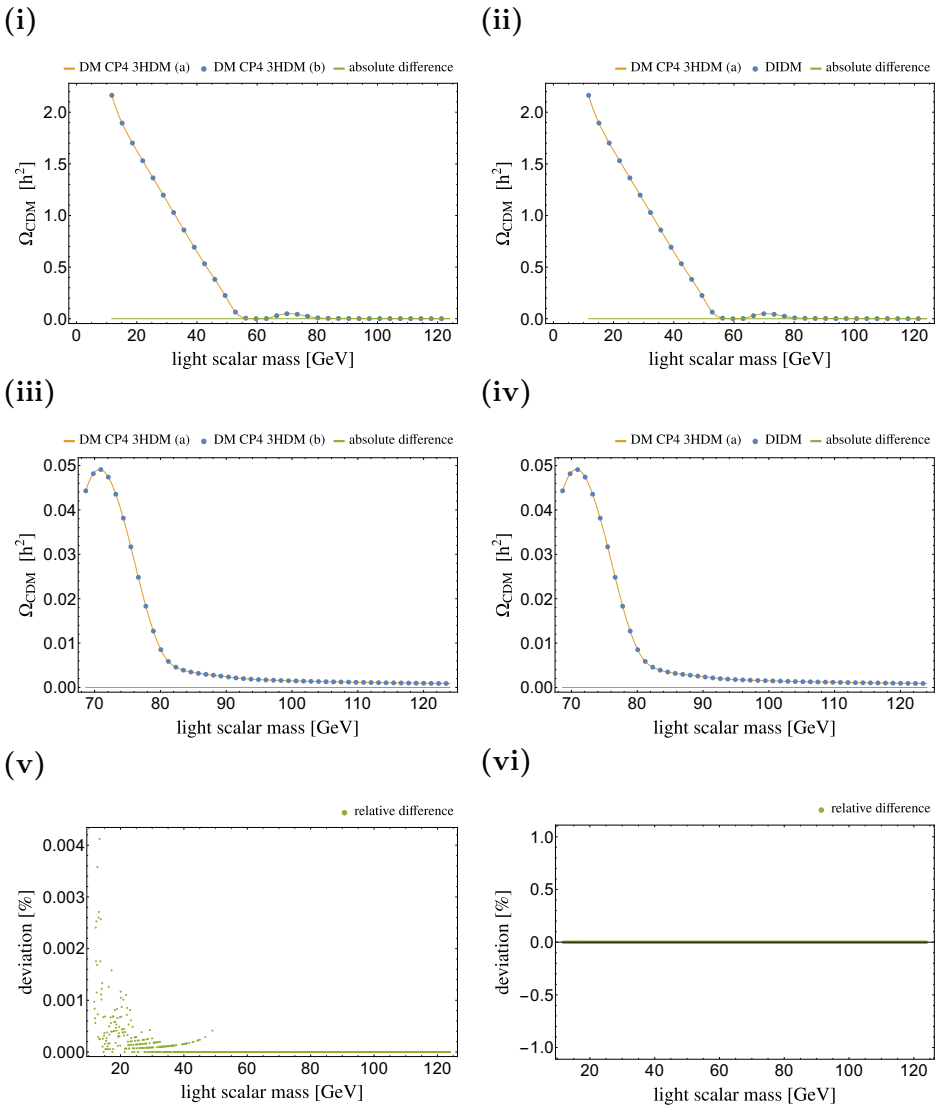

Figure 4.10: Comparison of the DM CP4 3HDM (a), DM CP4 3HDM (b) and the DIDM for the mass ordering lsch. (i)-(ii): full scan range. (iii)-(iv): zoomed scan range. (v): relative difference of DM CP4 3HDM (a) and DM CP4 3HDM (b). (vi): relative difference of DM CP4 3HDM (a) and DIDM.

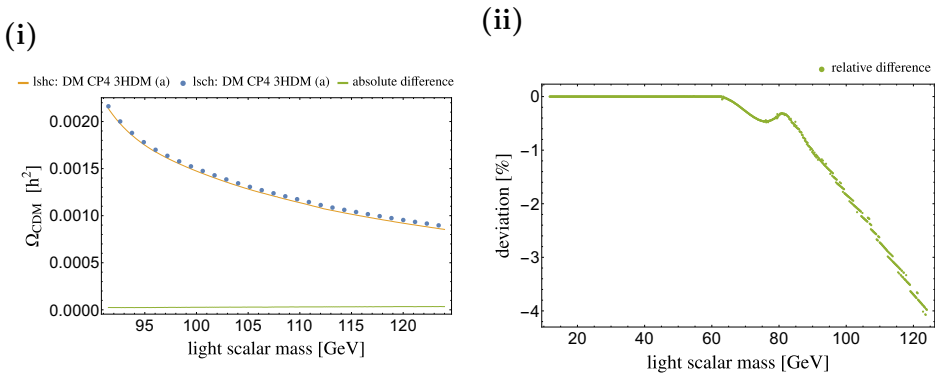

Figure 4.11: Comparison of the mass orderings lshc and lsch for the DM CP4 3HDM (a). (i) zoomed scan range. (ii) relative difference of lshc and lsch.

those of lshc. This agrees with the behavior in the comparison of slhc and slch in Figure 4.8. Here, the relic density is larger when the next-to-lightest (non-SM-like) scalar is charged and not neutral. The maximum enhancement is about 4 %. This is much less than the previous finding in the comparison of lhcs and lchs where the mass splitting between m_{light}, m_{heavy} and m_{charged} was smaller.

Type IV: lhsc

The mass region labeled by lhsc corresponds to a mass ordering with

$$m_{\text{light}} < m_{\text{heavy}} < m_{h_{\text{SM}}} < m_{\text{charged}} \ . \tag{4.28}$$

It is a type IV ordering. The DM candidate mass scan was done over the range

$$m_{\text{light}} \in [10\,\text{GeV}, 80\,\text{GeV}] \ . \tag{4.29}$$

The other masses are set to

$$\begin{aligned} m_{\text{heavy}} &= 81.0\,\text{GeV} \\ m_{\text{charged}} &= 501.0\,\text{GeV} \\ m_{h_{\text{SM}}} &= 125.09\,\text{GeV} \end{aligned} \tag{4.30}$$

to comply with the mass ordering.

Figure 4.12 shows the comparison of the parameter sets (a) and (b) for the DM CP4 3HDM and the comparison to the DIDM. The DM CP4 3HDM and the DIDM agree completely. There are deviations $\leq 0.005\,\%$ between the DM CP4 3HDM (a) and (b), which are randomly distributed. They can be attributed to numerical fluctuations. In this mass region, the models are equivalent with respect to the tested parameter sets.

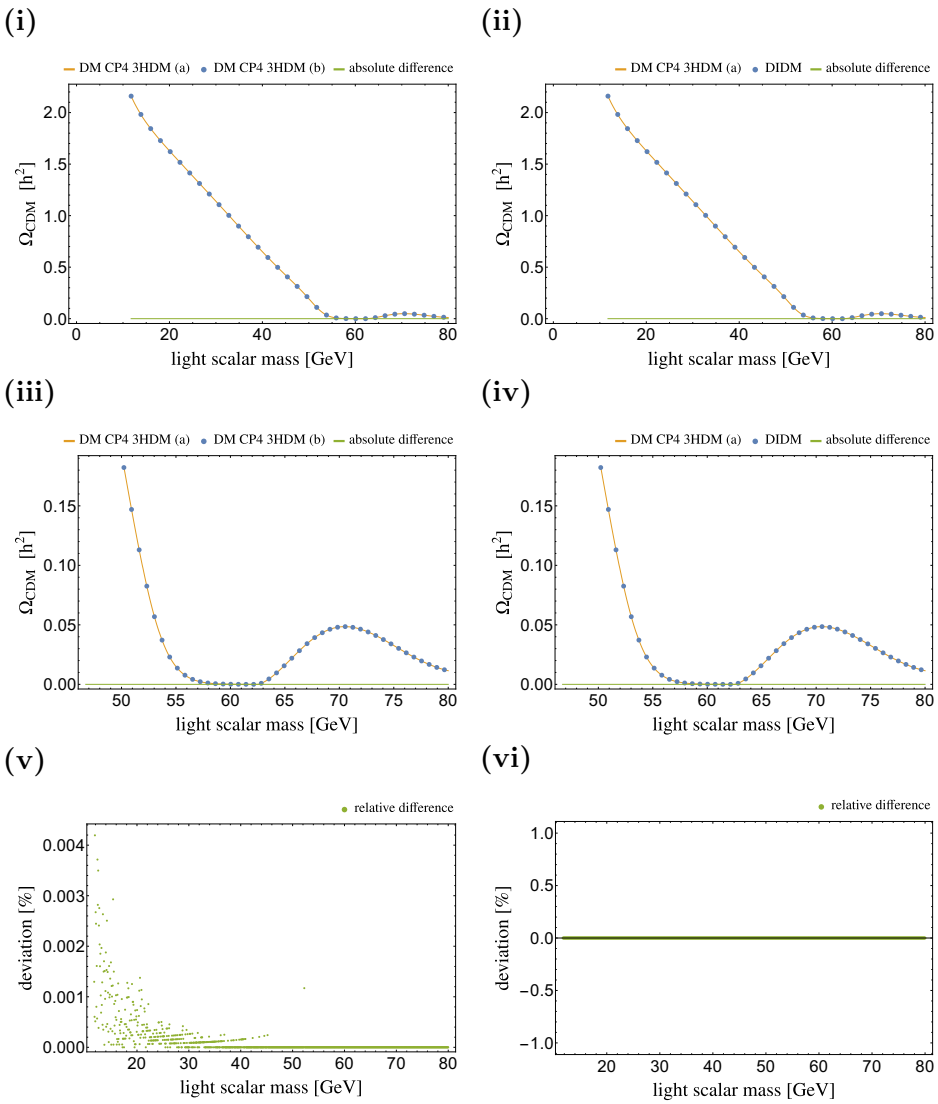

Figure 4.12: Comparison of the DM CP4 3HDM (a), DM CP4 3HDM (b) and the DIDM for the mass ordering lhsc. (i)-(ii): full scan range. (iii)-(iv): zoomed scan range. (v): relative difference of DM CP4 3HDM (a) and DM CP4 3HDM (b). (vi): relative difference of DM CP4 3HDM (a) and DIDM.

Type IV: lcsh

The mass region labeled by lcsh corresponds to a mass ordering with

$$m_{\text{light}} < m_{\text{charged}} < m_{h_{\text{SM}}} < m_{\text{heavy}} \ . \tag{4.31}$$

It is a type IV ordering. The DM candidate mass scan was performed over the range

$$m_{\text{light}} \in [10\,\text{GeV}, 80\,\text{GeV}] \ . \tag{4.32}$$

The other masses are set to

$$\begin{aligned} m_{\text{heavy}} &= 501.0\,\text{GeV} \\ m_{\text{charged}} &= 81.0\,\text{GeV} \\ m_{h_{\text{SM}}} &= 125.09\,\text{GeV} \end{aligned} \tag{4.33}$$

to comply with the mass ordering.

Figure 4.13 shows the comparison of the parameter sets (a) and (b) for the DM CP4 3HDM and the comparison to the DIDM. Again, the relic density values of the DM CP4 3HDM and the DIDM fully agree. Between the DM CP4 3HDM (a) and (b) there are deviations $\leq 0.005\,\%$. They are randomly distributed. Therefore, these deviations are just numerical fluctuations.

Compared to the mass ordering lhsc, the masses of the heavy and charged scalars were flipped. The direct comparison between lhsc and lcsh in Figure 4.14 shows that the relic density values of lcsh oscillate between enhancement and suppression compared to those of lshc. This agrees with the behavior in the comparison of lhcs and lchs in Figure 4.5. The maximum enhancement or suppression is about $8\,\%$. This is smaller than the previous finding because the mass splitting between charged and neutral scalars is larger. However, the enhancements and suppressions are more symmetric this time.

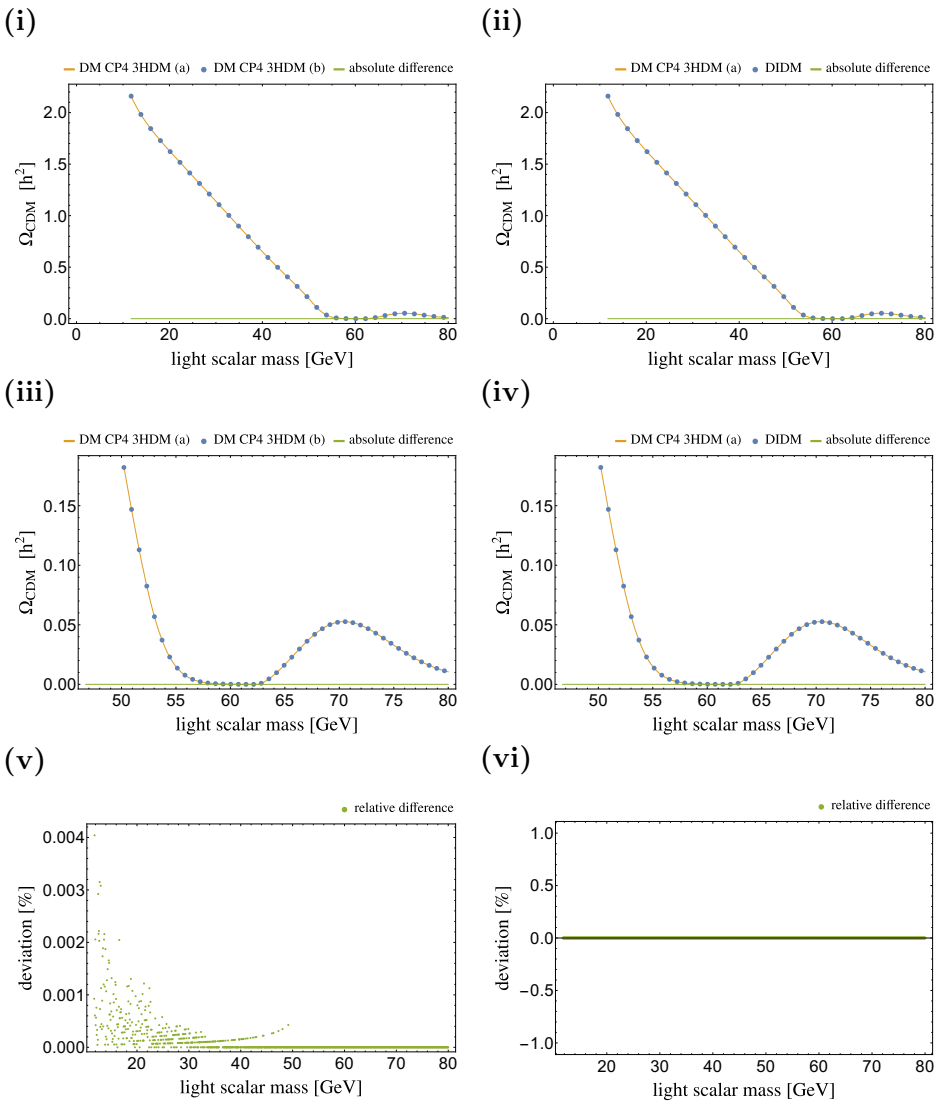

Figure 4.13: Comparison of the DM CP4 3HDM (a), DM CP4 3HDM (b) and the DIDM for the mass ordering lcsh. (i)-(ii): full scan range. (iii)-(iv): zoomed scan range. (v): relative difference of DM CP4 3HDM (a) and DM CP4 3HDM (b). (vi): relative difference of DM CP4 3HDM (a) and DIDM.

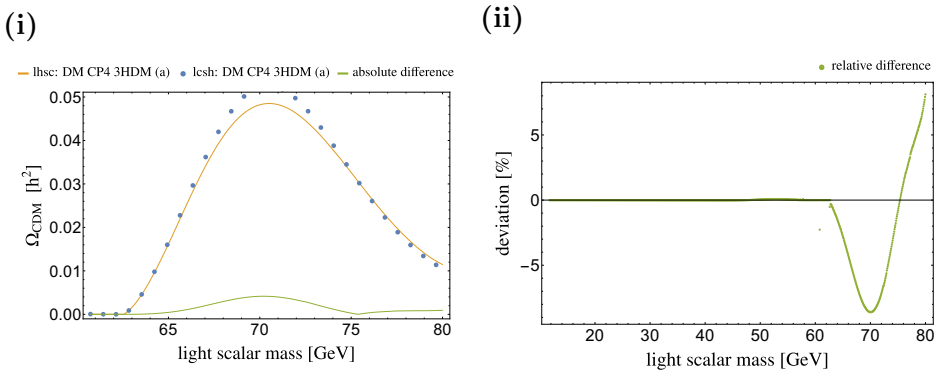

Figure 4.14: Comparison of the mass orderings lhsc and lcsh for the DM CP4 3HDM (a). (i) zoomed scan range. (ii) relative difference of lhsc and lcsh.

4.2.4 Conclusion

In the previous sections a systematic analysis of the dependence of the DM relic density on the quartic coupling parameters λ_2, λ_3', λ_4', λ_8 and λ_9 was given. Both models, the DM CP4 3HDM and the DIDM, were tested on two different parameter sets (a) and (b). The quartic couplings either vanished or had values with very large magnitude. Furthermore, the tests were conducted on all possible mass orderings within the scalar sector. Hence, the results are representative for all kinematically allowed decay and coannihilation channels that may influence the thermal evolution of the DM candidates. No dependence on the quartic couplings was found. All deviations can be attributed to numerical fluctuations of the used tools. Concerning the relic density of the DM candidates, none of the parameters λ_2, λ_3', λ_4', λ_8 or λ_9 has any influence.

When all these parameters are set to zero, there is still a difference in the potential of the DM CP4 3HDM and the DIDM. They differ by a factor of -1 in the λ_6 coupling of the second doublet. However, it has also been found that there is no difference due to this factor with respect to the relic density of the DM candidates. As has been argued in Section 3.1 and thereafter, the sign of λ_6 is not important and corresponds to an arbitrary choice of the mass ordering. Here it has been shown, that the relative sign of λ_6-like couplings of different doublets also has no influence on the relic density.

In conclusion, the DM relic density is not sensitive to the GCP structure of the examined 3HDMs. In fact, all couplings that involve only particles of the inert doublets have been found to be irrelevant for the thermal evolution. However, it is this inert interaction that encodes the CP4 symmetry of the DM CP4 3HDM. Unfortunately, the difference of a CP2 and CP4 symmetry

cannot be seen in this observable.

Finally, some remarks on the general behavior of the DM relic density for $g_{\mathrm{DM}} > 0$. The direct comparisons of the two different mass orderings within type II and type III show that higher relic density values are achieved over the whole scan range for mass orderings ch, i.e. orderings with $m_{\mathrm{charged}} < m_{\mathrm{heavy}}$. In type I and type IV the relic density can be either enhanced or suppressed. However, when the mass splitting between m_{light} and m_{heavy} gets smaller, then clearly hc orderings, i.e. $m_{\mathrm{heavy}} < m_{\mathrm{charged}}$, are preferred with respect to high relic density values.

In total, when the mass splitting between the light scalar and the next-to-lightest (non-SM-like) scalar approaches zero it holds that

- ch orderings are preferred when $m_{h_{\mathrm{SM}}}$ is smaller than both m_{heavy} and m_{charged} (type II and type III).
- hc orderings are preferred when $m_{h_{\mathrm{SM}}}$ is larger than either m_{heavy} or m_{charged} (type I and type IV).

Furthermore, to achieve maximum enhancement the mass splittings of all particles from the inert doublets should be small and the DM candidate mass should be far above the SM Higgs boson mass.

This discussion holds for $g_{\mathrm{DM}} > 0$. It was not tested for negative values and is likely to change in that range, because the mass ordering also induces an ordering on the couplings of the light, heavy and charged scalars to the SM Higgs boson. These are proportional to $\bar{\lambda}_{346}$, λ_{346} and λ_3 respectively (see Appendices A.1 and A.2).

For instance, an lhc ordering in relation to Eq. (3.18) or (3.33) also demands the ordering of couplings

$$\bar{\lambda}_{346} < \lambda_{346} < \lambda_3 \ . \tag{4.34}$$

For $g_{\mathrm{DM}} = \bar{\lambda}_{346} > 0$ this is equivalent to

$$|\bar{\lambda}_{346}| < |\lambda_{346}| < |\lambda_3| \ , \tag{4.35}$$

i.e. the magnitudes of couplings are ordered in the same way. Hence, for positive values there will be no qualitative change based on the actual magnitude of g_{DM}.

For $g_{\mathrm{DM}} < 0$ there are 3 possibilities

$$\begin{aligned} &\bar{\lambda}_{346} < \lambda_{346} < \lambda_3 < 0 \\ &\bar{\lambda}_{346} < \lambda_{346} < 0 < \lambda_3 \\ &\bar{\lambda}_{346} < 0 < \lambda_{346} < \lambda_3 \end{aligned} \tag{4.36}$$

In the first case, the magnitude ordering is flipped compared to Eq. (4.35) and the mass ordering. The second and third case do not allow a simple assignment of the magnitude ordering based on the mass ordering. Also, the relative signs of the couplings are different. This classification is out of scope for this thesis and was not performed.

The minimum mass splitting between the lightest and next-to-lightest (non-SM-like) scalar in this analysis is 1 GeV. For even smaller splittings, the next-to-lightest (non-SM-like) scalars can be sufficiently long lived to influence the thermal evolution of the DM candidates. MicrOmegas currently assumes that all other particles are in thermal equilibrium during the freeze-out of the DM relic density and is therefore unable to handle this case. The quartic couplings λ_3', λ_4', λ_8, λ_9 and therefore the GCP structure are likely to play an important role in this regime. It is a current topic of research which is also beyond the scope of this thesis.

4.3 Perturbative Unitarity

As we have seen in the last section, the DM relic density is not sensitive to the parameters λ_3', λ_4', λ_8 and λ_9 of the DM CP4 3HDM. The remaining quartic parameters λ_1, λ_2, λ_3, λ_4 and λ_6 are also present in the DIDM, which shows no difference to the DM CP4 3HDM with respect to the relic density.

The goal of this section is to demonstrate that all quartic coupling parameters of the DM CP4 3HDM are subject to perturbative unitarity constraints. Furthermore, it will be shown that the two sets

- set A: λ_1, λ_2, λ_3, λ_4 and λ_6
- set B: λ_3', λ_4', λ_8 and λ_9

are not independent of each other.

If they were independent, this would imply that the GCP structure is again phenomenologically irrelevant. One can think of it like this: The masses depend on the parameter set A. Hence, it is assured that this set has phenomenological significance. Without reference to other constraints or observables, if set B would completely decouple from set A then the GCP structure encoded in set B will have no effect on the phenomenological implications of set A. The parameters of set B occur only in quartic interactions of particles of the inert doublets (see Appendix A.1). These interactions and particles are extremely difficult to probe. Very high energies and luminosities or an abundance of inert particles would be needed. Such conditions are usually only met in astrophysical observations. However, one of them, the DM relic density, has already been shown to be independent of parameter set B. Hence, if the unitarity constraints of set B ought to have any currently testable implications, they must influence the constraints of set A.

All calculations have been done with the Mathematica package PUC [5] (see also Appendix B.1). For the DIDM the unitarity constraints can be given explicitly. The eigenvalues

$$\begin{aligned} e_1 &= 0 \\ e_{2/3} &= 3(\lambda_1+\lambda_2) \pm \sqrt{9(\lambda_1-\lambda_2)^2 + 2(2\lambda_3+\lambda_4)^2} \\ e_{4/5} &= (\lambda_1+\lambda_2) \pm \sqrt{(\lambda_1-\lambda_2)^2 + 2\lambda_4^2} \\ e_{6/7} &= (\lambda_1+\lambda_2) \pm \sqrt{(\lambda_1-\lambda_2)^2 + 2\lambda_6^2} \end{aligned} \tag{4.37}$$

$$\begin{aligned} e_{8/9} &= \lambda_3 + 2\lambda_4 \pm 3\lambda_6 \\ e_{10/11} &= \lambda_3 \pm \lambda_4 \\ e_{12/13} &= \lambda_3 \pm \lambda_6 \\ e_{14} &= 2\lambda_2 \\ e_{15} &= 6\lambda_2 \end{aligned} \tag{4.38}$$

of the 2-to-2 scattering matrix of Higgs sector scalars (including Goldstone bosons) must fulfill

$$|e_i| \leq 8\pi \ , \qquad i \in \{1, 2, \ldots, 15\} \ . \tag{4.39}$$

The constraints agree with the ones for the DM CP4 3HDM if parameter set B is set to zero. With non-zero parameters, however, some of the unitarity constraints of the DM CP4 3HDM cannot be given in terms of analytical inequalities [23]. Therefore, a numerical test has to be applied.

4.3.1 Numerical Test

Constraints of the form of Eq. (4.39) will effectively yield bounded intervals

$$\mathrm{lb}_j \leq \lambda_j \leq \mathrm{ub}_j \tag{4.40}$$

for the quartic coupling parameters λ_j. If the parameter is complex, then there will be a bounded interval for the real and imaginary part separately. Here, ub_j and lb_j are the upper and lower bound of that interval. In general, ub_j and lb_j will be functions of the other parameters. Each constrained eigenvalue gives rise to such bounds. Only the largest lower bound and the smallest upper bound will affect the actual unitarity constraint.

To demonstrate this, set all parameters but λ_1 and λ_6 in Eqs. (4.37) and (4.38) to zero. The constraints are then

$$\left| \ 6\lambda_1 \ \right| \leq 8\pi \tag{4.41}$$

$$\left| \ 2\lambda_1 \ \right| \leq 8\pi \tag{4.42}$$

$$\left| \ \lambda_1 + \sqrt{\lambda_1^2 + 2\lambda_6^2} \ \right| \leq 8\pi \tag{4.43}$$

$$\left| \ \lambda_1 - \sqrt{\lambda_1^2 + 2\lambda_6^2} \ \right| \leq 8\pi \tag{4.44}$$

$$\left| \ 3\lambda_6 \ \right| \leq 8\pi \tag{4.45}$$

$$\left| \ \lambda_6 \ \right| \leq 8\pi \ . \tag{4.46}$$

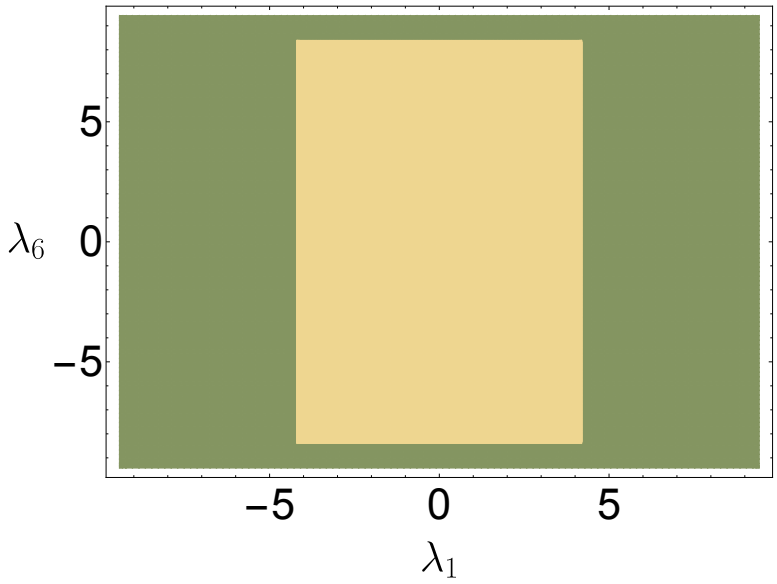

Figure 4.15: Exclusion plot for unitarity constraints in the (λ_1, λ_6) plane with all other parameters set to zero. The green region is excluded by a numerical scan with PUC, the yellow region is allowed.

The bounds of Eq. (4.42) are less restrictive than the ones of Eq. (4.41) and similar for Eq. (4.46) and (4.45). By applying the triangle inequality one can deduce that

$$\begin{aligned} &\left| \lambda_1 \pm \sqrt{\lambda_1^2 + 2\lambda_6^2} \right| \leq \left| \lambda_1 \right| + \left| \sqrt{\lambda_1^2 + 2\lambda_6^2} \right| \\ &\leq \left(\frac{8}{6} + \sqrt{\left(\frac{8}{6}\right)^2 + 2\left(\frac{8}{3}\right)^2} \right) \pi = \frac{16}{3}\pi \leq 8\pi \end{aligned} \tag{4.47}$$

such that the bounds of (4.43) and (4.44) are also less restrictive. Hence, the actual unitarity constraints can be written as

$$\begin{aligned} -\frac{8}{6}\pi \leq \lambda_1 \leq \frac{8}{6}\pi \\ -\frac{8}{3}\pi \leq \lambda_6 \leq \frac{8}{3}\pi \ . \end{aligned} \tag{4.48}$$

There is another important thing to observe here: the upper and lower bounds are constant. Figure 4.15 shows how this would look like in a planar exclusion plot. As one can see, the allowed region is rectangular with sides parallel to the axes. The parameters λ_1 and λ_6 are independent of each other. Inversely, if the allowed region has a different shape, then the bounds of the

parameters will not be constant. The bounds will depend on the respective parameters, that have been varied in the plane.

As has been just demonstrated, for the check on the pairwise dependence of unitarity constraints of two parameters it is not sufficient to derive all constraining inequalities. Equations (4.43) and (4.44) seemed to indicate a dependence of λ_1 and λ_6 even though there was none.

However, the finding of independence could be a specific property of the parameter point that was fixed with the remaining parameters. A different parameter point might make an upper or lower bound with an actual dependence more restrictive than a constant one, resulting in a non-rectangular shape in the respective planar exclusion plot. Hence, with this method one can only check for the pairwise dependence of two parameters. This is what will be done in the next sections.

Dependence Test for λ_1

To generate the planar exclusion plots one has to fix all remaining parameters. The following default values have been used in the plots unless stated otherwise.

- default values d0:

$$\begin{aligned} &\lambda_1 = \lambda_2 = \lambda_3 = \lambda_3' = \lambda_4 = \lambda_4' = \lambda_6 = 0 \\ &\mathrm{Re}(\lambda_8) = \mathrm{Im}(\lambda_8) = \mathrm{Re}(\lambda_9) = \mathrm{Im}(\lambda_9) = 0 \end{aligned} \tag{4.49}$$

- default values d1:

$$\begin{aligned} &\lambda_1 = \lambda_2 = \lambda_3 = \lambda_3' = \lambda_4 = \lambda_4' = \lambda_6 = 1 \\ &\mathrm{Re}(\lambda_8) = \mathrm{Im}(\lambda_8) = \mathrm{Re}(\lambda_9) = \mathrm{Im}(\lambda_9) = 1 \end{aligned} \tag{4.50}$$

Needless to say, the parameters of the plot axes have not been fixed to these values.

Figure 4.16 shows the exclusion plots of all combinations of λ_1 with the parameters of set B. The (λ_1, λ_3') and (λ_1, λ_4') plane clearly show a non-rectangular shape of the allowed region and therefore a pairwise dependence of the unitarity constraints of these parameters.

Neither the bounds of $\mathrm{Re}(\lambda_8)$ and $\mathrm{Im}(\lambda_8)$ nor the bounds of $\mathrm{Re}(\lambda_9)$ and $\mathrm{Im}(\lambda_9)$ show any dependence on λ_1. This could be an artifact of the parameter point that has been fixed with the default values d0 or d1. However, the dependence on λ_8 and λ_9 was tested on several different parameter points as well. No dependence was found. As has been said before, the dependence cannot be disproved by this method. It is very unlikely that there is any, though.

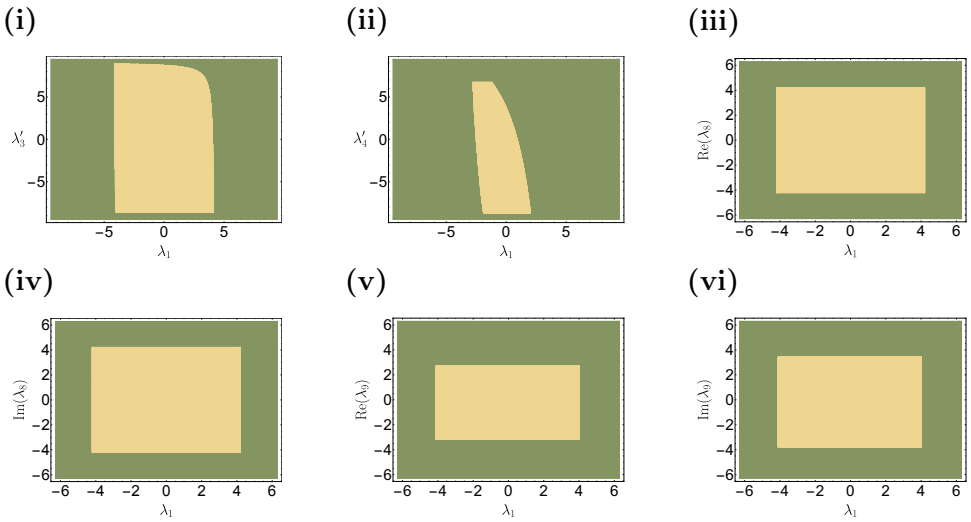

Figure 4.16: Exclusion plots for unitarity constraints of λ_1 and parameter set B. The green region is excluded, the yellow region is allowed. The default values are (i) d1, (ii) d1 with $\lambda_3 = 6$, (iii) d0, (iv) d0, (v) d1, (vi) d1.

Dependence Test for λ_2

Figure 4.17 shows the exclusion plots of all combinations of λ_2 with the parameters of set B. All parameter planes show a dependence of λ_2 on each of the parameters of set B and vice versa.

Dependence Test for λ_3

Figure 4.18 shows the exclusion plots of all combinations of λ_3 with the parameters of set B. The planes (λ_3, λ_3') and (λ_3, λ_4') show a pairwise dependence of the respective parameters.

However, the exclusion plots indicate that λ_3 does not depend on λ_8 and λ_9. This coincides with the expressions in [23, Eqs. (4.24) - (4.32)], where none of the possible eigenvalues of the 2-to-2 scattering matrix simultaneously involve the parameters of any of the pairs (λ_3, λ_8) or (λ_3, λ_9). Hence, no bounding inequality will simultaneously involve the parameters of these pairs such that the effective upper and lower bounds will be constant with respect to λ_3, λ_8 and λ_9. The independence found here is exact.

Dependence Test for λ_4

Figure 4.19 shows the exclusion plots of all combinations of λ_4 with the parameters of set B. The pictures that emerges here is very much similar to

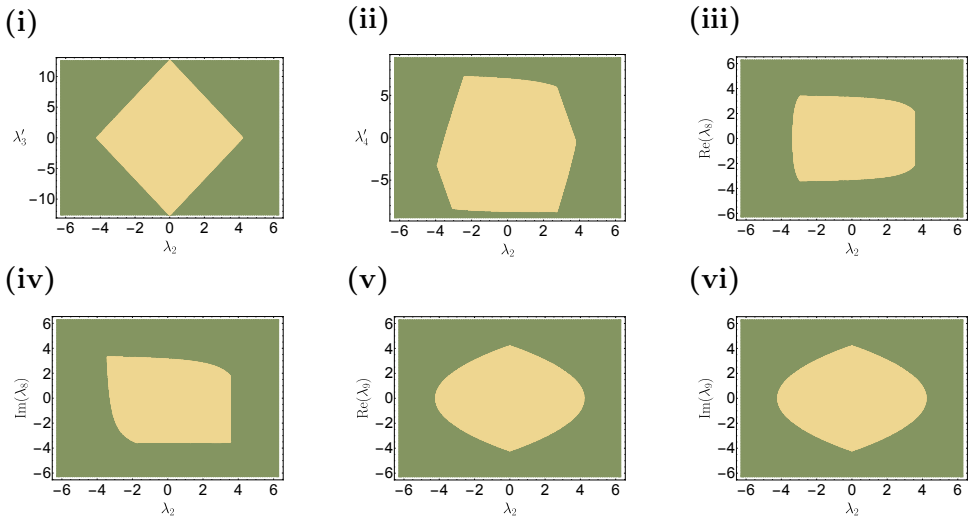

Figure 4.17: Exclusion plots for unitarity constraints of λ_2 and parameter set B. The green region is excluded, the yellow region is allowed. The default values are (i) d0, (ii) d1, (iii) d1, (iv) d1, (v) d0, (vi) d0.

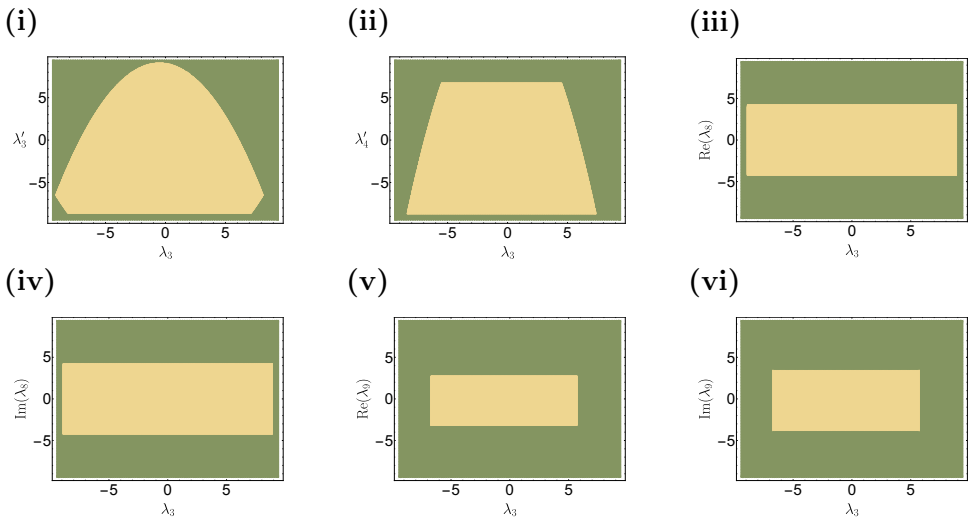

Figure 4.18: Exclusion plots for unitarity constraints of λ_3 and parameter set B. The green region is excluded, the yellow region is allowed. The default values are (i) d1, (ii) d1, (iii) d0, (iv) d0, (v) d1, (vi) d1.

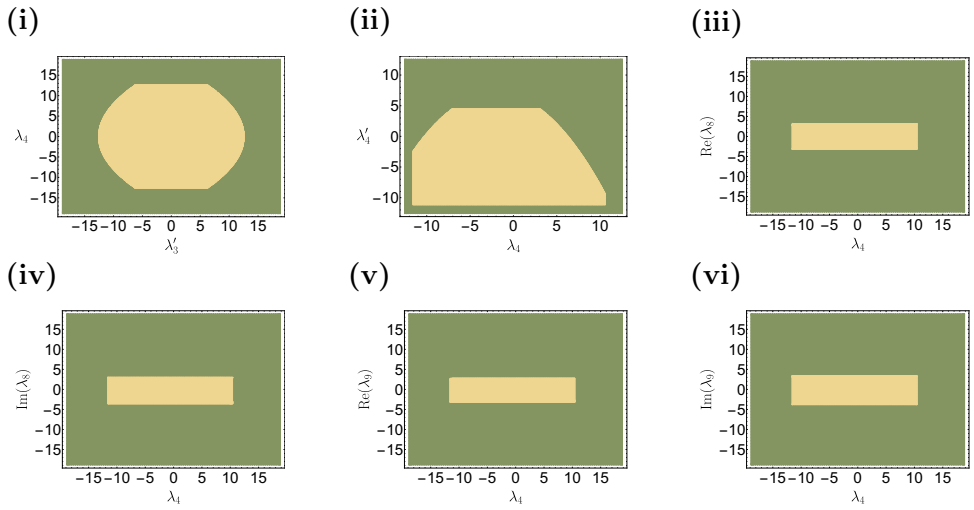

Figure 4.19: Exclusion plots for unitarity constraints of λ_4 and parameter set B. The green region is excluded, the yellow region is allowed. The default values are (i) d0, (ii) d1 with $\lambda_3' = 6$, (iii) d1, (iv) d1, (v) d1, (vi) d1.

the one for λ_3. The parameters λ_3' and λ_4' show a dependence while λ_8 and λ_9 do not influence the constraints of λ_4. In fact, this independence is again exact as suggested by the expressions in [23, Eqs. (4.24) - (4.32)]. None of the possible eigenvalues of the 2-to-2 scattering matrix simultaneously involve the parameters of the pairs (λ_4, λ_8) or (λ_4, λ_9). All possible points of parameter space different from the default values d0 and d1 will show the constancy of upper and lower bounds as well.

Dependence Test for λ_6

Figure 4.20 shows the exclusion plots of all combinations of λ_6 with the parameters of set B. Similar to the discussion of Eqs. (4.41) to (4.48) one can show explicitly that λ_6 does not depend on any of the parameters of set B if the remaining ones are set to zero. Furthermore, λ_6 shows no dependence in the exclusion plots when the default values d1 are used. The tests were conducted on several different parameter points. They did not show any dependence as well. Therefore, it is very likely that λ_6 does not depend on any of the parameters of set B.

4.3.2 Comparison of Unitarity Constraints

Now that we know the dependencies of the parameters of set A from the ones of set B, we can have a look at how they will influence the unitarity

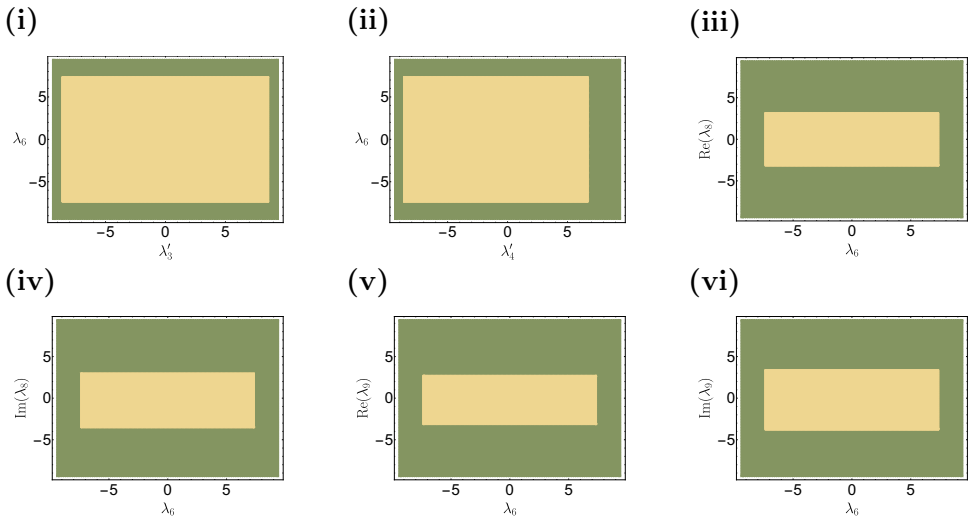

Figure 4.20: Exclusion plots for unitarity constraints of λ_6 and parameter set B. The green region is excluded, the yellow region is allowed. The default values are (i) d1, (ii) d1, (iii) d1, (iv) d1, (v) d1, (vi) d1.

constraints compared to the DIDM. This will be done based on a selection of planar exclusion plots, where one axis is λ_6, a parameter that is not influenced by parameter set B. Therefore, any deviation between the DM CP4 3HDM and the DIDM can be examined with respect to one parameter only.

Figure 4.21 shows a collection of exclusion plots. The green regions are excluded in the DM CP4 3HDM, while the yellow regions are allowed. The black points are valid points with respect to the unitarity constraints of the DIDM.

As one can see in Figures 4.21 (i) and (ii), some of the parameter space region can be freed up, while some of it is even more constrained due to the presence of parameter set B. However, these two effects do not have to occur at the same time. Figures 4.21 (iii) and (iv) show exclusion plots where the parameter space of the DM CP4 3HDM is more constrained than the one of the DIDM. On the contrary, Figures 4.21 (v) and (vi) show the exact opposite behavior, the only causal difference being the sign of λ_3'.

4.3.3 Conclusion

In the previous sections a systematic analysis of the unitarity constraints of the DM CP4 3HDM was given. There are 11 free parameters influencing the quartic couplings of this model. To get a hold on them, they were separated into two sets. Set A consists of the parameters λ_1, λ_2, λ_3, λ_4 and λ_6, all of

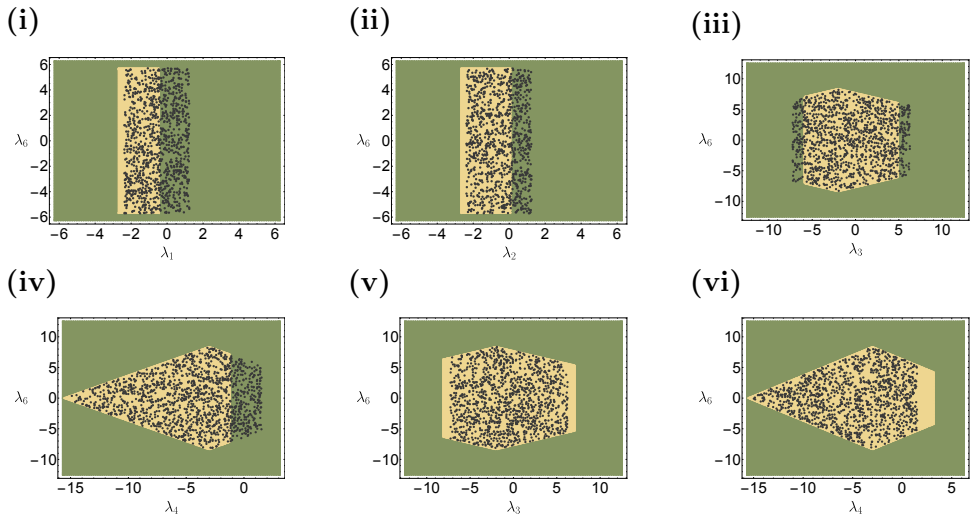

Figure 4.21: Comparison of unitarity constraints of parameter set A for the DM CP4 3HDM and the DIDM. The green region is excluded, the yellow region is allowed in the DM CP4 3HDM. The black points are allowed in the DIDM according to a scan with PUC. The default values are (i) d1 with $\lambda_3 = 6$ and $\lambda_3' = 3$, (ii) d1 with $\lambda_3 = 6$ and $\lambda_3' = 3$, (iii) d1 with $\lambda_3' = 3$, (iv) d1 with $\lambda_3 = 6$ and $\lambda_3' = 3$, (v) d1 with $\lambda_3' = -3$, (vi) d1 with $\lambda_3 = 6$ and $\lambda_3' = -3$.

which are present in the DIDM, too. Set B is constituted by λ_3', λ_4', λ_8 and λ_9. They are responsible for the presence of the GCP symmetry in the DM CP4 3HDM.

As as been argued in the beginning of Section 4.3, parameter set B does not contribute to the masses nor to the trilinear couplings of the DM CP4 3HDM. Therefore, it is difficult to probe these parameters in experiments. Moreover, in Section 4.2 it has been shown that parameter set B does not influence the DM relic density, at least for mass splittings larger than 1 GeV. Hence, if the unitarity constraints of parameter set B ought to have any phenomenological significance they have to be related to the constraints of set A.

The parameter λ_6 showed no dependence on set B. However, it was the only parameter that had this property. All other parameters of set A were at least dependent on λ_3' and λ_4'. Only λ_2 is able to influence λ_8 and λ_9 and vice versa. Thus, the unitarity constraints of parameter set B constitute a real phenomenological difference between the DM CP4 3HDM and the DIDM. That being said, the phenomenological significance of λ_8 and λ_9 can still be regarded as questionable at the current stage of analysis, because λ_2 is itself

a parameter that does not occur in the expressions for the masses and the trilinear couplings (see for example Appendices A.1 and A.2).

As the direct comparison of the unitarity constraints of the DM CP4 3HDM and the DIDM in Section 4.3.2 has shown, with the help of set B certain parameter space regions of set A can be either opened up or even more restricted. This allows for two different interpretations. Firstly, the addition of more quartic coupling parameters to an inert Higgs model can be regarded as a convenient model building tool, if the parameters do not occur in expressions for masses and trilinear couplings. Previously excluded parameter points can be valid again, without altering direct experimental predictions. Secondly, if the constraints can be weakened or strengthened by incorporating parameters, whose values are not to be measured with current collider technologies and other experiments in the near future, then these constraints are perhaps not as strict as usually considered.

This latter point of view has a limitation, though. The allowed parameter space regions can never be arbitrarily enlarged. After all, the upper limit of approximately 8π will always be a valid bound for the values of the quartic parameters. Only their internal dependencies with respect to the unitarity constraints can be altered by additional parameters. Hence, one should be cautious with heavily overconstrained or underconstrained parameter regions, as these regions could easily change in a phenomenologically equivalent model. To circumvent this, one could think about assessing the unitarity constraints of a given inert multi-Higgs model always with respect to the unitarity constraints of the most general multi-Higgs model of the same type, i.e. with all possible quartic interactions enabled.

In conclusion, it has been shown that out of the 6 free parameters λ_3', λ_4', $\mathrm{Re}(\lambda_8)$, $\mathrm{Im}(\lambda_8)$, $\mathrm{Re}(\lambda_9)$ and $\mathrm{Im}(\lambda_9)$, only the first two have been identified to have a phenomenological significance with respect to unitarity constraints. Also, the unitarity constraints can in principle be used to distinguish between the DM CP4 3HDM and the DIDM.

It is not clear how this picture is extended if one also considers the theoretical constraints of Higgs potential boundedness. For the DM CP4 3HDM and the DIDM there are currently only sufficient conditions for boundedness. Because they are not necessary, any implication beyond boundedness, e.g. on the dependence of quartic parameters, will neither be sufficient nor necessary for the model under consideration. Hence, the analysis on the phenomenological significance of these constraints is currently not feasible. The next chapter presents a new and general method to derive such necessary and sufficient conditions for any multi-Higgs model. However, the current implementation of the algorithms is not yet fully adequate for 3HDMs in terms of runtime.

Chapter 5

Boundedness of Higgs Potentials

5.1 Motivation

The potential of the SM Higgs boson with a mass of about 125 GeV is only stable at tree level. If one incorporates loop corrections, the RGE running eventually pushes the Higgs potential parameters into regions where it is not bounded from below. Hence, the vacuum state is not stable and the quantum field theory is ill defined. There are several ways to stabilize the theory. The most prominent one is probably to extend the scalar sector. This is the case for SUSY theories like the Minimal Supersymmetric Standard Model (MSSM) [24, 25, 26, 27, 28] or the Next-to-Minimal Supersymmetric Standard Model (NMSSM) [28, 29, 30, 31] but also for most non-supersymmetric GUT theories (see for example [32]). Multi-Higgs models have been studied independently as well, for example in [33].

While it is easy to check boundedness for the SM Higgs potential by constraining the quartic self-coupling parameter to positive values, it is a rather challenging task to find necessary and sufficient conditions for extended scalar sectors. First attempts date back to 1985 [34]. Sufficient constraints are more easy to find and where studied even earlier in [35]. In fact, the first conditions for the IDM were written down in 1978 in [22]. Over the years, there have been several approaches to this problem, identifying and confirming constraints with different methods. A rather elegant one was applied in [20], where a Minkowski space structure of the Higgs potential was used to derive necessary and sufficient constraints for the most general 2HDM. The most recent method is probably [21], which gives necessary and sufficient conditions for a whole class of Higgs potentials.

All these methods have one thing in common: They were designed and studied for a specific model or work with a very limited subset of Higgs

potentials only. In particular, there is currently no way to obtain necessary conditions for the 3HDMs described in Chapter 3. The following sections outline a general method to derive necessary and sufficient conditions of boundedness for any Higgs potential. One of the insights will be that for some Higgs potentials these constraints cannot be given in terms of analytical inequalities as it is the case in the 2HDM. There is, however, a different analytical structure that can serve as a tool for fast numerical checks of boundedness.

5.2 The Idea

Suppose there is a general Higgs potential V which is a function of SU(2) singlets, doublets, triplets, etc. These fields will be complex valued in general. However, by splitting up the singlets, doublets, triplets, etc. into their real and imaginary parts, one can rewrite the potential V in terms of real scalar fields only. The potential V is then an ordinary real valued function of real variables $\vec{x} \in \mathbb{R}^n$ for some $n \in \mathbb{N}$.

$$\begin{aligned} V : \mathbb{R}^n &\to \mathbb{R} \\ \vec{x} &\mapsto V(\vec{x}) \ . \end{aligned} \tag{5.1}$$

As a matter of fact, V is an algebraic function of the original field variables and therefore also of $\vec{x}$. The maximum total power, that is the sum of powers of products of the x_i, $i = 1, \ldots, n$, is 4 due to renormalizability. Hence one can expand V in a sum of tensor contractions

$$V = C + F_i \cdot x_i + S_{ij} \cdot x_i x_j + T_{ijk} \cdot x_i x_j x_k + Q_{ijkl} \cdot x_i x_j x_k x_l \ , \tag{5.2}$$

where for instance

$$Q_{ijkl} = \left[\frac{1}{4!} \frac{\partial^4 V}{\partial x_i \partial x_j \partial x_k \partial x_l} \right]_{\vec{x}=0} \tag{5.3}$$

is the 4th order coefficient tensor of a usual Taylor expansion in $\vec{x}$ around 0. The ray $\alpha \cdot \vec{x}$ for some $\vec{x} \neq 0$ has a distinctive behavior for the different tensor contractions. For instance, the absolute value

$$|\alpha|^4 \cdot |Q_{ijkl} \cdot x_i x_j x_k x_l| \tag{5.4}$$

grows with a power of 4 in α compared to

$$|\alpha|^3 \cdot |T_{ijk} \cdot x_i x_j x_k| \ , \tag{5.5}$$

which only grows with a power of 3. Unless, there is a direction $\vec{x} \neq 0$ for which $Q_{ijkl} \cdot x_i x_j x_k x_l = 0$, the large scale behavior of V will be dominated by Q because any of the lower order tensor contractions will be negligible for $|\vec{x}| \gg 1$.

So the question of whether or not a given Higgs potential V is bounded from below, that is if V remains larger than any of its minima for $|\vec{x}| \to \infty$, reduces to the question of whether or not the tensor Q is positive definite:

$$Q_{ijkl} \cdot x_i x_j x_k x_l > 0 \quad \forall\, \vec{x} \in \mathbb{R}^n \setminus \{0\} \; . \tag{5.6}$$

If it is only positive semidefinite, one has to consider lower order tensors as well. For example, one has to check that the kernel of Q

$$\mathrm{Ker}(Q) = \{\vec{x} \in \mathbb{R}^n \mid Q_{ijkl} \cdot x_i x_j x_k x_l = 0\} \tag{5.7}$$

is mapped entirely to 0 by T and that S is positive definite on that kernel. This is because tensors of uneven order such as T cannot be positive definite as a contraction of $\vec{x} \neq 0$ with T will be mapped to the negative of the contraction of $-\vec{x}$. Also, as one usually deals with positive mass squared values, e.g. non-tachyonic particles, the positivity of S can be easily decided on the mass spectrum (S is nothing but the mass matrix). It is clear that this special case of positive semidefiniteness of Q will depend on the numerical values of the Higgs potential parameters and will usually only occur on isolated points or similar null sets of the parameter space. Hence, it will be disregarded in the following.

The decision problem of positive definiteness of tensors has been solved recently in 2005 by Lim [36] and Qi [37] in a form that can be done computationally. To understand this approach the following section will give a short introduction into some general notions of algebraic geometry.

5.3 Algebraic Geometry

In this section some notions of algebraic geometry will be described in order to set the terminological foundation for Section 5.4, which introduces the spectral theory of tensors. First, polynomial rings and ideals are discussed. In this context polynomial division and Gröbner bases play an important role. Lastly, the concept of multivariate resultants, which is a key ingredient for spectral theory, is introduced.

5.3.1 Polynomial Rings

A polynomial in one variable x is for instance

$$p := a \cdot x^2 + b \cdot x + c \ . \tag{5.8}$$

Depending on the coefficients a, b, c one says that p is part of the polynomial ring $\mathbb{F}[x]$ when $a, b, c \in \mathbb{F}$ for some field $\mathbb{F}$, e.g. $\mathbb{Q}$, $\mathbb{R}$ or $\mathbb{C}$. A ring is similar to a field, however, it need not have multiplicative inverses, 1 and commutativity. In polynomial rings only inverses may be absent. A polynomial ring in several variables $x_1, x_2, \ldots, x_n$ is written $\mathbb{F}[x_1, x_2, \ldots, x_n]$. The polynomial $f \in \mathbb{F}[x_1, x_2, \ldots, x_n]$ is then called multivariate while $p \in \mathbb{F}[x]$ is univariate.

A monomial in $\mathbb{F}[x_1, x_2, \ldots, x_n]$ is an expression of the form

$$x_1^{d_1} x_2^{d_2} \ldots x_n^{d_n} \ . \tag{5.9}$$

Its (total) degree is the sum of all powers d_i:

$$\deg\left(x_1^{d_1} x_2^{d_2} \ldots x_n^{d_n}\right) = \sum_{i=1}^{n} d_i \ . \tag{5.10}$$

The (total) degree of a polynomial is the highest degree of all of its monomials. A polynomial is called homogeneous if all of its monomials have the same degree. For instance

$$x_1^5 - 4 \cdot x_1^2 x_3^3 + x_1 x_2^3 x_3 \tag{5.11}$$

is called a homogeneous, multivariate polynomial in the variables x_1, x_2, x_3 with coefficients in $\mathbb{Q}$.

5.3.2 Ideals and Polynomial Division

Polynomial division in one variable can be expressed by the following theorem: For all $f, g \in \mathbb{F}[x]$ there are unique $q, r \in \mathbb{F}[x]$ such that

$$f = q \cdot g + r \ , \tag{5.12}$$

with either $r = 0$ or $\deg(r) < \deg(g)$. One calls r the remainder of the polynomial division of f by g. f is divisible by g if $r = 0$. The set of all f that are divisible by g is an ideal I

$$I := \langle g \rangle = \{q \cdot g \mid q \in \mathbb{F}[x]\} \ . \tag{5.13}$$

The formal definition of a polynomial ideal is a subring $I \subseteq \mathbb{F}[x]$ such that I is closed under multiplication in the whole ring:

$$\forall\ i \in I, r \in \mathbb{F}[x] :\ r \cdot i \in I\ . \tag{5.14}$$

However, one can show by Hilbert's basis theorem (see for example [38, p. 4]), that every ideal has the form of Eq. (5.13). Similarly, every ideal I of a multivariate polynomial ring $R := \mathbb{F}[x_1, x_2, \ldots, x_n]$ can be written

$$I = \langle g_1, g_2, \ldots, g_m \rangle = \{q_1 \cdot g_1 + q_2 \cdot g_2 + \cdots + q_m \cdot g_m \mid q_i \in R\} \tag{5.15}$$

for some $m \in \mathbb{N}$. The g_i are called generators of I. Hence, every polynomial ideal is finitely generated.

Ideals are closely connected to the concept of polynomial division. However, for multivariate polynomials some adjustments have to be made. First of all, for 2 or more variables one can think of dividing a polynomial by a whole set of other polynomials. For example, one can ask if there is a linear combination of the form

$$f = q_1 \cdot g_1 + q_2 \cdot g_2 + \cdots + q_m \cdot g_m + r \tag{5.16}$$

for $f, g_1, g_2, \ldots, g_m \in \mathbb{F}[x_1, x_2, \ldots, x_n]$ with some minimal remainder r. As one can see in the case of $f := x_1^2 x_2 + x_1 x_2^2 + x_2^2$, $g_1 := x_1 x_2 - 1$, $g_2 := x_2^2 - 1$ there are at least two such remainders:

$$\begin{aligned} f &= (x_1 + x_2) \cdot g_1 + 1 \cdot g_2 + (x_1 + x_2 + 1) \\ f &= x_1 \cdot g_1 + (x_1 + 1) \cdot g_2 + (2x_1 + 1)\ . \end{aligned} \tag{5.17}$$

The uniqueness of the q_i and r is lost compared to the univariate case. To understand why this happened one has to look at the explicit algorithm used to derive these results.

In the first example of Eq. (5.17) the term $(x+y) \cdot g_1$ cancels both of the terms of highest degree in f, while in the second example $x \cdot g_1$ only cancels the first one. For univariate polynomials this does not happen since there is no ambiguity in deciding what the leading order term is. To fix that one has to introduce a so-called monomial order, which uniquely identifies for every polynomial a leading term: First define an order on the different variables

$$x_1 > x_2 > \cdots > x_n \tag{5.18}$$

and let $d := (d_1, d_2, \ldots, d_n)$ and $e := (e_1, e_2, \ldots, e_n)$ be the in this way ordered tuple of powers of two monomials. The lexicographic order (lex) is defined by the rule that

$$x_1^{d_1} x_2^{d_2} \ldots x_n^{d_n} > x_1^{e_1} x_2^{e_2} \ldots x_n^{e_n} \tag{5.19}$$

if in the difference $d - e$ the left-most non-zero entry is positive. This is analogous to orderings in dictionaries. The graded reverse lexicographic order (grevlex) is defined by the rule that Eq. (5.19) holds if $\sum_{i=1}^{n} d_i > \sum_{i=1}^{n} e_i$ or both sums are equal and in the difference $d - e$ the right-most non-zero entry is negative. This is an ordering based on the degree of monomials with an additional rule concerning equality of degrees. The leading term of a polynomial is then the biggest monomial considering the order that has been chosen. Monomial orders are in a sense the substitution for the degree ordering of univariate polynomials.

Considering lex (or grevlex) one has for the example in Eq. (5.17) that $x_1^2 x_2 > x_1 x_2^2$. Hence, one should try to cancel that term first. This can either be done with g_1 or g_2. Again, both choices will differ in the resulting q_i and r. However, considering the fact that polynomial division is nothing but an algorithm to decide ideal membership, there should be no ordering required, since ideals do not impose any order on the g_i beforehand.

There is no solution that can restore uniqueness for all possible sets of g_i. Despite that, one can define an equivalent set of polynomials, which span the same ideal and for which this uniqueness is restored. For every set of g_i there exists set of $\tilde{g}_i$ called a Gröbner basis such that

$$I = \langle g_1, g_2, \ldots, g_m \rangle = \langle \tilde{g}_1, \tilde{g}_2, \ldots, \tilde{g}_{\tilde{m}} \rangle \tag{5.20}$$

and for all $f \in I$ there is a $\tilde{g}_i$ such that the leading term of f is divisible by the leading term of $\tilde{g}_i$. In a sense a Gröbner basis is the smallest generating set for I. Not only is it possible to find such a set but there exists also an algorithm to do so due to Buchberger (see for example [38, p. 15]). Most computer algebra systems like Mathematica (function call: GroebnerBasis) and Maple (package: Groebner, function call: Basis) implement this or similar algorithms.

So, rather than thinking about division by a set of polynomials one should think about division by a given ideal. The Gröbner basis is a convenient choice of a generating set to make the results of a certain division algorithm unique. Closely related to this is the notion of quotient rings.

5.3.3 Quotient Rings

For a polynomial Ring $\mathbb{F}[x_1, x_2, \ldots, x_n]$ and an ideal $I = \langle g_1, g_2, \ldots, g_m \rangle$ with a Gröbner basis g_i the quotient ring

$$\mathbb{F}[x_1, x_2, \ldots, x_n] / \langle g_1, g_2, \ldots, g_m \rangle \tag{5.21}$$

consists of the (equivalence classes of) remainders $[r]$ of the division of all $f \in \mathbb{F}[x_1, x_2, \ldots, x_n]$ by the g_i. For instance $f \in [r]$ if

$$f = q_1 \cdot g_1 + q_2 \cdot g_2 + \cdots + q_m \cdot g_m + r \tag{5.22}$$

and also obviously $r \in [r]$. The quotient ring encodes all possible outcomes of division of some f by the g_i. As such, calculating in it is the same as calculating in $\mathbb{F}[x_1, x_2, \ldots, x_n]$ modulo the g_i.

$$\begin{aligned} [r_1] + [r_2] &= [r_1 + r_2] \\ [r_1] \cdot [r_2] &= [r_1 \cdot r_2] \end{aligned} \tag{5.23}$$

Practically, one would take two representatives $f_1 \in [r_1]$ and $f_2 \in [r_2]$, perform the calculation and expand the outcome afterwards in the g_i (polynomial division). For the multiplication of f_1 and f_2 we have

$$f_1 \cdot f_2 = q_1' \cdot g_1 + q_2' \cdot g_2 + \cdots + q_m' \cdot g_m + r' \tag{5.24}$$

such that $f_1 \cdot f_2 \in [r_1 \cdot r_2]$ and $r' \in [r_1 \cdot r_2]$.

5.3.4 Resultants

There is a generalization of determinants in the case of non-linear polynomial equations, called resultants. First take a homogeneous, square, linear system of equations in two variables x_1, x_2

$$\begin{aligned} a \cdot x_1 + b \cdot x_2 &= 0 \\ c \cdot x_1 + d \cdot x_2 &= 0 \end{aligned} \tag{5.25}$$

and rewrite it in matrix form

$$\underbrace{\begin{pmatrix} a & b \\ c & d \end{pmatrix}}_{:=M} \cdot \begin{pmatrix} x_1 \\ x_2 \end{pmatrix} = \begin{pmatrix} 0 \\ 0 \end{pmatrix} \ . \tag{5.26}$$

This system has non-trivial solutions $\vec{x} \neq 0$ if and only if

$$\det(M) = ad - bc = 0 \ , \tag{5.27}$$

i.e. if the matrix M is not invertible. One can also think of the determinant in Eq. (5.27) as a polynomial in the variables a, b, c, d, which are the coefficients of Eq. (5.25).

For a homogeneous, square, non-linear polynomial system of equations

$$f_1 = f_2 = \cdots = f_n = 0 \tag{5.28}$$

with $f_i \in \mathbb{F}[x_1, x_2, \ldots, x_n]$, there exists a similar polynomial

$$\mathrm{Res}(f_1, f_2, \ldots, f_n) \tag{5.29}$$

called the resultant, which is a polynomial in the coefficients of the f_i. It holds that $\mathrm{Res}(f_1, f_2, \ldots, f_n) = 0$ if and only if there are non-trivial solutions $\vec{x} \neq 0$ of the system of Eqs. (5.28). Unfortunately, resultants are not as easy to calculate as determinants. In fact, for fields $\mathbb{F} = \mathbb{Q}, \mathbb{R}, \mathbb{C}$ the calculation is at least NP-hard [39]. Every NP-problem has an algorithm for which the execution time scales exponentially with the input. The calculation time is thus extremely sensitive to the number n of polynomials and to their respective degrees.

The first one to study multivariate resultants was Macaulay [40]. This is why one sometimes calls it a Macaulay resultant, too. Due to him there is an algorithm that expresses the resultant as a quotient of the determinants of two matrices. The size of these two matrices grows rapidly with the number n of variables / polynomials and their respective polynomial degrees $d_i := \deg(f_i)$. Hence, this algorithm is not very space efficient.

5.3.5 An explicit Resultant Algorithm

Another more economical algorithm can be found in [38, theorem 3.4], which uses a recursive approach: Given homogeneous polynomials $f_1, f_2, \ldots, f_n \in \mathbb{C}[x_1, x_2, \ldots x_n]$ with degrees $d_i := \deg(f_i)$ that form a square system of Eqs. (5.28), define new polynomials

$$\begin{aligned} \bar{f}_i &:= f_i(0, x_2, \ldots, x_n) \\ F_i &:= f_i(1, x_2, \ldots, x_n) \ . \end{aligned} \tag{5.30}$$

Then, if $\mathrm{Res}(\bar{f}_2, \ldots, \bar{f}_n) \neq 0$ one has

$$\mathrm{Res}(f_1, f_2, \ldots, f_n) = \mathrm{Res}(\bar{f}_2, \ldots, \bar{f}_n)^{d_1} \cdot \det M_1 \ , \tag{5.31}$$

where the matrix M_1 is defined by the map

$$\begin{aligned} m_{F_1} : V &\to V \\ [r] &\mapsto [F_1] \cdot [r] = [F_1 \cdot r] \ , \end{aligned} \tag{5.32}$$

with the quotient ring $V := \mathbb{C}[x_2, \ldots, x_n]/\langle F_2, \ldots, F_n \rangle$ being a $\mathbb{C}$ vector space of dimension $D := d_2 \ldots d_n$.

Let us asses how this theorem enables one to the calculate the resultant: Eq. (5.31) gives the resultant in terms of the determinant of some

matrix times another resultant of now $n-1$ polynomials $\bar{f}_i$ and variables $x_2, \ldots, x_n$. These polynomials are still homogeneous and of the same degree $\deg(\bar{f}_i) = \deg(f_i)$, because setting one variable to zero $x_1 = 0$ does not alter these properties unless the polynomial is identical to zero. However, this case is excluded by the condition $\mathrm{Res}(\bar{f}_2, \ldots, \bar{f}_n) \neq 0$. If one $\bar{f}_i \equiv 0$ then $\mathrm{Res}(\bar{f}_2, \ldots, \bar{f}_n) = 0$ because the system $\bar{f}_2 = \ldots \bar{f}_n = 0$ is underdetermined and thus there are non-trivial solutions (recall the definition of the resultant). Applying the theorem $n-1$ times, one ends up with a resultant of a single homogeneous polynomial $\tilde{f}_n$ in one variable x_n of degree d_n. The only possible form for this polynomial is

$$\tilde{f}_n(x_n) = \alpha \cdot x_n^{d_n} \ , \tag{5.33}$$

with some $\alpha \in \mathbb{C}$. Because the resultant $\mathrm{Res}(\tilde{f}_n)$ is zero if and only if there are non-trivial solutions to $\tilde{f}_n = 0$ it holds that

$$\mathrm{Res}(\tilde{f}_n) = \alpha \ . \tag{5.34}$$

Hence, after $n-1$ steps the calculation of the resultant terminates with a trivial relation.

The essential part of the calculation is setting up the matrix M_1 and its sequential successors. To do so, one has to first find a basis $[b_i]$ of the vector space $V = \mathbb{C}[x_2, \ldots, x_n]/\langle F_2, \ldots F_n \rangle$. The most straightforward way is to look for a monomial basis by scanning through all possible monomials

$$m := x_2^{e_2} \ldots x_n^{e_n} \tag{5.35}$$

of ascending total degree $\deg(m) = \sum_{i=2}^{n} e_i = 0, 1, 2$, etc. The goal is to find in total D unique, non-zero, linear independent monomial remainders b_i of a polynomial division of the monomials m by a Gröbner basis G_i of the ideal $\langle F_2, \ldots, F_n \rangle$. Then one has to multiply the b_i by F_1 and find the remainder r_i modulo the Gröbner basis,

$$b_i \cdot F_1 = Q_1 \cdot G_1 + Q_2 \cdot G_2 + \cdots + Q_m \cdot G_m + r_i \ , \tag{5.36}$$

and express it as a linear combination of the b_i:

$$r_i = c_{1i} \cdot b_1 + c_{2i} \cdot b_2 + \cdots + c_{Di} \cdot b_D \ . \tag{5.37}$$

Here, the c_{ij} are the (i, j) elements of the matrix M_1.

It may happen that the condition $\mathrm{Res}(\bar{f}_2, \ldots, \bar{f}_n) \neq 0$ cannot be fulfilled because there are always at least two $\bar{f}_i$ that are identical to zero (if it is just one, one must choose this polynomial for elimination instead of f_1). In this

case, the starting resultant is zero. Intuitively, this result is clear. Suppose there are two polynomials, say f_1, f_2, such that $\bar{f}_1 \equiv \bar{f}_2 \equiv 0$. Then both of them are proportional to x_1:

$$\begin{aligned} f_1 &= x_1 \cdot f_1' \\ f_2 &= x_1 \cdot f_2' \ . \end{aligned} \tag{5.38}$$

For $f_1 = 0$ it follows that $x_1 = 0$ or $f_1' = 0$. In the first case $x_1 = 0$, the second polynomial is identical to zero $f_2 \equiv 0$, e.g. $f_2 = 0$ is a trivial relation. Hence, the $n-1$ variables are underdetermined due to the remaining $n-2$ Eqs. (5.28), such that there is a non-trivial solution $\vec{x} \neq 0$. Therefore one has $\mathrm{Res}(f_1, f_2, \ldots, f_n) = 0$. If $x_1 \neq 0$ this already implies a non-trivial solution and again $\mathrm{Res}(f_1, f_2, \ldots, f_n) = 0$. As one can see, depending on the specific form of the polynomials f_i the algorithm may indeed be very fast or a different kind of algorithm may be applicable. Some further consequences of this are discussed in Section 5.7.

5.3.6 Exemplary Calculation of Resultants

To get a feeling for the algorithm of Section 5.3.5 the following examples may be helpful. Take the system of equations

$$\begin{aligned} f_1 &:= a \cdot x + b \cdot y = 0 \\ f_2 &:= c \cdot x + d \cdot y = 0 \\ f_3 &:= x + y + z = 0 \end{aligned} \tag{5.39}$$

and calculate $\mathrm{Res}(f_1, f_2, f_3)$. There are in total 3 equations, such that Eq. (5.31) has to be applied two times. For the first iteration define

$$\begin{aligned} \bar{f}_2 &:= f_2(x = 0, y, z) = d \cdot y \\ \bar{f}_3 &:= f_3(x = 0, y, z) = y + z \\ F_1 &:= f_1(x = 1, y, z) = a + b \cdot y \\ F_2 &:= f_2(x = 1, y, z) = c + d \cdot y \\ F_3 &:= f_3(x = 1, y, z) = 1 + y + z \ . \end{aligned} \tag{5.40}$$

A Gröbner basis of $\langle F_2, F_3 \rangle$ is

$$\begin{aligned} G_2 &:= -c + d + d \cdot z \\ G_3 &:= 1 + y + z \ . \end{aligned} \tag{5.41}$$

The degrees of the f_i are $d_i = 1$. Thus, the quotient ring and vector space $\mathbb{C}[y, z]/\langle F_2, F_3 \rangle$ has dimension $D = d_2 \cdot d_3 = 1$. A basis vector is (the equivalence class of) the constant polynomial [1] because the division

$$1 = 0 \cdot G_2 + 0 \cdot G_3 + 1 \tag{5.42}$$

shows that 1 is a unique remainder. The first (and only) element of the matrix M_1 can be read off by

$$1 \cdot F_1 = (-\frac{b}{d}) \cdot G_2 + b \cdot G_3 + \frac{ad-bc}{d} \tag{5.43}$$

and therefore

$$[1] \cdot [F_1] = \left[\frac{ad-bc}{d}\right] = \frac{ad-bc}{d} \cdot [1] = c_{11} \cdot [1] \tag{5.44}$$

such that $\det(M_1) = c_{11} = \frac{ad-bc}{d}$. For the second iteration calculate $\mathrm{Res}(\bar{f}_2, \bar{f}_3)$ and define

$$\begin{aligned} \bar{\bar{f}}_3 &:= \bar{f}_3(y=0,z) = z \\ \bar{F}_2 &:= \bar{f}_2(y=1,z) = d \\ \bar{F}_3 &:= \bar{f}_3(y=1,z) = 1+z \ . \end{aligned} \tag{5.45}$$

A Gröbner basis of $\langle \bar{F}_3 \rangle$ is

$$\bar{G}_3 := 1 + z \ , \tag{5.46}$$

i.e. $\bar{F}_3$ is already a Gröbner basis. Again, the dimension of the quotient ring and vector space is $\bar{D} = \bar{d}_3 = \deg(\bar{f}_3) = 1$ such that a unique remainder is [1]. The matrix element of $\bar{M}_2$ is given by

$$1 \cdot \bar{F}_2 = 0 \cdot \bar{G}_3 + d \tag{5.47}$$

and therefore

$$[1] \cdot [\bar{F}_2] = [d] = d \cdot [1] \ , \tag{5.48}$$

which gives $\det(\bar{M}_2) = d$. Lastly, one has $\mathrm{Res}(\bar{\bar{f}}_3) = 1$. In total this yields

$$\begin{aligned} \mathrm{Res}(f_1, f_2, f_3) &= \mathrm{Res}(\bar{f}_2, \bar{f}_3)^{d_1} \cdot \det(M_1) \\ &= \left(\mathrm{Res}(\bar{\bar{f}}_3)^{\bar{d}_2} \cdot \det(\bar{M}_2)\right)^{d_1} \cdot \det(M_1) \\ &= \left(1^1 \cdot d\right)^1 \cdot \frac{ad-bc}{d} \\ &= ad - bc \ . \end{aligned} \tag{5.49}$$

It is no coincidence that this agrees with

$$\det \begin{pmatrix} a & b & 0 \\ c & d & 0 \\ 1 & 1 & 1 \end{pmatrix} = ad - bc \tag{5.50}$$

Table 5.1: Remainders r of a polynomial division of low degree monomials m by the Gröbner basis G_2, G_3.

monomial $m =$	1	y	z	y^2	yz	z^2	y^3	y^2z	yz^2	z^3
remainder $r =$	1	z^3	z	$-z^2$	-1	z^2	z	$-z^3$	$-z$	z^3

because both, the determinant of the matrix of the linear system of Eqs. (5.39) and its resultant, give sufficient and necessary conditions for non-trivial solutions to exist.

To further understand the process of finding a basis for a quotient ring $\mathbb{C}[y,z]/\langle F_2, F_3\rangle$ and the matrix M_1, take a more complicated example than in Eq. (5.40). Let

$$\begin{aligned} f_1 &:= x^3 - xyz + y^2z \\ f_2 &:= x^2 + yz \\ f_3 &:= y^2 + z^2 \\ F_1 &:= f_1(x=1,y,z) = y^2z - yz + 1 \\ F_2 &:= f_2(x=1,y,z) = yz + 1 \\ F_3 &:= f_3(x=1,y,z) = y^2 + z^2 \end{aligned} \tag{5.51}$$

be a new set of polynomials. A Gröbner basis of $\langle F_2, F_3\rangle$ is

$$\begin{aligned} G_2 &:= z^4 + 1 \\ G_3 &:= y - z^3 \ . \end{aligned} \tag{5.52}$$

The degrees are $d_1 = \deg(f_1) = 3$ and $d_2 = \deg(f_2) = d_3 = \deg(f_3) = 2$ such that the quotient ring and vector space $\mathbb{C}[y,z]/\langle F_2, F_3\rangle$ has a dimension $D = d_2 \cdot d_3 = 4$. Table 5.1 shows a list of remainders r for a division of monomials m of degree $\deg(m) \leq 3$. After the first four divisions one can already identify the unique monomial remainders $1, z, z^2, z^3$ which form the basis $[b_1] := [1]$, $[b_2] := [z]$, $[b_3] := [z^2]$ and $[b_4] := [z^3]$. The remaining divisions show the repeating pattern of these remainders. Now perform the polynomial division of the products $b_i \cdot F_1$,

$$\begin{aligned} b_1 \cdot F_1 &= (y-1)\cdot G_2 &&+ (yz - z - 1)\cdot G_3 &&+ (2 - z^3) \\ b_2 \cdot F_1 &= (yz - z - 1)\cdot G_2 &&+ (yz^2 - z^2 - z)\cdot G_3 &&+ (1 + 2\cdot z) \\ b_3 \cdot F_1 &= (yz^2 - z^2 - z)\cdot G_2 &&+ (yz^3 - z^3 - z^2)\cdot G_3 &&+ (z + 2\cdot z^2) \\ b_4 \cdot F_1 &= (y^2 - z^2 - y)\cdot G_2 &&+ (-z^3 - y + 1)\cdot G_3 &&+ (z^2 + 2\cdot z^3) \end{aligned} \tag{5.53}$$

and expand the remainders in the basis vectors $[b_i]$,

$$\begin{aligned}
[b_1]\cdot[F_1] &= [2-z^3] &&= 2\cdot[b_1] && && -1\cdot[b_4]\\
[b_2]\cdot[F_1] &= [1+2\cdot z] &&= 1\cdot[b_1]+2\cdot[b_2] && &&\\
[b_3]\cdot[F_1] &= [z+2\cdot z^2] &&= && +1\cdot[b_2]+2\cdot[b_3] &&\\
[b_4]\cdot[F_1] &= [z^2+2\cdot z^3] &&= && && +1\cdot[b_3]+2\cdot[b_4]\ .
\end{aligned} \tag{5.54}$$

From this one can read off the matrix

$$M_1 := \begin{pmatrix} 2 & 1 & 0 & 0\\ 0 & 2 & 1 & 0\\ 0 & 0 & 2 & 1\\ -1 & 0 & 0 & 2 \end{pmatrix} \tag{5.55}$$

with determinant $\det(M_1) = 17$.

5.4 Spectral Theory of Tensors

In 2005 Lim [36] and Qi [37] independently defined eigenvalues of tensors and thus created a general spectral theory of tensors. However, most of the presented material can also be found in the more recent review [41] or the book [42]. This section relies on the terminology introduced in Section 5.3, especially on the concept of multivariate resultants. Eigenvalues are the key to the decision problem of positive definiteness of tensors and therefore also for the boundedness of Higgs potentials.

5.4.1 Eigenvalues

There are several different ways to generalize the notion of eigenvalues. One of which is the following: Let Q be a real, symmetric tensor of order $m \in \mathbb{N}$ over a vector space $\mathbb{C}^n$. Then $\lambda \in \mathbb{C}$ is called an eigenvalue of Q if

$$Q_{i_1 i_2 \ldots i_m} \cdot x_{i_2} \ldots x_{i_m} = \lambda \cdot x_{i_1}^{m-1} \tag{5.56}$$

has non-trivial solutions $\vec{x} \in \mathbb{C}^n \setminus \{0\}$. These solutions $\vec{x}$ are then called eigenvectors. An H-eigenvalue of Q is an eigenvalue λ such that there exists at least one real eigenvector $\vec{x} \in \mathbb{R}^n \setminus \{0\}$. This eigenvector is then called an H-eigenvector. There is always at least one H-eigenvalue. For $m = 2$, the definition of Eq. (5.56) reduces to the one of matrices.

In contrast to matrices, eigenvalues of a real, symmetric tensor Q can be complex for $m > 2$. Also, eigenvalues and in particular H-eigenvalues are in

general not invariant under orthogonal transformations. Let $R \in \mathrm{O}(n)$ and define the transformed tensor

$$Q'_{j_1 j_2 \ldots j_m} := Q_{i_1 i_2 \ldots i_m} \cdot R^{\top}_{i_1 j_1} R^{\top}_{i_2 j_2} \ldots R^{\top}_{i_m j_m} \tag{5.57}$$

and vector

$$\vec{x}\,' := R \cdot \vec{x} \tag{5.58}$$

such that

$$\begin{aligned} & Q'_{j_1 j_2 \ldots j_m} \cdot x'_{j_1} x'_{j_2} \ldots x'_{j_m} = R^{\top}_{i_1 j_1} \cdot Q_{i_1 i_2 \ldots i_m} \cdot x_{i_2} \ldots x_{i_m} \\ & = R^{\top}_{i_1 j_1} \cdot \lambda \cdot x_{i_1}^{m-1} \\ & = \lambda \cdot \left(R_{j_1 1} \cdot x_1^{m-1} + R_{j_1 2} \cdot x_2^{m-1} + \cdots + R_{j_1 n} \cdot x_n^{m-1} \right) \\ & \neq \lambda \cdot (x'_{j_1})^{m-1} \end{aligned} \tag{5.59}$$

for $m > 2$, because raising x_{i_1} to the power of $m - 1 > 1$ is not compatible with linear transformations.

This is why there is yet another definition of eigenvalues: $\lambda \in \mathbb{C}$ is called an E-eigenvalue if for the set of equations

$$\begin{aligned} Q_{i_1 i_2 \ldots i_m} \cdot x_{i_2} \ldots x_{i_m} &= \lambda \cdot x_{i_1} \\ \vec{x}^{\top} \cdot \vec{x} &= 1 \end{aligned} \tag{5.60}$$

there is a non-trivial (E-eigen)vector $\vec{x} \in \mathbb{C} \setminus \{0\}$. If an E-eigenvalue has a real E-eigenvector, it is called a Z-eigenvalue with a (real) Z-eigenvector. There is always at least one Z-eigenvalue. For $m = 2$ this is not the usual definition of eigenvectors, because $\vec{x}^{\top} \cdot \vec{x} = 1$ is an additional restriction, which allows only normalized real eigenvectors and may even single out some complex solutions. The eigenvalues of a real, symmetric matrix are, however, Z-eigenvalues. As one can see, both Eqs. (5.60) are form-invariant under orthogonal transformations. Hence, E-eigenvalues and Z-eigenvalues are $\mathrm{O}(n)$ invariant.

A comparison of some of the properties of the different concepts of eigenvalues and eigenvectors is given in Table 5.2. The last line refers to the next Section 5.4.2.

5.4.2 Characteristic Polynomial

The discussion of Section 5.4.1 enables one to look for eigenvectors $\vec{x} \in \mathbb{C}^n \setminus \{0\}$ by simply checking if they satisfy the relation of Eq. (5.56) or Eq. (5.60). However, there is yet no way of determining all eigenvalues $\lambda \in \mathbb{C}$ systematically.

Table 5.2: Comparison of different definitions of eigenvalues and eigenvectors. The term "normal" refers to the definition given in Eq. (5.56).

	normal	H	E	Z
real	possible	always	possible	always
O(n) behavior	-	-	invariant	invariant
reduces to matrix definition	yes	yes	only eigenvalues	only eigenvalues
eigenvalues from Char(Q, λ)	yes	yes	only if regular	only if regular

For matrices, this is done by rewriting the defining linear equations of eigenvalues in matrix form and demanding that the determinant vanishes. As discussed in Section 5.3.5 this is equivalent to the requirement that eigenvectors shall be non-trivial, $\vec{x} \neq 0$. There is a straightforward generalization to eigenvalues of tensors: The eigenvalues $\lambda \in \mathbb{C}$ are again chosen such that there is a non-trivial solution to Eq. (5.56). By rewriting these equations one gets

$$\begin{aligned} f_1 &:= Q_{1i_2\ldots i_m} \cdot x_{i_2} \ldots x_{i_m} - \lambda \cdot x_1^{m-1} = 0 \\ f_2 &:= Q_{2i_2\ldots i_m} \cdot x_{i_2} \ldots x_{i_m} - \lambda \cdot x_2^{m-1} = 0 \\ &\ldots \\ f_n &:= Q_{ni_2\ldots i_m} \cdot x_{i_2} \ldots x_{i_m} - \lambda \cdot x_n^{m-1} = 0 \ , \end{aligned} \tag{5.61}$$

which actually is a system of n homogeneous polynomial equations in n variables. The requirement of non-triviality of the solutions is equivalent to the vanishing of the respective resultant. Hence, one defines the characteristic polynomial by

$$\text{Char}(Q, \lambda) := \text{Res}(f_1, f_2, \ldots, f_n) \ . \tag{5.62}$$

The eigenvalues are then the roots λ of $\text{Char}(Q, \lambda) = 0$.

For E-eigenvalues the situation is different because Eq. (5.60) cannot be rewritten in terms of homogeneous polynomials. Nevertheless, one can define for an even order tensor Q the set of equations

$$\begin{aligned} e_1 &:= Q_{1i_2\ldots i_m} \cdot x_{i_2} \ldots x_{i_m} - \lambda \cdot \left(\vec{x}^\top \cdot \vec{x}\right)^{\frac{m-2}{2}} \cdot x_1 = 0 \\ e_2 &:= Q_{2i_2\ldots i_m} \cdot x_{i_2} \ldots x_{i_m} - \lambda \cdot \left(\vec{x}^\top \cdot \vec{x}\right)^{\frac{m-2}{2}} \cdot x_2 = 0 \\ &\ldots \\ e_n &:= Q_{ni_2\ldots i_m} \cdot x_{i_2} \ldots x_{i_m} - \lambda \cdot \left(\vec{x}^\top \cdot \vec{x}\right)^{\frac{m-2}{2}} \cdot x_n = 0 \ , \end{aligned} \tag{5.63}$$

where the e_i are homogeneous polynomials. An E-characteristic polynomial is then given by

$$\mathrm{Char}(Q,\lambda) := \mathrm{Res}(e_1, e_2, \ldots, e_n) \ . \tag{5.64}$$

Equation (5.63) combines the two defining relations. One calls Q regular if the set of equations

$$\begin{aligned} Q_{i_1 i_2 \ldots i_m} \cdot x_{i_2} \ldots x_{i_m} &= 0 \\ \vec{x}^{\top} \cdot \vec{x} &= 0 \end{aligned} \tag{5.65}$$

has only the trivial solution $\vec{x} = 0$. If Q is regular, then $\lambda \in \mathbb{C}$ is an E-eigenvalue if and only if it is a root of the E-characteristic polynomial, $\mathrm{Char}(Q,\lambda) = 0$. One needs this extra condition of regularity because in (5.63) there are fewer equations than the original definition of E-eigenvalues used. If Q is not regular, then solutions of Eq. (5.65) will also solve Eq. (5.63) with any choice of $\lambda \in \mathbb{C}$. Hence, there is no distinctive set of eigenvalues to be derived from $\mathrm{Char}(Q,\lambda) = 0$.

5.4.3 Positive Definiteness

As has been outlined in Section 5.2, the essential part for the check of boundedness of a Higgs potential is to test positive definiteness of a order 4 tensor. Similar as for matrices, one can do that with eigenvalues.

Let $k \in \mathbb{N}$ and $m = 2k$ be the (even) order of a real, symmetric tensor Q. Then Q is positive definite, that is

$$Q_{i_1 i_2 \ldots i_m} \cdot x_{i_1} x_{i_2} \ldots x_{i_m} > 0 \quad \forall\ \vec{x} \in \mathbb{R}^n \setminus \{0\} \tag{5.66}$$

if and only if

1. all of its H-eigenvalues are positive.

2. all of its Z-eigenvalues are positive.

It suffices to test either 1 or 2 because they are equivalent. For a definition of H- and Z-eigenvalues refer to Section 5.4.1.

It is interesting to note that even though H-eigenvalues are not $\mathrm{O}(n)$ invariant, Z-eigenvalues are indeed invariant. Thus H-eigenvalues may change their values under orthogonal transformations but the property of all of them being positive will never do so.

5.5 The Algorithm

Based on the previous section one can now formulate an algorithm to test boundedness of a general Higgs potential V. Where possible, tools and their function calls that are able to calculate intermediate steps are referenced. There exists a working implementation, based on Mathematica [43] and Macaulay2 [44], called BFB [4] available at GitHub.

Due to the reason that for Z-eigenvalues the regularity of a given tensor has to be tested first, the following algorithm is based on H-eigenvalues. However, possible advantages of Z-eigenvalues that have not been tested yet are described in Section 5.7.

For a given Higgs potential V one has to do the following steps to check boundedness:

1. Rewrite V in terms of real, scalar fields $\vec{x} \in \mathbb{R}^n$ by expanding the singlets, doublets, triplets, etc. in terms of their real and imaginary parts.
2. Calculate the order 4 tensor $Q_{ijkl} := \left[\frac{1}{4!}\frac{\partial^4 V}{\partial x_i \partial x_j \partial x_k \partial x_l}\right]_{\vec{x}=0}$.
3. Set up the polynomials $f_i := Q_{ijkl} \cdot x_j x_k x_l - \lambda \cdot x_i^3$.
4. Calculate $\mathrm{Char}(Q, \lambda) = \mathrm{Res}(f_1, f_2, \ldots, f_n)$.
5. Find all real roots $\lambda \in \mathbb{R}$ in $\mathrm{Char}(Q, \lambda) = 0$.
6. Check all non-positive roots $\lambda \leq 0$ for real solutions $\vec{x} \in \mathbb{R}^n$ to the equations $f_1 = f_2 = \cdots = f_n = 0$.
7. V is bounded from below if and only if none of the non-positive roots have such real solutions.

For step 1 it is important that the real scalar fields x_i can in principle map to any value in $\mathbb{R}$ and not just some subset of it. For instance, there should not be a periodic function $x_i \in [0, 2\pi]$ or a purely non-negative function $x_i \in [0, \infty)$ (these situations have been tested by so called copositivity criteria [21] but the method is not generally applicable). If this condition is not met, the algorithm might only yield sufficient but not necessary constraints on the Higgs potential parameters, simply because positive definiteness of Q is too restrictive for fields that will not acquire the whole range of values $x_i \in \mathbb{R}$. However, the real and imaginary part of usual singlets, doublets, triplets, etc. will always meet the condition.

Step 2 and 3 can be done by most computer algebra systems such as Mathematica [43] or Maple [45].

Step 4, however, is more complicated. Both, Mathematica and Maple, have implementations for the calculation of resultants for two polynomials in a maximum of two variables. But there is no general implementation for the calculation of multivariate resultants. Either, one can go ahead and implement the resultant algorithm of Section 5.3.5 within Mathematica/Maple with their support for polynomial division algorithms such as finding Gröbner bases etc. Alternatively, one can try to use a more specialized computer algebra system such as Macaulay2 [44] that was designed for problems in algebraic geometry. It allows for symbolic manipulation of polynomials and calculation within quotient rings and ideals over the field of integers or rational numbers. The implementation of multivariate resultants is provided as a package called Resultants [46]. The currently tested version of BFB [4] uses this package.

In step 5 for analytic Higgs potential parameters, it is not clear if it is in general possible to decide whether a root is real or not. Hence, most of the time this has to be decided after numeric values have been chosen.

Step 6 is, similar as the calculation of resultants, a mathematical problem that can be rather involved. It reduces to a proof of existence of real solutions for a given set of polynomial equations. In the univariate case this problem can be tackled by a so called Sturm sequence. For the more interesting multivariate case, the decision problem of real solutions has been solved by the so called Tarski-Seidenberg theorem [47]. The implementation of BFB uses Mathematica's function call FindInstance to construct a real solution if possible.

In practice there are two different scenarios for which one would apply this algorithm. Firstly, to have a numerical check of boundedness for a given point in the parameters space of the Higgs potential. The Higgs potential will have numeric coefficients only.

Secondly, one would want to derive analytic constraints that can be later evaluated numerically. The constraints then should be the analytic form of all H-eigenvalues restricted to positive values. In principle the algorithm is capable of doing this, however, the calculation of analytic H-eigenvalues can be either extremely time consuming or actually impossible.

The Abel-Ruffini theorem states that there is no algebraic solution to a univariate, generic polynomial equation of degree five or higher with arbitrary coefficients. H-eigenvalues are the roots of the characteristic polynomial which is a univariate polynomial in λ of usually very high degree. Thus, there might not even exists an analytic expression in terms of inequalities that can decide boundedness of a given Higgs potential. The only analytic form that

encodes all information about boundedness is the characteristic polynomial $\mathrm{Char}(Q, \lambda)$. Because calculating resultants is NP-hard [39] step 4 can be very challenging. Finding the analytic form of the resultant easily exceeds a time scale of several weeks for the 2HDM with the current implementation of BFB. Approaches to this problem are discussed in Section 5.7. Once the resultant is known, however, the numerical calculations in step 5 to 7 do not take more time than several seconds.

5.6 Proof of Concept

This section shows the validation of the algorithm formulated in the previous Section 5.5 based on some exemplary potentials. All results have been calculated with the Mathematica package BFB [4].

5.6.1 2HDM

The 2HDM potential is given by

$$\begin{aligned} V = {} & m_{11}^2|\phi_1|^2 + \lambda_1|\phi_1|^4 + m_{22}^2|\phi_2|^2 + \lambda_2|\phi_2|^4 \\ & + \lambda_3|\phi_1|^2|\phi_2|^2 + \lambda_4|\phi_1^\dagger\phi_2|^2 + \frac{\lambda_5}{2}\Big((\phi_1^\dagger\phi_2)^2 + (\phi_1^\dagger\phi_2)^2\Big) \end{aligned} \tag{5.67}$$

with Higgs potential parameters $m_{11}^2, m_{22}^2, \lambda_1, \lambda_2, \lambda_3, \lambda_4, \lambda_5 \in \mathbb{R}$ and SU(2) doublets $\phi_1, \phi_2 \in \mathbb{C}^2$. The analytic constraints for boundedness are known and can be found in [20, 21, 22]:

$$\begin{aligned} \lambda_1 &> 0 \\ \lambda_2 &> 0 \\ \lambda_3 + 2\sqrt{\lambda_1\lambda_2} &> 0 \\ \lambda_4 - |\lambda_5| + \lambda_3 + 2\sqrt{\lambda_1\lambda_2} &> 0\ . \end{aligned} \tag{5.68}$$

As one can see, it is sufficient to restrict all parameters to positive values but also that it is not necessary to do so. In fact, λ_5 can be arbitrarily negative as long as its absolute value is smaller than some combination of the other parameters. It is this necessary part of the constraint that is usually very hard to proof.

The Figures 5.1 to 5.6 show exclusion plots of two parameter planes. The green region is excluded by the analytic constraints of Eq. (5.68). The yellow region is allowed. As one can see, the parameter scan with BFB, denoted by black points, shows perfect agreement.

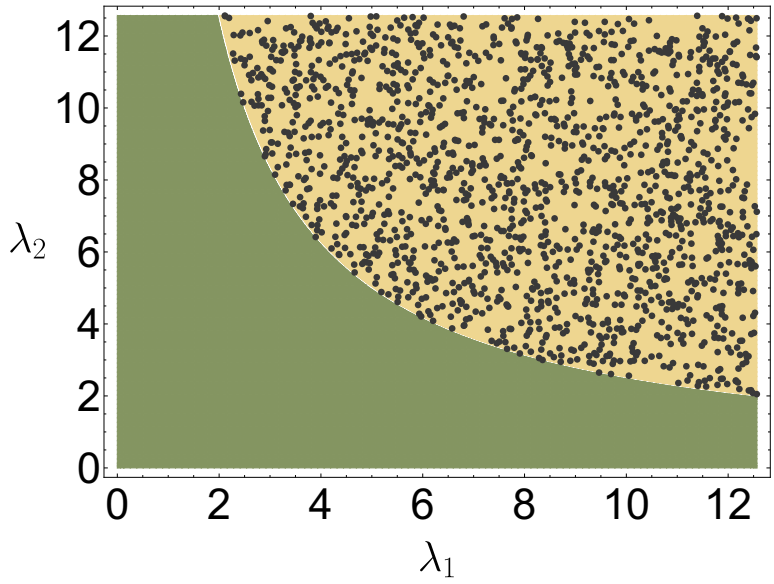

Figure 5.1: Exclusion plot for the λ_1, λ_2 plane with $\lambda_3 = -10$ and $\lambda_4 = \lambda_5 = 1$. The green region is excluded by analytic constraints, the yellow region is allowed. Black points are allowed according to a parameter scan with BFB.

The scan was done numerically, that is, the Higgs potential parameters were assigned numerical values before running the algorithm. To reduce the complexity of the problem, the SU(2) symmetry of the Higgs potential has been exploited. A given potential value V at a certain point $\vec{x} \in \mathbb{R}^8$ of variables can be equally expressed by a different point $\vec{x}\,' \in \mathbb{R}^8$ if the two points are connected through an SU(2) transformation of the two Higgs doublets. Hence by an appropriate choice of transformation, one can make three of the eight variables vanish. This corresponds to the calculation of the constraints in unitary gauge.

Also, within Macaulay2 [44] one can choose to calculate the resultant not over a field but over the ring of integers. This is on average faster because the intermediate polynomial division steps also require the division of the coefficients. Within the ring of integers this is effectively done by a modulo operation which is much faster than an actual division. The computation time varied a lot and ranged from 3 hours to 8 hours per parameter point. Almost the whole time was spent for the calculation of the resultant. There is a strong dependence on the calculation time based on the complexity of the input parameters. For example, simpler coefficients like $\frac{1}{10}$ would result in a faster calculation than coefficients like $\frac{743}{999}$. This is because the resultant is a

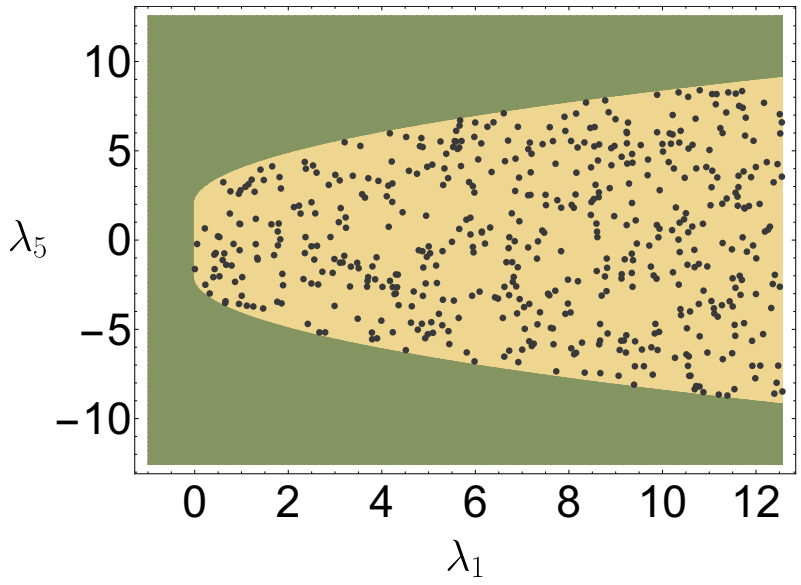

Figure 5.2: Exclusion plot for the λ_1, λ_5 plane with $\lambda_2 = \lambda_3 = \lambda_4 = 1$. The green region is excluded by analytic constraints, the yellow region is allowed. Black points are allowed according to a parameter scan with BFB.

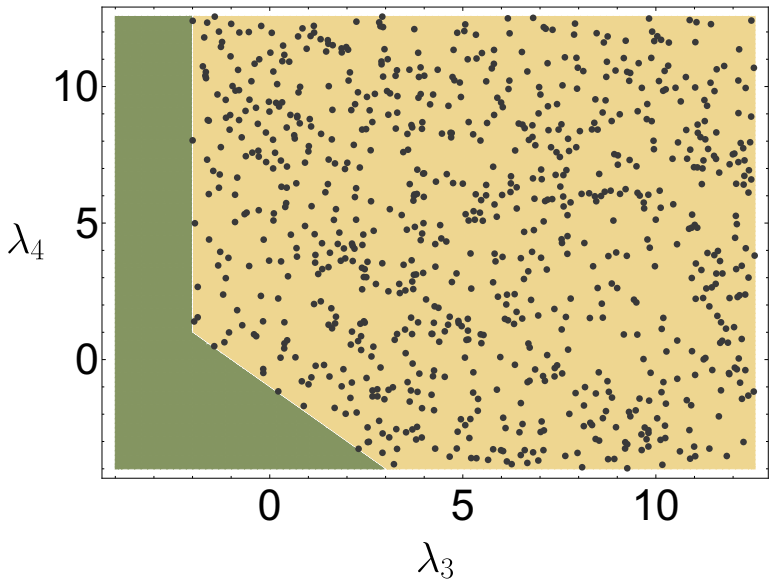

Figure 5.3: Exclusion plot for the λ_3, λ_4 plane with $\lambda_1 = \lambda_2 = \lambda_5 = 1$. The green region is excluded by analytic constraints, the yellow region is allowed. Black points are allowed according to a parameter scan with BFB.

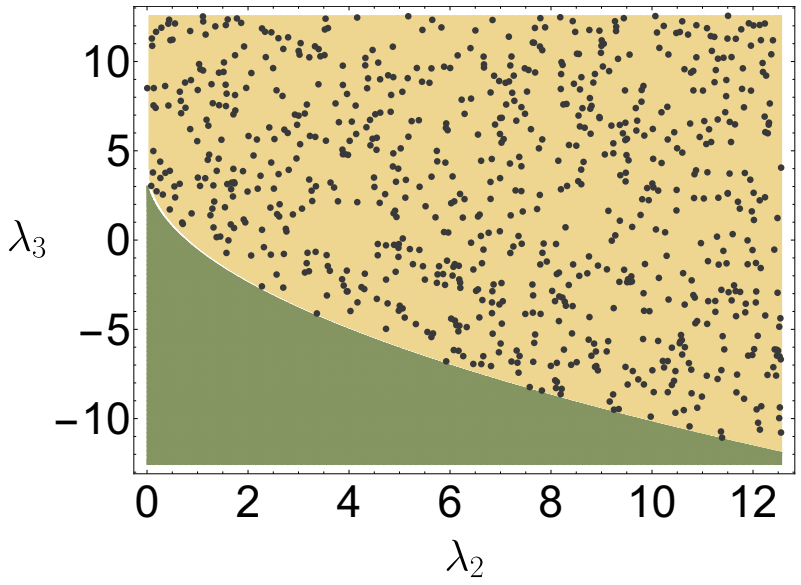

Figure 5.4: Exclusion plot for the λ_2, λ_3 plane with $\lambda_1 = \lambda_5 = 5$ and $\lambda_4 = 1$. The green region is excluded by analytic constraints, the yellow region is allowed. Black points are allowed according to a parameter scan with BFB.

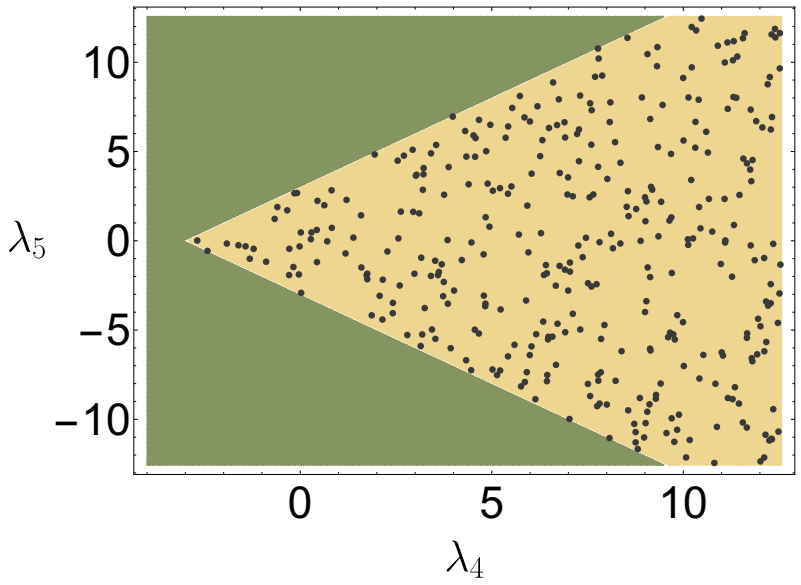

Figure 5.5: Exclusion plot for the λ_4, λ_5 plane with $\lambda_1 = \lambda_2 = \lambda_3 = 1$. The green region is excluded by analytic constraints, the yellow region is allowed. Black points are allowed according to a parameter scan with BFB.

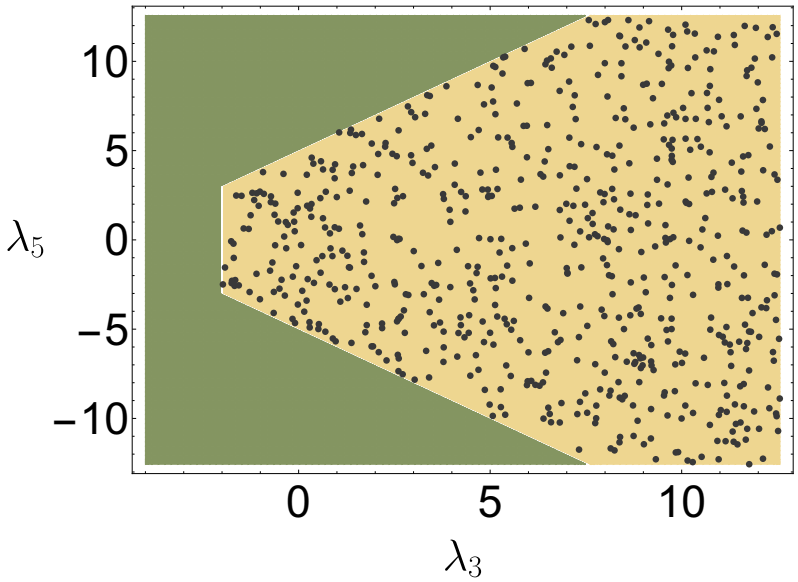

Figure 5.6: Exclusion plot for the λ_3, λ_5 plane with $\lambda_4 = 3$ and $\lambda_1 = \lambda_2 = 1$. The green region is excluded by analytic constraints, the yellow region is allowed. Black points are allowed according to a parameter scan with BFB.

polynomial in the coefficients. For the 5 variable version of the 2HDM within the ring of integers the highest degree of this polynomial was 405. Hence the initial parameters will approximately be raised to this total power making the resulting nominator and denominator a huge number which cannot be stored in CPU registers. For instance, for $\lambda_1 = \lambda_2 = \lambda_3 = 1$, $\lambda_4 = 9.01587$ and $\lambda_5 = -10.2132$ the largest coefficient of the characteristic polynomial is of order

$$\approx 3.452 \cdot 10^{1137} \, . \tag{5.69}$$

Thus special libraries for integer manipulation, that emulate the CPU's arithmetic logic unit, have to be used instead. Possible solutions to this problem are discussed in Section 5.7.

The runtime of the remaining algorithm, after the calculation of the resultant / characteristic polynomial, is negligible. For the above parameter point, calculating and testing all H-eigenvalues takes no longer than ≈ 3 seconds. As discussed in Section 5.5, this shows that the characteristic polynomial is essentially equivalent to having exact analytic constraints.

5.6.2 Potential in two Variables

Consider a very simple potential in two variables

$$V = a \cdot x^4 + b \cdot x^2 y^2 + c \cdot y^4 \tag{5.70}$$

with parameters $a, b, c \in \mathbb{R}$. The corresponding eigenvalue equations for the check of boundedness are

$$\begin{aligned} f_1 &:= a \cdot x^3 + \frac{1}{2} b \cdot x y^2 - \lambda \cdot x^3 = 0 \\ f_2 &:= c \cdot y^3 + \frac{1}{2} b \cdot x^2 y - \lambda \cdot y^3 = 0 \ . \end{aligned} \tag{5.71}$$

BFB can calculate the characteristic polynomial, resulting in

$$\begin{aligned} &\mathrm{Char}(Q, \lambda) = \mathrm{Res}(f_1, f_2) = a^3 c^3 - 3a^3 c^2 \lambda + 3a^3 c \lambda^2 - a^3 \lambda^3 - \frac{1}{2} a^2 b^2 c^2 \\ &+ a^2 b^2 c \lambda - \frac{1}{2} a^2 b^2 \lambda^2 - 3a^2 c^3 \lambda + 9a^2 c^2 \lambda^2 - 9a^2 c \lambda^3 + 3a^2 \lambda^4 + \frac{1}{16} a b^4 c \\ &- \frac{1}{16} a b^4 \lambda + a b^2 c^2 \lambda - 2a b^2 c \lambda^2 + a b^2 \lambda^3 + 3a c^3 \lambda^2 - 9a c^2 \lambda^3 + 9a c \lambda^4 \\ &- 3a \lambda^5 - \frac{1}{16} b^4 c \lambda + \frac{1}{16} b^4 \lambda^2 - \frac{1}{2} b^2 c^2 \lambda^2 + b^2 c \lambda^3 - \frac{1}{2} b^2 \lambda^4 - c^3 \lambda^3 + 3c^2 \lambda^4 \\ &- 3c \lambda^5 + \lambda^6 \ . \end{aligned} \tag{5.72}$$

Solving $\mathrm{Char}(Q, \lambda) = 0$ yields the eigenvalues

$$\begin{aligned} \lambda_1 &:= a \\ \lambda_2 &:= c \\ \lambda_{3/4} &:= \frac{1}{2} \left(a + c \pm \sqrt{(a-c)^2 + b^2} \right) \ , \end{aligned} \tag{5.73}$$

which are always real. However, some of them might not matter for the boundedness check. Looking at the Eq. (5.71) with λ set to λ_1

$$\begin{aligned} f_1\Big|_{\lambda=\lambda_1} &= \left(\frac{1}{2} b \cdot x y \right) y = 0 \\ f_2\Big|_{\lambda=\lambda_1} &= \left(c \cdot y^2 + \frac{1}{2} b \cdot x^2 - a \cdot y^2 \right) y = 0 \end{aligned} \tag{5.74}$$

one can see that $x \in \mathbb{R}$ and $y = 0$ will always be a solution. Hence, there are non-trivial real solutions and λ_1 is an H-eigenvalue. The same is true for λ_2 and $x = 0$, $y \in \mathbb{R}$.

The discussion for $\lambda_{3/4}$ is a bit more involved. For $b = 0$ there is only the trivial solution $x = y = 0$ when $a \neq c$. So $\lambda_{3/4}$ is no H-eigenvalue. For $b = 0$ and $a = c$, any vector $(x, y)^\top \in \mathbb{R}^2$ is a solution, thus making $\lambda_{3/4} = a = c$ an H-eigenvalue. The non-trivial real solutions for $b \neq 0$ are of the form

$$\begin{aligned} x &\in \mathbb{R} \\ y &= \pm\sqrt{\frac{(c - a + \sqrt{(a-c)^2 + b^2}\ ) \cdot x^2}{b}}\ . \end{aligned} \tag{5.75}$$

The inner square root will always be greater than $|c - a|$. So all non-trivial solutions ($x \neq 0$) for λ_3 will be real or complex depending on whether $b > 0$ or $b < 0$. Therefore, λ_3 is an H-eigenvalue if $b > 0$. In a similar way one can see that λ_4 is an H-eigenvalue if $b < 0$. In total there are four cases for which the boundedness constraints are

1. $b = 0$ and $a \neq c$:

$$\begin{aligned} \lambda_1 &= a > 0 \\ \lambda_2 &= c > 0 \end{aligned} \tag{5.76}$$

2. $b = 0$ and $a = c$:

$$\begin{aligned} \lambda_1 &= a > 0 \\ \lambda_2 &= c > 0 \\ \lambda_{3/4} &= \frac{1}{2}(a + c) = a = c > 0 \end{aligned} \tag{5.77}$$

3. $b > 0$:

$$\begin{aligned} \lambda_1 &= a > 0 \\ \lambda_2 &= c > 0 \\ \lambda_3 &= \frac{1}{2}\left(a + c + \sqrt{(a-c)^2 + b^2}\right) > 0 \end{aligned} \tag{5.78}$$

4. $b < 0$:

$$\begin{aligned} \lambda_1 &= a > 0 \\ \lambda_2 &= c > 0 \\ \lambda_4 &= \frac{1}{2}\left(a + c - \sqrt{(a-c)^2 + b^2}\right) > 0 \end{aligned} \tag{5.79}$$

All of those cases effectively reduce to the constraint $a > 0$ and $c > 0$ except for the last one, which adds another constraint $b + 2\sqrt{ac} > 0$.

The important thing to observe is that the feature of an eigenvalue being an H-eigenvalue can change based on the actual numerical value of the Higgs potential parameters. In this example the different parameter space regions can be derived easily. However, due to the reason of them being solutions to polynomial equations and the Abel-Ruffini theorem (see Section 5.5), there might not even be a simple analytic expression of the points of change (here $a = c$ or $b = 0$) nor of the eigenvalues themselves.

It is thus in general not feasible to derive analytic constraints in terms of inequalities. They simply might not exist for a given Higgs potential. The only analytic expression that does encode all information about boundedness in all cases is the characteristic polynomial.

5.7 Future Work

The previous sections raised some open problems or possibilities for improvement. In the following, some of these questions will be addressed. The presented algorithm of Section 5.5 is capable of constructing boundedness constraints for any Higgs potential. The bottleneck of runtime is the calculation of the characteristic polynomial. There are essentially four different approaches that may increase the speed drastically.

Firstly, the current implementation of BFB [4] uses no parallelization even though there is great potential to do so. This is mainly because the whole calculation of the resultant has been outsourced to the computer algebra system Macaulay2 [44]. There are two critical algorithms that may be subject to improvement: the calculation of Gröbner bases and the calculation of the resultant. Both of them are under steady investigation of the mathematical community. For Gröbner bases there are Faugére's algorithms F4 [48] and F5 [49] both of which are highly parallelizable. Macaulay2 includes already four different algorithms for the calculation of the resultant. The presented algorithm of Section 5.3.5 from [38, theorem 3.4] is one of them. Part of it is the calculation of the intermediate matrices $M_1, \bar{M}_2$, etc. Currently, the elements are obtained in a linear way on one CPU only. However, each row can be calculated independently. For the 2HDM test of Section 5.6 M_1 already has 81 rows, so here is a huge potential for parallelization. Also, the calculation of the basis of the quotient ring is a simple scan through low degree polynomials and can be distributed over any number of cores. Macaulay2 implements also the classic algorithm by Macaulay [40]. It is less space efficient but may be more time efficient when it comes to the calculation

of resultants of polynomials with many variables. Furthermore, Macaulay2 implements a variation of these two algorithms that makes use of polynomial interpolation (see for instance [50] and [51]).

Secondly, as one can probably already conclude, not only the possibility of parallelization may speed up the process of resultant calculations, but the choice of the respective algorithm as well. There is a multitude of publications on this topic. Depending on the specific form of the input polynomials there might exist much faster algorithms than the presented ones. For instance, Macaulay proposed a modified version of his algorithm that can be used if all polynomials share the same degree [52]. This is applicable to the current case of Higgs potential boundedness and should definitely be tested. It is this approach that might bypass the NP-hardness [39] of resultant calculations.

Thirdly, for the 2HDM tests of Section 5.6 it has been shown that the SU(2) symmetry of the Higgs potential can be used to reduce the complexity of the problem from 8 to 5 variables. It is plausible that additional symmetries of higher order Higgs potentials (N2HDM, 3HDM, etc.) can be exploited in a similar way. This holds for discrete symmetries, too. Furthermore, as has been discussed in Section 5.4.3, the problem of deciding positive definiteness is $\mathrm{O}(n)$ invariant. This symmetry appears independently to the ones of the Higgs potential and might result in a further reduction of variables. In this context, the E-eigenvalues of Section 5.4.1 are of special importance because they are invariant under orthogonal transformations while H-eigenvalues do not possess this feature. By choosing a transformation that is block diagonal with submatrices

$$\begin{pmatrix} \cos(\alpha) & -\sin(\alpha) \\ \sin(\alpha) & \cos(\alpha) \end{pmatrix} , \tag{5.80}$$

one can always rotate one variable to zero. The resulting problem will be another decision problem of positive definiteness of now $n-1$ variables. However, the new tensor Q' will have a much more complicated dependence on analytic parameters such as the rotation angles α. There are algorithms that operate faster on less variables even though there was a trade-off in the complexity of analytic coefficients. The problematic part will then be the test of regularity of Q' (see Section 5.4.2). It is not clear whether or not the approach with E-eigenvalues can actually be faster.

Lastly, in Section 5.6 for the 2HDM test it has been stated that choosing the ring of integers as polynomial coefficients can change the runtime. Rational numbers $\mathbb{Q}$ might be the worst choice because they incorporate an inefficient division algorithm (finding greatest common divisors etc.) and have a bad scaling with powers (numerator and denominator can get very large). Integers $\mathbb{Z}$ are more efficient when it comes to the used division operations (modulo operations) but still possess a bad scaling with powers. Macaulay2

only allows for these two options. The field of real numbers $\mathbb{R}$ may be an intermediate solution that trades accuracy for runtime. The division algorithm is not as fast as for integers but calculations of powers are faster and more space efficient (floating point numbers store powers separately). Currently there exists no implementation of resultant algorithms that work with both analytic parameters and real numbers. There is a working framework called MARS [53] that can handle the calculation of the resultant numerically. It is possible to perform a scan over a bounded range of values for the eigenvalues λ and test for the numerical vanishing of the resultant. This is very unstable though, since the resultant is in general a high degree polynomial in λ and accuracy will play an important role here. Nevertheless, this is a feasible approach.

The long term goal is to have an algorithm that can produce the analytic form of the characteristic polynomial for many different Higgs potentials (steps 1 to 4 in Section 5.5). These polynomials can then be published and distributed for fast checks of boundedness. Without some effort in parallelization and other optimizations and possibly some advances in the field of elimination theory, this will not be possible. So the intermediate goal is to have a fast, reliable, numerical check of boundedness. The presented approaches are promising and will be applied to the case of the 3HDM in the future.

Chapter 6

Conclusion

In the first part of this thesis an introduction to GCP transformations was given. The two 3HDMs under consideration, the DM CP4 3HDM which has a GCP symmetry and the DIDM which has an ordinary CP symmetry, were introduced.

The phenomenological comparison of both models was done in Chapter 4. The DM relic density scans with a minimum mass splitting of 1 GeV between the DM candidate and the next-to-lightest scalar showed the following:

- The relic density does not depend on the quartic coupling parameters λ_2, λ_3', λ_4', λ_8 and λ_9 of the DM CP4 3HDM.
- The DM CP4 3HDM and the DIDM are completely equivalent in terms of the relic density.

Therefore, the GCP structure is not important here. However, smaller mass splittings are currently investigated and are likely to show a difference between the models.

Collider observables have not been considered in this thesis, because they are unlikely to show a measurable difference between the models. The main difference is in the quartic couplings, which are difficult to probe for inert models.

In the analysis of the perturbative unitarity constraints of the DM CP4 3HDM, the following was found:

- The unitarity constraints of λ_6 do not depend on the parameters λ_3', λ_4', λ_8 and λ_9.
- The unitarity constraints of λ_2 do depend on all the parameters λ_3', λ_4', λ_8 and λ_9.

- The unitarity constraints of λ_1, λ_3 and λ_4 do depend on λ_3' and λ_4' but not on λ_8 and λ_9.
- The unitarity constraints of the DM CP4 3HDM can be stronger or weaker compared to the ones of the DIDM depending on the values of λ_3', λ_4', λ_8 and λ_9.

Therefore, unitarity constraints possess the potential of distinguishing between the DM CP4 3HDM and the DIDM and the respective GCP structure encoded in the quartic couplings. For instance, a given point in parameter space that is excluded in the DIDM can still be allowed in the DM CP4 3HDM, ruling out the DIDM but not the DM CP4 3HDM even though they are very similar in terms of collider and astrophysical observables. Also, one should try to probe for the parameters λ_3' and λ_4' because they can influence the constraints of masses and trilinear couplings. The parameters λ_8 and λ_9 are less significant in terms of phenomenological considerations.

It is plausible that a similar picture would emerge for boundedness constraints. However, this hypothesis could not be tested here, because there are currently no necessary and sufficient conditions for boundedness of the Higgs potentials of both models. An attempt has been made in Chapter 5 to find these conditions with a completely new method that can be applied to any multi-Higgs model. Currently, the implementation of BFB [4] is lacking the speed to calculate the constraints. In [54], a different problem for the NMSSM Higgs sector has been demonstrated to be solvable with multivariate polynomial division algorithms. The restrictions of these algorithms and the one presented in Section 5.5 are very similar. Hence, the vast possibilities for improvement described in Section 5.7 are promising. Calculating the boundedness constraints of 3HDMs is a feasible task that will be completed in the future.

Part II

Appendix

Appendix A

Feynman Rules

The vertex factors in the tables below were generated with the Mathematica package PUC [5]. For further reference see also Appendix B.1. For vertices with a derivative another momentum factor of ip_μ or $-ip_\mu$ has to be added depending on whether there is an incoming or outgoing (anti-) particle. The Mathematica functions and symbols have the following meaning:

$$\begin{aligned}
&\text{Abs}[x] \to |x| && \text{(absolute value of } x\text{)} \\
&\text{Conjugate}[x] \to x^* && \text{(complex conjugate of } x\text{)} \\
&\text{Csc}[x] \to \frac{1}{\sin(x)} && \text{(cosecant of } x\text{)} \\
&\text{Sec}[x] \to \frac{1}{\cos(x)} && \text{(secant of } x\text{)} \\
&\text{Cot}[x] \to \frac{\cos(x)}{\sin(x)} && \text{(cotangent of } x\text{) .}
\end{aligned} \tag{A.1}$$

Also, $\mathrm{e_{EM}}$ is the electromagnetic charge of the positron, θ_W is the Weinberg angle and $g^{\mu\nu} = \mathrm{diag}(1, -1, -1, -1)$ is the Minkowski metric.

A.1 DM CP4 3HDM

The particle labels in the following differ from the ones used in Section 3.2:

$$\begin{aligned}
h_2 &= h \\
a_2 &= a \\
h_3 &= H \\
a_3 &= A \ .
\end{aligned} \tag{A.2}$$

They were chosen such that there is no confusion regarding the photon label A_μ. Also, $\hat{\lambda}_3$ is λ'_3 and $\hat{\lambda}_4$ is λ'_4.

Table A.1: Table of 3-vertex Feynman rules for the DM CP4 3HDM

$-6\,i\,\text{Abs}[m_{1,1}]\,\sqrt{\lambda_1}$	$\{h_{SM}, h_{SM}, h_{SM}\}$
$-\frac{i\,\text{Abs}[m_{1,1}]\,(\lambda_3+\lambda_4-\lambda_6)}{\sqrt{\lambda_1}}$	$\{h_{SM}, h_2, h_2\}$
$-\frac{i\,\text{Abs}[m_{1,1}]\,(\lambda_3+\lambda_4-\lambda_6)}{\sqrt{\lambda_1}}$	$\{h_{SM}, a_2, a_2\}$
$-\frac{i\,\text{Abs}[m_{1,1}]\,(\lambda_3+\lambda_4+\lambda_6)}{\sqrt{\lambda_1}}$	$\{h_{SM}, h_3, h_3\}$
$-\frac{i\,\text{Abs}[m_{1,1}]\,(\lambda_3+\lambda_4+\lambda_6)}{\sqrt{\lambda_1}}$	$\{h_{SM}, a_3, a_3\}$
$-\frac{i\,\text{Abs}[m_{1,1}]\,\lambda_3}{\sqrt{\lambda_1}}$	$\{h_{SM}, H_2^+, H_2^-\}$
$-\frac{i\,\text{Abs}[m_{1,1}]\,\lambda_3}{\sqrt{\lambda_1}}$	$\{h_{SM}, H_3^+, H_3^-\}$
$\frac{i\,\text{Abs}[m_{1,1}]\,\text{Csc}[\theta_W]^2\,e_{EM}^2}{2\sqrt{\lambda_1}}\,g^{\mu\nu}$	$\{h_{SM}, W_\mu^+, W_\nu^-\}$
$\frac{2\,i\,\text{Abs}[m_{1,1}]\,\text{Csc}[2\,\theta_W]^2\,e_{EM}^2}{\sqrt{\lambda_1}}\,g^{\mu\nu}$	$\{h_{SM}, Z_\mu, Z_\nu\}$
$-i\,\text{Csc}[2\,\theta_W]\,e_{EM}\,g^{\mu\nu}$	$\{h_2, \partial_\mu a_3, Z_\nu\}$
$\frac{1}{2}\,\text{Csc}[\theta_W]\,e_{EM}\,g^{\mu\nu}$	$\{h_2, \partial_\mu H_3^+, W_\nu^-\}$
$-\frac{1}{2}\,\text{Csc}[\theta_W]\,e_{EM}\,g^{\mu\nu}$	$\{h_2, \partial_\mu H_3^-, W_\nu^+\}$
$i\,\text{Csc}[2\,\theta_W]\,e_{EM}\,g^{\mu\nu}$	$\{a_2, \partial_\mu h_3, Z_\nu\}$
$-\frac{1}{2}\,i\,\text{Csc}[\theta_W]\,e_{EM}\,g^{\mu\nu}$	$\{a_2, \partial_\mu H_2^+, W_\nu^-\}$
$-\frac{1}{2}\,i\,\text{Csc}[\theta_W]\,e_{EM}\,g^{\mu\nu}$	$\{a_2, \partial_\mu H_2^-, W_\nu^+\}$
$-i\,\text{Csc}[2\,\theta_W]\,e_{EM}\,g^{\mu\nu}$	$\{h_3, \partial_\mu a_2, Z_\nu\}$
$\frac{1}{2}\,\text{Csc}[\theta_W]\,e_{EM}\,g^{\mu\nu}$	$\{h_3, \partial_\mu H_2^+, W_\nu^-\}$
$-\frac{1}{2}\,\text{Csc}[\theta_W]\,e_{EM}\,g^{\mu\nu}$	$\{h_3, \partial_\mu H_2^-, W_\nu^+\}$
$i\,\text{Csc}[2\,\theta_W]\,e_{EM}\,g^{\mu\nu}$	$\{a_3, \partial_\mu h_2, Z_\nu\}$
$-\frac{1}{2}\,i\,\text{Csc}[\theta_W]\,e_{EM}\,g^{\mu\nu}$	$\{a_3, \partial_\mu H_3^+, W_\nu^-\}$
$-\frac{1}{2}\,i\,\text{Csc}[\theta_W]\,e_{EM}\,g^{\mu\nu}$	$\{a_3, \partial_\mu H_3^-, W_\nu^+\}$
$\frac{1}{2}\,i\,\text{Csc}[\theta_W]\,e_{EM}\,g^{\mu\nu}$	$\{H_2^+, \partial_\mu a_2, W_\nu^-\}$
$-\frac{1}{2}\,\text{Csc}[\theta_W]\,e_{EM}\,g^{\mu\nu}$	$\{H_2^+, \partial_\mu h_3, W_\nu^-\}$
$-\text{Cot}[2\,\theta_W]\,e_{EM}\,g^{\mu\nu}$	$\{H_2^+, \partial_\mu H_2^-, Z_\nu\}$
$-e_{EM}\,g^{\mu\nu}$	$\{H_2^+, \partial_\mu H_2^-, A_\nu\}$
$\frac{1}{2}\,i\,\text{Csc}[\theta_W]\,e_{EM}\,g^{\mu\nu}$	$\{H_2^-, \partial_\mu a_2, W_\nu^+\}$
$\frac{1}{2}\,\text{Csc}[\theta_W]\,e_{EM}\,g^{\mu\nu}$	$\{H_2^-, \partial_\mu h_3, W_\nu^+\}$
$\text{Cot}[2\,\theta_W]\,e_{EM}\,g^{\mu\nu}$	$\{H_2^-, \partial_\mu H_2^+, Z_\nu\}$
$e_{EM}\,g^{\mu\nu}$	$\{H_2^-, \partial_\mu H_2^+, A_\nu\}$
$-\frac{1}{2}\,\text{Csc}[\theta_W]\,e_{EM}\,g^{\mu\nu}$	$\{H_3^+, \partial_\mu h_2, W_\nu^-\}$
$\frac{1}{2}\,i\,\text{Csc}[\theta_W]\,e_{EM}\,g^{\mu\nu}$	$\{H_3^+, \partial_\mu a_3, W_\nu^-\}$
$-\text{Cot}[2\,\theta_W]\,e_{EM}\,g^{\mu\nu}$	$\{H_3^+, \partial_\mu H_3^-, Z_\nu\}$
$-e_{EM}\,g^{\mu\nu}$	$\{H_3^+, \partial_\mu H_3^-, A_\nu\}$
$\frac{1}{2}\,\text{Csc}[\theta_W]\,e_{EM}\,g^{\mu\nu}$	$\{H_3^-, \partial_\mu h_2, W_\nu^+\}$
$\frac{1}{2}\,i\,\text{Csc}[\theta_W]\,e_{EM}\,g^{\mu\nu}$	$\{H_3^-, \partial_\mu a_3, W_\nu^+\}$
$\text{Cot}[2\,\theta_W]\,e_{EM}\,g^{\mu\nu}$	$\{H_3^-, \partial_\mu H_3^+, Z_\nu\}$
$e_{EM}\,g^{\mu\nu}$	$\{H_3^-, \partial_\mu H_3^+, A_\nu\}$

Table A.2: Table of 4-vertex Feynman rules for the DM CP4 3HDM

$-6\,i\,\lambda_1$	$\{h_{SM}, h_{SM}, h_{SM}, h_{SM}\}$
$-i\,(\lambda_3+\lambda_4-\lambda_6)$	$\{h_{SM}, h_{SM}, h_2, h_2\}$
$-i\,(\lambda_3+\lambda_4-\lambda_6)$	$\{h_{SM}, h_{SM}, a_2, a_2\}$
$-i\,(\lambda_3+\lambda_4+\lambda_6)$	$\{h_{SM}, h_{SM}, h_3, h_3\}$
$-i\,(\lambda_3+\lambda_4+\lambda_6)$	$\{h_{SM}, h_{SM}, a_3, a_3\}$
$-i\,\lambda_3$	$\{h_{SM}, h_{SM}, H_2^+, H_2^-\}$
$-i\,\lambda_3$	$\{h_{SM}, h_{SM}, H_3^+, H_3^-\}$
$-6\,i\,\lambda_2$	$\{h_2, h_2, h_2, h_2\}$
$-\frac{3}{2}\left(\text{Conjugate}[\lambda_9]-\lambda_9\right)$	$\{h_2, h_2, h_2, a_2\}$
$\frac{3}{2}\,i\left(\text{Conjugate}[\lambda_9]+\lambda_9\right)$	$\{h_2, h_2, h_2, h_3\}$
$-i\left(-\text{Conjugate}[\lambda_8]+\hat{\lambda_3}+\hat{\lambda_4}-\lambda_8\right)$	$\{h_2, h_2, a_2, a_2\}$
$\text{Conjugate}[\lambda_8]-\lambda_8$	$\{h_2, h_2, a_2, h_3\}$
$-\frac{1}{2}\,i\left(-\text{Conjugate}[\lambda_9]-\lambda_9\right)$	$\{h_2, h_2, a_2, a_3\}$
$-i\left(\text{Conjugate}[\lambda_8]+\hat{\lambda_3}+\hat{\lambda_4}+\lambda_8\right)$	$\{h_2, h_2, h_3, h_3\}$
$\frac{1}{2}\left(\text{Conjugate}[\lambda_9]-\lambda_9\right)$	$\{h_2, h_2, h_3, a_3\}$
$-2\,i\,\lambda_2$	$\{h_2, h_2, a_3, a_3\}$
$-i\,\hat{\lambda_3}$	$\{h_2, h_2, H_2^+, H_2^-\}$
$i\,\text{Conjugate}[\lambda_9]$	$\{h_2, h_2, H_2^+, H_3^-\}$
$i\,\lambda_9$	$\{h_2, h_2, H_2^-, H_3^+\}$
$-2\,i\,\lambda_2$	$\{h_2, h_2, H_3^+, H_3^-\}$
$\frac{3}{2}\left(\text{Conjugate}[\lambda_9]-\lambda_9\right)$	$\{h_2, a_2, a_2, a_2\}$
$-\frac{1}{2}\,i\left(\text{Conjugate}[\lambda_9]+\lambda_9\right)$	$\{h_2, a_2, a_2, h_3\}$
$\text{Conjugate}[\lambda_8]-\lambda_8$	$\{h_2, a_2, a_2, a_3\}$
$\frac{1}{2}\left(\text{Conjugate}[\lambda_9]-\lambda_9\right)$	$\{h_2, a_2, h_3, h_3\}$
$-i\left(\text{Conjugate}[\lambda_8]+\lambda_8\right)$	$\{h_2, a_2, h_3, a_3\}$
$\frac{1}{2}\left(-\text{Conjugate}[\lambda_9]+\lambda_9\right)$	$\{h_2, a_2, a_3, a_3\}$
$\frac{1}{2}\left(\text{Conjugate}[\lambda_9]-\lambda_9\right)$	$\{h_2, a_2, H_2^+, H_2^-\}$
$\frac{1}{2}\left(2\,\text{Conjugate}[\lambda_8]-\hat{\lambda_4}\right)$	$\{h_2, a_2, H_2^+, H_3^-\}$
$\frac{1}{2}\left(\hat{\lambda_4}-2\,\lambda_8\right)$	$\{h_2, a_2, H_2^-, H_3^+\}$
$\frac{1}{2}\left(-\text{Conjugate}[\lambda_9]+\lambda_9\right)$	$\{h_2, a_2, H_3^+, H_3^-\}$
$-\frac{3}{2}\,i\left(\text{Conjugate}[\lambda_9]+\lambda_9\right)$	$\{h_2, h_3, h_3, h_3\}$
$-\text{Conjugate}[\lambda_8]+\lambda_8$	$\{h_2, h_3, h_3, a_3\}$
$-\frac{1}{2}\,i\left(-\text{Conjugate}[\lambda_9]-\lambda_9\right)$	$\{h_2, h_3, a_3, a_3\}$
$-\frac{1}{2}\,i\left(\text{Conjugate}[\lambda_9]+\lambda_9\right)$	$\{h_2, h_3, H_2^+, H_2^-\}$
$-i\left(\text{Conjugate}[\lambda_8]+\frac{\hat{\lambda_4}}{2}\right)$	$\{h_2, h_3, H_2^+, H_3^-\}$
$-i\left(\frac{\hat{\lambda_4}}{2}+\lambda_8\right)$	$\{h_2, h_3, H_2^-, H_3^+\}$
$-\frac{1}{2}\,i\left(-\text{Conjugate}[\lambda_9]-\lambda_9\right)$	$\{h_2, h_3, H_3^+, H_3^-\}$
$-6\,i\,\lambda_2$	$\{a_2, a_2, a_2, a_2\}$
$-\frac{3}{2}\,i\left(\text{Conjugate}[\lambda_9]+\lambda_9\right)$	$\{a_2, a_2, a_2, a_3\}$
$-2\,i\,\lambda_2$	$\{a_2, a_2, h_3, h_3\}$
$\frac{1}{2}\left(-\text{Conjugate}[\lambda_9]+\lambda_9\right)$	$\{a_2, a_2, h_3, a_3\}$
$-i\left(\text{Conjugate}[\lambda_8]+\hat{\lambda_3}+\hat{\lambda_4}+\lambda_8\right)$	$\{a_2, a_2, a_3, a_3\}$
$-2\,i\,\lambda_2$	$\{a_2, a_2, H_2^+, H_2^-\}$
$-i\,\text{Conjugate}[\lambda_9]$	$\{a_2, a_2, H_2^+, H_3^-\}$
$-i\,\lambda_9$	$\{a_2, a_2, H_2^-, H_3^+\}$
$-i\,\hat{\lambda_3}$	$\{a_2, a_2, H_3^+, H_3^-\}$
$-\frac{1}{2}\,i\left(\text{Conjugate}[\lambda_9]+\lambda_9\right)$	$\{a_2, h_3, h_3, a_3\}$
$-\text{Conjugate}[\lambda_8]+\lambda_8$	$\{a_2, h_3, a_3, a_3\}$
$\frac{3}{2}\,i\left(\text{Conjugate}[\lambda_9]+\lambda_9\right)$	$\{a_2, a_3, a_3, a_3\}$
$-\frac{1}{2}\,i\left(\text{Conjugate}[\lambda_9]+\lambda_9\right)$	$\{a_2, a_3, H_2^+, H_2^-\}$
$-i\left(\text{Conjugate}[\lambda_8]+\frac{\hat{\lambda_4}}{2}\right)$	$\{a_2, a_3, H_2^+, H_3^-\}$
$-i\left(\frac{\hat{\lambda_4}}{2}+\lambda_8\right)$	$\{a_2, a_3, H_2^-, H_3^+\}$
$-\frac{1}{2}\,i\left(-\text{Conjugate}[\lambda_9]-\lambda_9\right)$	$\{a_2, a_3, H_3^+, H_3^-\}$
$-6\,i\,\lambda_2$	$\{h_3, h_3, h_3, h_3\}$
$-\frac{3}{2}\left(\text{Conjugate}[\lambda_9]-\lambda_9\right)$	$\{h_3, h_3, h_3, a_3\}$
$-i\left(-\text{Conjugate}[\lambda_8]+\hat{\lambda_3}+\hat{\lambda_4}-\lambda_8\right)$	$\{h_3, h_3, a_3, a_3\}$
$-2\,i\,\lambda_2$	$\{h_3, h_3, H_2^+, H_2^-\}$
$-i\,\text{Conjugate}[\lambda_9]$	$\{h_3, h_3, H_2^+, H_3^-\}$
$-i\,\lambda_9$	$\{h_3, h_3, H_2^-, H_3^+\}$
$-i\,\hat{\lambda_3}$	$\{h_3, h_3, H_3^+, H_3^-\}$

Table A.3: Table of 4-vertex Feynman rules for the DM CP4 3HDM

$\frac{3}{2}\left(\text{Conjugate}[\lambda_9]-\lambda_9\right)$	$\{h_3, a_3, a_3, a_3\}$
$\frac{1}{2}\left(-\text{Conjugate}[\lambda_9]+\lambda_9\right)$	$\{h_3, a_3, H_2^+, H_2^-\}$
$-i\left(-i\,\text{Conjugate}[\lambda_8]+\frac{i\hat{\lambda}_4}{2}\right)$	$\{h_3, a_3, H_2^+, H_3^-\}$
$\frac{1}{2}\left(-\hat{\lambda}_4+2\lambda_8\right)$	$\{h_3, a_3, H_2^-, H_3^+\}$
$\frac{1}{2}\left(\text{Conjugate}[\lambda_9]-\lambda_9\right)$	$\{h_3, a_3, H_3^+, H_3^-\}$
$-6\,i\,\lambda_2$	$\{a_3, a_3, a_3, a_3\}$
$-i\,\hat{\lambda}_3$	$\{a_3, a_3, H_2^+, H_2^-\}$
$i\,\text{Conjugate}[\lambda_9]$	$\{a_3, a_3, H_2^+, H_3^-\}$
$i\,\lambda_9$	$\{a_3, a_3, H_2^-, H_3^+\}$
$-2\,i\,\lambda_2$	$\{a_3, a_3, H_3^+, H_3^-\}$
$-4\,i\,\lambda_2$	$\{H_2^+, H_2^+, H_2^-, H_2^-\}$
$-2\,i\,\text{Conjugate}[\lambda_9]$	$\{H_2^+, H_2^+, H_2^-, H_3^-\}$
$-4\,i\,\text{Conjugate}[\lambda_8]$	$\{H_2^+, H_2^+, H_3^-, H_3^-\}$
$-2\,i\,\lambda_9$	$\{H_2^+, H_2^-, H_2^-, H_3^+\}$
$-i\left(\hat{\lambda}_3+\hat{\lambda}_4\right)$	$\{H_2^+, H_2^-, H_3^+, H_3^-\}$
$2\,i\,\text{Conjugate}[\lambda_9]$	$\{H_2^+, H_3^+, H_3^-, H_3^-\}$
$-4\,i\,\lambda_8$	$\{H_2^-, H_2^-, H_3^+, H_3^+\}$
$2\,i\,\lambda_9$	$\{H_2^-, H_3^+, H_3^+, H_3^-\}$
$-4\,i\,\lambda_2$	$\{H_3^+, H_3^+, H_3^-, H_3^-\}$
$\frac{1}{2}\,i\,\text{Csc}[\theta_W]^2\,e_{EM}^2\,g^{\mu\nu}$	$\{h_{SM}, h_{SM}, W_\mu^+, W_\nu^-\}$
$2\,i\,\text{Csc}[2\,\theta_W]^2\,e_{EM}^2\,g^{\mu\nu}$	$\{h_{SM}, h_{SM}, Z_\mu, Z_\nu\}$
$\frac{1}{2}\,i\,\text{Csc}[\theta_W]^2\,e_{EM}^2\,g^{\mu\nu}$	$\{h_2, h_2, W_\mu^+, W_\nu^-\}$
$2\,i\,\text{Csc}[2\,\theta_W]^2\,e_{EM}^2\,g^{\mu\nu}$	$\{h_2, h_2, Z_\mu, Z_\nu\}$
$-\frac{1}{2}\,i\,\text{Sec}[\theta_W]\,e_{EM}^2\,g^{\mu\nu}$	$\{h_2, H_3^+, W_\mu^-, Z_\nu\}$
$\frac{1}{2}\,i\,\text{Csc}[\theta_W]\,e_{EM}^2\,g^{\mu\nu}$	$\{h_2, H_3^+, W_\mu^-, A_\nu\}$
$-\frac{1}{2}\,i\,\text{Sec}[\theta_W]\,e_{EM}^2\,g^{\mu\nu}$	$\{h_2, H_3^-, W_\mu^+, Z_\nu\}$
$\frac{1}{2}\,i\,\text{Csc}[\theta_W]\,e_{EM}^2\,g^{\mu\nu}$	$\{h_2, H_3^-, W_\mu^+, A_\nu\}$
$\frac{1}{2}\,i\,\text{Csc}[\theta_W]^2\,e_{EM}^2\,g^{\mu\nu}$	$\{a_2, a_2, W_\mu^+, W_\nu^-\}$
$2\,i\,\text{Csc}[2\,\theta_W]^2\,e_{EM}^2\,g^{\mu\nu}$	$\{a_2, a_2, Z_\mu, Z_\nu\}$
$-\frac{1}{2}\,\text{Sec}[\theta_W]\,e_{EM}^2\,g^{\mu\nu}$	$\{a_2, H_2^+, W_\mu^-, Z_\nu\}$
$\frac{1}{2}\,\text{Csc}[\theta_W]\,e_{EM}^2\,g^{\mu\nu}$	$\{a_2, H_2^+, W_\mu^-, A_\nu\}$
$\frac{1}{2}\,\text{Sec}[\theta_W]\,e_{EM}^2\,g^{\mu\nu}$	$\{a_2, H_2^-, W_\mu^+, Z_\nu\}$
$-\frac{1}{2}\,\text{Csc}[\theta_W]\,e_{EM}^2\,g^{\mu\nu}$	$\{a_2, H_2^-, W_\mu^+, A_\nu\}$
$\frac{1}{2}\,i\,\text{Csc}[\theta_W]^2\,e_{EM}^2\,g^{\mu\nu}$	$\{h_3, h_3, W_\mu^+, W_\nu^-\}$
$2\,i\,\text{Csc}[2\,\theta_W]^2\,e_{EM}^2\,g^{\mu\nu}$	$\{h_3, h_3, Z_\mu, Z_\nu\}$
$-\frac{1}{2}\,i\,\text{Sec}[\theta_W]\,e_{EM}^2\,g^{\mu\nu}$	$\{h_3, H_2^+, W_\mu^-, Z_\nu\}$
$\frac{1}{2}\,i\,\text{Csc}[\theta_W]\,e_{EM}^2\,g^{\mu\nu}$	$\{h_3, H_2^+, W_\mu^-, A_\nu\}$
$-\frac{1}{2}\,i\,\text{Sec}[\theta_W]\,e_{EM}^2\,g^{\mu\nu}$	$\{h_3, H_2^-, W_\mu^+, Z_\nu\}$
$\frac{1}{2}\,i\,\text{Csc}[\theta_W]\,e_{EM}^2\,g^{\mu\nu}$	$\{h_3, H_2^-, W_\mu^+, A_\nu\}$
$\frac{1}{2}\,i\,\text{Csc}[\theta_W]^2\,e_{EM}^2\,g^{\mu\nu}$	$\{a_3, a_3, W_\mu^+, W_\nu^-\}$
$2\,i\,\text{Csc}[2\,\theta_W]^2\,e_{EM}^2\,g^{\mu\nu}$	$\{a_3, a_3, Z_\mu, Z_\nu\}$
$-\frac{1}{2}\,\text{Sec}[\theta_W]\,e_{EM}^2\,g^{\mu\nu}$	$\{a_3, H_3^+, W_\mu^-, Z_\nu\}$
$\frac{1}{2}\,\text{Csc}[\theta_W]\,e_{EM}^2\,g^{\mu\nu}$	$\{a_3, H_3^+, W_\mu^-, A_\nu\}$
$\frac{1}{2}\,\text{Sec}[\theta_W]\,e_{EM}^2\,g^{\mu\nu}$	$\{a_3, H_3^-, W_\mu^+, Z_\nu\}$
$-\frac{1}{2}\,\text{Csc}[\theta_W]\,e_{EM}^2\,g^{\mu\nu}$	$\{a_3, H_3^-, W_\mu^+, A_\nu\}$
$\frac{1}{2}\,i\,\text{Csc}[\theta_W]^2\,e_{EM}^2\,g^{\mu\nu}$	$\{H_2^+, H_2^-, W_\mu^+, W_\nu^-\}$
$2\,i\,\text{Cot}[2\,\theta_W]^2\,e_{EM}^2\,g^{\mu\nu}$	$\{H_2^+, H_2^-, Z_\mu, Z_\nu\}$
$2\,i\,\text{Cot}[2\,\theta_W]\,e_{EM}^2\,g^{\mu\nu}$	$\{H_2^+, H_2^-, Z_\mu, A_\nu\}$
$2\,i\,e_{EM}^2\,g^{\mu\nu}$	$\{H_2^+, H_2^-, A_\mu, A_\nu\}$
$\frac{1}{2}\,i\,\text{Csc}[\theta_W]^2\,e_{EM}^2\,g^{\mu\nu}$	$\{H_3^+, H_3^-, W_\mu^+, W_\nu^-\}$
$2\,i\,\text{Cot}[2\,\theta_W]^2\,e_{EM}^2\,g^{\mu\nu}$	$\{H_3^+, H_3^-, Z_\mu, Z_\nu\}$
$2\,i\,\text{Cot}[2\,\theta_W]\,e_{EM}^2\,g^{\mu\nu}$	$\{H_3^+, H_3^-, Z_\mu, A_\nu\}$
$2\,i\,e_{EM}^2\,g^{\mu\nu}$	$\{H_3^+, H_3^-, A_\mu, A_\nu\}$

A.2 DIDM

Table A.4: Table of 3-vertex Feynman rules for the DIDM

$-6\,i\,\text{Abs}[m_{1,1}]\,\sqrt{\lambda_1}$	$\{h_{SM}, h_{SM}, h_{SM}\}$
$-\frac{i\,\text{Abs}[m_{1,1}]\,(\lambda_3+\lambda_4-\lambda_6)}{\sqrt{\lambda_1}}$	$\{h_{SM}, h_2, h_2\}$
$-\frac{i\,\text{Abs}[m_{1,1}]\,(\lambda_3+\lambda_4+\lambda_6)}{\sqrt{\lambda_1}}$	$\{h_{SM}, a_2, a_2\}$
$-\frac{i\,\text{Abs}[m_{1,1}]\,(\lambda_3+\lambda_4-\lambda_6)}{\sqrt{\lambda_1}}$	$\{h_{SM}, h_3, h_3\}$
$-\frac{i\,\text{Abs}[m_{1,1}]\,(\lambda_3+\lambda_4+\lambda_6)}{\sqrt{\lambda_1}}$	$\{h_{SM}, a_3, a_3\}$
$-\frac{i\,\text{Abs}[m_{1,1}]\,\lambda_3}{\sqrt{\lambda_1}}$	$\{h_{SM}, H_2^+, H_2^-\}$
$-\frac{i\,\text{Abs}[m_{1,1}]\,\lambda_3}{\sqrt{\lambda_1}}$	$\{h_{SM}, H_3^+, H_3^-\}$
$\frac{i\,\text{Abs}[m_{1,1}]\,\text{Csc}[\theta_W]^2\,e_{EM}^2}{2\sqrt{\lambda_1}}\,g^{\mu\nu}$	$\{h_{SM}, W_\mu^+, W_\nu^-\}$
$\frac{2\,i\,\text{Abs}[m_{1,1}]\,\text{Csc}[2\,\theta_W]^2\,e_{EM}^2}{\sqrt{\lambda_1}}\,g^{\mu\nu}$	$\{h_{SM}, Z_\mu, Z_\nu\}$
$-i\,\text{Csc}[2\,\theta_W]\,e_{EM}\,g^{\mu\nu}$	$\{h_2, \partial_\mu a_2, Z_\nu\}$
$\frac{1}{2}\,\text{Csc}[\theta_W]\,e_{EM}\,g^{\mu\nu}$	$\{h_2, \partial_\mu H_2^+, W_\nu^-\}$
$-\frac{1}{2}\,\text{Csc}[\theta_W]\,e_{EM}\,g^{\mu\nu}$	$\{h_2, \partial_\mu H_2^-, W_\nu^+\}$
$i\,\text{Csc}[2\,\theta_W]\,e_{EM}\,g^{\mu\nu}$	$\{a_2, \partial_\mu h_2, Z_\nu\}$
$-\frac{1}{2}\,i\,\text{Csc}[\theta_W]\,e_{EM}\,g^{\mu\nu}$	$\{a_2, \partial_\mu H_2^+, W_\nu^-\}$
$-\frac{1}{2}\,i\,\text{Csc}[\theta_W]\,e_{EM}\,g^{\mu\nu}$	$\{a_2, \partial_\mu H_2^-, W_\nu^+\}$
$-i\,\text{Csc}[2\,\theta_W]\,e_{EM}\,g^{\mu\nu}$	$\{h_3, \partial_\mu a_3, Z_\nu\}$
$\frac{1}{2}\,\text{Csc}[\theta_W]\,e_{EM}\,g^{\mu\nu}$	$\{h_3, \partial_\mu H_3^+, W_\nu^-\}$
$-\frac{1}{2}\,\text{Csc}[\theta_W]\,e_{EM}\,g^{\mu\nu}$	$\{h_3, \partial_\mu H_3^-, W_\nu^+\}$
$i\,\text{Csc}[2\,\theta_W]\,e_{EM}\,g^{\mu\nu}$	$\{a_3, \partial_\mu h_3, Z_\nu\}$
$-\frac{1}{2}\,i\,\text{Csc}[\theta_W]\,e_{EM}\,g^{\mu\nu}$	$\{a_3, \partial_\mu H_3^+, W_\nu^-\}$
$-\frac{1}{2}\,i\,\text{Csc}[\theta_W]\,e_{EM}\,g^{\mu\nu}$	$\{a_3, \partial_\mu H_3^-, W_\nu^+\}$
$-\frac{1}{2}\,\text{Csc}[\theta_W]\,e_{EM}\,g^{\mu\nu}$	$\{H_2^+, \partial_\mu h_2, W_\nu^-\}$
$\frac{1}{2}\,i\,\text{Csc}[\theta_W]\,e_{EM}\,g^{\mu\nu}$	$\{H_2^+, \partial_\mu a_2, W_\nu^-\}$
$-\text{Cot}[2\,\theta_W]\,e_{EM}\,g^{\mu\nu}$	$\{H_2^+, \partial_\mu H_2^-, Z_\nu\}$
$-e_{EM}\,g^{\mu\nu}$	$\{H_2^+, \partial_\mu H_2^-, A_\nu\}$
$\frac{1}{2}\,\text{Csc}[\theta_W]\,e_{EM}\,g^{\mu\nu}$	$\{H_2^-, \partial_\mu h_2, W_\nu^+\}$
$\frac{1}{2}\,i\,\text{Csc}[\theta_W]\,e_{EM}\,g^{\mu\nu}$	$\{H_2^-, \partial_\mu a_2, W_\nu^+\}$
$\text{Cot}[2\,\theta_W]\,e_{EM}\,g^{\mu\nu}$	$\{H_2^-, \partial_\mu H_2^+, Z_\nu\}$
$e_{EM}\,g^{\mu\nu}$	$\{H_2^-, \partial_\mu H_2^+, A_\nu\}$
$-\frac{1}{2}\,\text{Csc}[\theta_W]\,e_{EM}\,g^{\mu\nu}$	$\{H_3^+, \partial_\mu h_3, W_\nu^-\}$
$\frac{1}{2}\,i\,\text{Csc}[\theta_W]\,e_{EM}\,g^{\mu\nu}$	$\{H_3^+, \partial_\mu a_3, W_\nu^-\}$
$-\text{Cot}[2\,\theta_W]\,e_{EM}\,g^{\mu\nu}$	$\{H_3^+, \partial_\mu H_3^-, Z_\nu\}$
$-e_{EM}\,g^{\mu\nu}$	$\{H_3^+, \partial_\mu H_3^-, A_\nu\}$
$\frac{1}{2}\,\text{Csc}[\theta_W]\,e_{EM}\,g^{\mu\nu}$	$\{H_3^-, \partial_\mu h_3, W_\nu^+\}$
$\frac{1}{2}\,i\,\text{Csc}[\theta_W]\,e_{EM}\,g^{\mu\nu}$	$\{H_3^-, \partial_\mu a_3, W_\nu^+\}$
$\text{Cot}[2\,\theta_W]\,e_{EM}\,g^{\mu\nu}$	$\{H_3^-, \partial_\mu H_3^+, Z_\nu\}$
$e_{EM}\,g^{\mu\nu}$	$\{H_3^-, \partial_\mu H_3^+, A_\nu\}$

Table A.5: Table of 4-vertex Feynman rules for the DIDM

$-6\,i\,\lambda_1$	$\{h_{SM}, h_{SM}, h_{SM}, h_{SM}\}$
$-i\,(\lambda_3+\lambda_4-\lambda_6)$	$\{h_{SM}, h_{SM}, h_2, h_2\}$
$-i\,(\lambda_3+\lambda_4+\lambda_6)$	$\{h_{SM}, h_{SM}, a_2, a_2\}$
$-i\,(\lambda_3+\lambda_4-\lambda_6)$	$\{h_{SM}, h_{SM}, h_3, h_3\}$
$-i\,(\lambda_3+\lambda_4+\lambda_6)$	$\{h_{SM}, h_{SM}, a_3, a_3\}$
$-i\,\lambda_3$	$\{h_{SM}, h_{SM}, H_2^+, H_2^-\}$
$-i\,\lambda_3$	$\{h_{SM}, h_{SM}, H_3^+, H_3^-\}$
$-6\,i\,\lambda_2$	$\{h_2, h_2, h_2, h_2\}$
$-2\,i\,\lambda_2$	$\{h_2, h_2, a_2, a_2\}$
$-2\,i\,\lambda_2$	$\{h_2, h_2, H_2^+, H_2^-\}$
$-6\,i\,\lambda_2$	$\{a_2, a_2, a_2, a_2\}$
$-2\,i\,\lambda_2$	$\{a_2, a_2, H_2^+, H_2^-\}$
$-6\,i\,\lambda_2$	$\{h_3, h_3, h_3, h_3\}$
$-2\,i\,\lambda_2$	$\{h_3, h_3, a_3, a_3\}$
$-2\,i\,\lambda_2$	$\{h_3, h_3, H_3^+, H_3^-\}$
$-6\,i\,\lambda_2$	$\{a_3, a_3, a_3, a_3\}$
$-2\,i\,\lambda_2$	$\{a_3, a_3, H_3^+, H_3^-\}$
$-4\,i\,\lambda_2$	$\{H_2^+, H_2^+, H_2^-, H_2^-\}$
$-4\,i\,\lambda_2$	$\{H_3^+, H_3^+, H_3^-, H_3^-\}$
$\frac{1}{2}\,i\,\csc[\theta_W]^2\,e_{EM}^2\,g^{\mu\nu}$	$\{h_{SM}, h_{SM}, W_\mu^+, W_\nu^-\}$
$2\,i\,\csc[2\,\theta_W]^2\,e_{EM}^2\,g^{\mu\nu}$	$\{h_{SM}, h_{SM}, Z_\mu, Z_\nu\}$
$\frac{1}{2}\,i\,\csc[\theta_W]^2\,e_{EM}^2\,g^{\mu\nu}$	$\{h_2, h_2, W_\mu^+, W_\nu^-\}$
$2\,i\,\csc[2\,\theta_W]^2\,e_{EM}^2\,g^{\mu\nu}$	$\{h_2, h_2, Z_\mu, Z_\nu\}$
$-\frac{1}{2}\,i\,\sec[\theta_W]\,e_{EM}^2\,g^{\mu\nu}$	$\{h_2, H_2^+, W_\mu^-, Z_\nu\}$
$\frac{1}{2}\,i\,\csc[\theta_W]\,e_{EM}^2\,g^{\mu\nu}$	$\{h_2, H_2^+, W_\mu^-, A_\nu\}$
$-\frac{1}{2}\,i\,\sec[\theta_W]\,e_{EM}^2\,g^{\mu\nu}$	$\{h_2, H_2^-, W_\mu^+, Z_\nu\}$
$\frac{1}{2}\,i\,\csc[\theta_W]\,e_{EM}^2\,g^{\mu\nu}$	$\{h_2, H_2^-, W_\mu^+, A_\nu\}$
$\frac{1}{2}\,i\,\csc[\theta_W]^2\,e_{EM}^2\,g^{\mu\nu}$	$\{a_2, a_2, W_\mu^+, W_\nu^-\}$
$2\,i\,\csc[2\,\theta_W]^2\,e_{EM}^2\,g^{\mu\nu}$	$\{a_2, a_2, Z_\mu, Z_\nu\}$
$-\frac{1}{2}\,\sec[\theta_W]\,e_{EM}^2\,g^{\mu\nu}$	$\{a_2, H_2^+, W_\mu^-, Z_\nu\}$
$\frac{1}{2}\,\csc[\theta_W]\,e_{EM}^2\,g^{\mu\nu}$	$\{a_2, H_2^+, W_\mu^-, A_\nu\}$
$\frac{1}{2}\,\sec[\theta_W]\,e_{EM}^2\,g^{\mu\nu}$	$\{a_2, H_2^-, W_\mu^+, Z_\nu\}$
$-\frac{1}{2}\,\csc[\theta_W]\,e_{EM}^2\,g^{\mu\nu}$	$\{a_2, H_2^-, W_\mu^+, A_\nu\}$
$\frac{1}{2}\,i\,\csc[\theta_W]^2\,e_{EM}^2\,g^{\mu\nu}$	$\{h_3, h_3, W_\mu^+, W_\nu^-\}$
$2\,i\,\csc[2\,\theta_W]^2\,e_{EM}^2\,g^{\mu\nu}$	$\{h_3, h_3, Z_\mu, Z_\nu\}$
$-\frac{1}{2}\,i\,\sec[\theta_W]\,e_{EM}^2\,g^{\mu\nu}$	$\{h_3, H_3^+, W_\mu^-, Z_\nu\}$
$\frac{1}{2}\,i\,\csc[\theta_W]\,e_{EM}^2\,g^{\mu\nu}$	$\{h_3, H_3^+, W_\mu^-, A_\nu\}$
$-\frac{1}{2}\,i\,\sec[\theta_W]\,e_{EM}^2\,g^{\mu\nu}$	$\{h_3, H_3^-, W_\mu^+, Z_\nu\}$
$\frac{1}{2}\,i\,\csc[\theta_W]\,e_{EM}^2\,g^{\mu\nu}$	$\{h_3, H_3^-, W_\mu^+, A_\nu\}$
$\frac{1}{2}\,i\,\csc[\theta_W]^2\,e_{EM}^2\,g^{\mu\nu}$	$\{a_3, a_3, W_\mu^+, W_\nu^-\}$
$2\,i\,\csc[2\,\theta_W]^2\,e_{EM}^2\,g^{\mu\nu}$	$\{a_3, a_3, Z_\mu, Z_\nu\}$
$-\frac{1}{2}\,\sec[\theta_W]\,e_{EM}^2\,g^{\mu\nu}$	$\{a_3, H_3^+, W_\mu^-, Z_\nu\}$
$\frac{1}{2}\,\csc[\theta_W]\,e_{EM}^2\,g^{\mu\nu}$	$\{a_3, H_3^+, W_\mu^-, A_\nu\}$
$\frac{1}{2}\,\sec[\theta_W]\,e_{EM}^2\,g^{\mu\nu}$	$\{a_3, H_3^-, W_\mu^+, Z_\nu\}$
$-\frac{1}{2}\,\csc[\theta_W]\,e_{EM}^2\,g^{\mu\nu}$	$\{a_3, H_3^-, W_\mu^+, A_\nu\}$
$\frac{1}{2}\,i\,\csc[\theta_W]^2\,e_{EM}^2\,g^{\mu\nu}$	$\{H_2^+, H_2^-, W_\mu^+, W_\nu^-\}$
$2\,i\,\cot[2\,\theta_W]^2\,e_{EM}^2\,g^{\mu\nu}$	$\{H_2^+, H_2^-, Z_\mu, Z_\nu\}$
$2\,i\,\cot[2\,\theta_W]\,e_{EM}^2\,g^{\mu\nu}$	$\{H_2^+, H_2^-, Z_\mu, A_\nu\}$
$2\,i\,e_{EM}^2\,g^{\mu\nu}$	$\{H_2^+, H_2^-, A_\mu, A_\nu\}$
$\frac{1}{2}\,i\,\csc[\theta_W]^2\,e_{EM}^2\,g^{\mu\nu}$	$\{H_3^+, H_3^-, W_\mu^+, W_\nu^-\}$
$2\,i\,\cot[2\,\theta_W]^2\,e_{EM}^2\,g^{\mu\nu}$	$\{H_3^+, H_3^-, Z_\mu, Z_\nu\}$
$2\,i\,\cot[2\,\theta_W]\,e_{EM}^2\,g^{\mu\nu}$	$\{H_3^+, H_3^-, Z_\mu, A_\nu\}$
$2\,i\,e_{EM}^2\,g^{\mu\nu}$	$\{H_3^+, H_3^-, A_\mu, A_\nu\}$

Appendix B

Published Code

B.1 PUC

Perturbative Unitarity Check (PUC) [5] is a Mathematica package written for the studies of this thesis. It is available at GitHub under `https://git.io/vb2Hh`. Currently, it allows for the calculation of tree-level, perturbative unitarity constraints for both of the 3HDMs of Chapter 3, the DM CP4 3HDM and the DIDM. However, it is easily extensible to any other multi-Higgs model.

The package utilizes the methods developed in [55, 56, 57]. Effectively, one calculates the 2-to-2 scattering matrix S of all scalars of the Higgs sector, including the Goldstone bosons. Then the absolute value of the eigenvalues e_i of S are constrained to

$$|e_i| \leq 8\pi \ . \tag{B.1}$$

As a side product for setting up the scattering matrix S, PUC can also calculate all vertex factors of the Feynman rules of Higgs-to-Higgs and gauge boson-to-Higgs couplings. The listings in Appendix A were calculated with PUC. They have been cross-checked with similar tools such as MadGraph [58] and FeynRules [59].

To use PUC one has to load the package via the file `"FRWG.m"`. One can then go ahead and list all vertex factors and the mass matrix with

```
Get["<path-to-package>/FRWG.m"];

rFR3Vertex // RGM
rFR4Vertex // RGM
massmatrix // RCM
```

This will not display vertex factors for Goldstone bosons. To include them use RCM instead of RGM.

A convenient way to list the eigenvalues of the S matrix is

```
Get["<path-to-package>/FRWG.m"];

DeleteDuplicates[Eigenvalues[smatrix]] // RCN
```

RCN is almost the same as RCM. It will remove the Mathematica context names from the variables but it will not display the result in matrix form.

It can happen that the eigenvalues e_i of the S matrix cannot be calculated explicitly, because the S matrix is too large or the eigenvalues cannot be given by analytic expressions. Either way, one can use

```
Get["<path-to-package>/FRWG.m"];

CheckUnitarity[{0.1, 0.2, 0.3, 0.4, 0.5, 0.6, 0.7, 0.8, 0.9}]
```

to check if perturbative unitarity constraints can be fulfilled by the list of parameter values given to CheckUnitarity. The length of this list depends on the specific model under consideration.

PUC has been cross-checked with 3 different models: SM, IDM and DM CP4 3HDM. It can reproduce the SM eigenvalues

$$\begin{aligned} e_1 &= 0 \\ e_2 &= 2\lambda \\ e_3 &= 6\lambda \end{aligned} \tag{B.2}$$

given in [23, Eq. (4.17)]. Here, λ is the quartic coupling parameter of the SM Higgs doublet ϕ with the potential $V = -m_{11}^2 \, |\phi|^2 + \lambda \, |\phi|^4$.

For the IDM defined in Section 3.1 the eigenvalues calculated by PUC are

$$\begin{aligned} e_1 &= 0 \\ e_{2/3} &= 3(\lambda_1 + \lambda_2) \pm \sqrt{9(\lambda_1 - \lambda_2)^2 + (2\lambda_3 + \lambda_4)^2} \\ e_{4/5} &= (\lambda_1 + \lambda_2) \pm \sqrt{(\lambda_1 - \lambda_2)^2 + \lambda_4^2} \\ e_{6/7} &= (\lambda_1 + \lambda_2) \pm \sqrt{(\lambda_1 - \lambda_2)^2 + \lambda_5^2} \\ e_{8/9} &= \lambda_3 + 2\lambda_4 \pm 3\lambda_5 \\ e_{10/11} &= \lambda_3 \pm \lambda_4 \\ e_{12/13} &= \lambda_3 \pm \lambda_5 \ . \end{aligned} \tag{B.3}$$

Up to a redefinition of λ_1 and λ_2, they agree with the ones given in [7, Eqs. (363) - (371)].

For the DM CP4 3HDM defined in Section 3.2 not all eigenvalues of the S matrix can be given as analytic expressions. Some of them are given as roots of polynomial equations in [23, Eqs. (4.30) - (4.32)]. Therefore a numerical check was applied. Figures B.1 to B.4 show exclusion plots for all possible parameter planes. The points are generated by PUC and the contours by the expressions given in [23]. The values

$$\begin{aligned} &\lambda_1 = \lambda_2 = \lambda_3 = \lambda_3' = \lambda_4 = \lambda_4' = \lambda_6 = 1 \\ &\mathrm{Re}(\lambda_8) = \mathrm{Im}(\lambda_8) = \mathrm{Re}(\lambda_9) = \mathrm{Im}(\lambda_9) = 1 \end{aligned} \tag{B.4}$$

are fixed unless they were varied in their respective parameter plane in the plots. As one can see, there is no deviation.

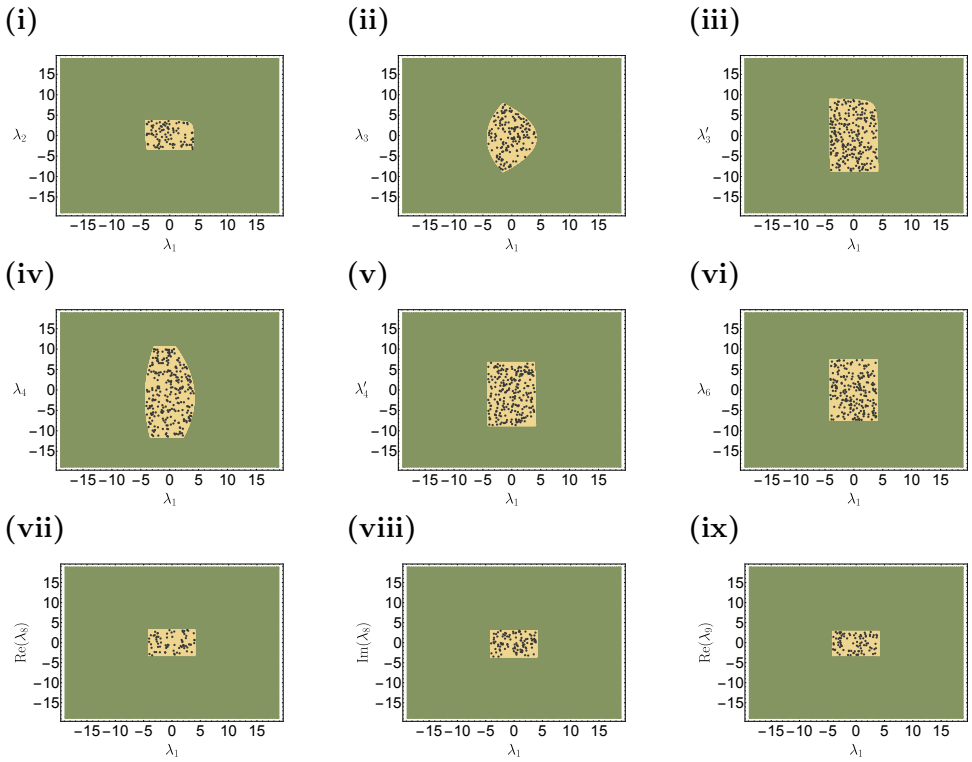

Figure B.1: Various exclusion plots for unitarity constraints in different parameter planes. The green region is excluded by the expressions in [23], the yellow region is allowed. Black points indicate valid parameter points according to a scan with PUC.

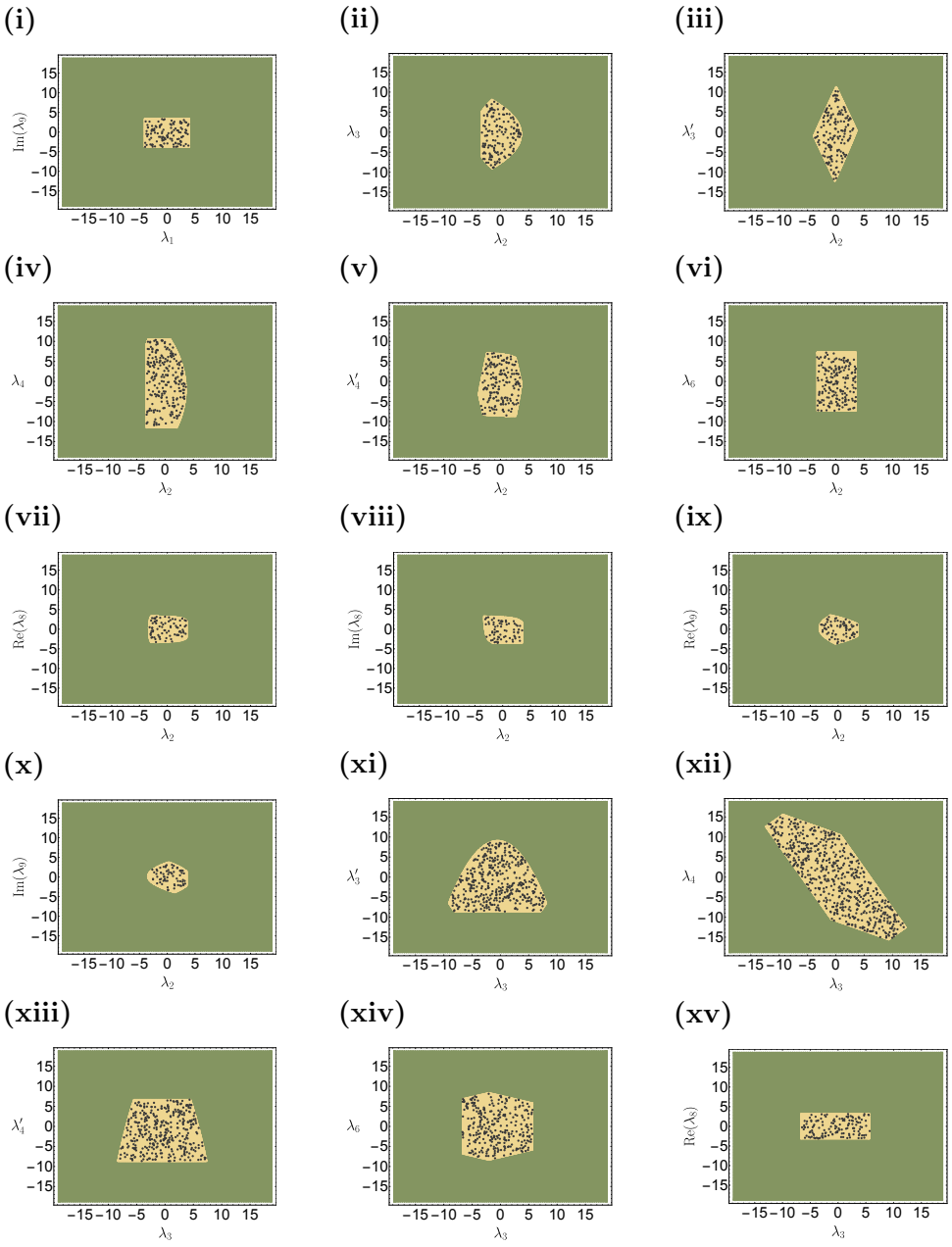

Figure B.2: Various exclusion plots for unitarity constraints in different parameter planes. The green region is excluded by the expressions in [23], the yellow region is allowed. Black points indicate valid parameter points according to a scan with PUC.

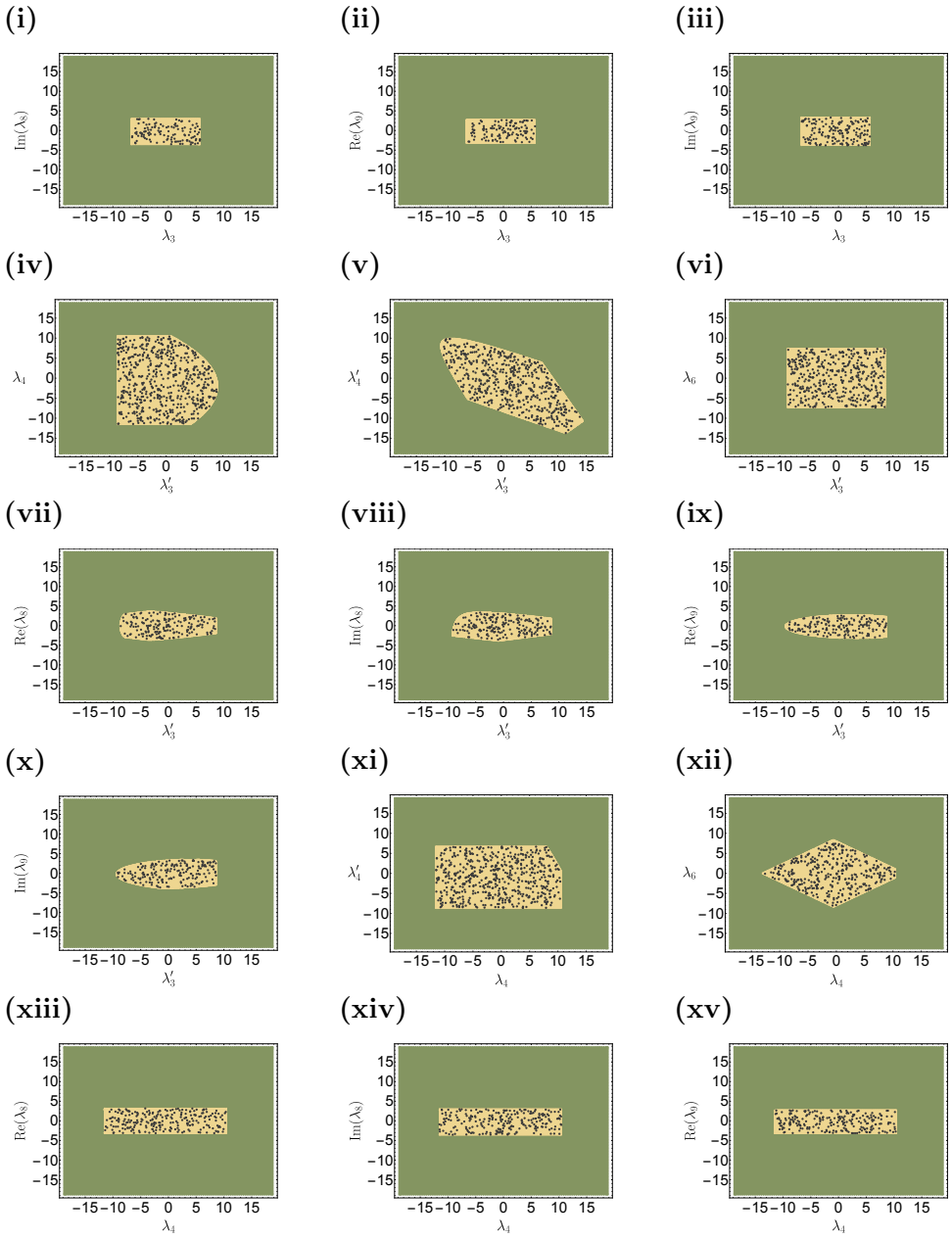

Figure B.3: Various exclusion plots for unitarity constraints in different parameter planes. The green region is excluded by the expressions in [23], the yellow region is allowed. Black points indicate valid parameter points according to a scan with PUC.

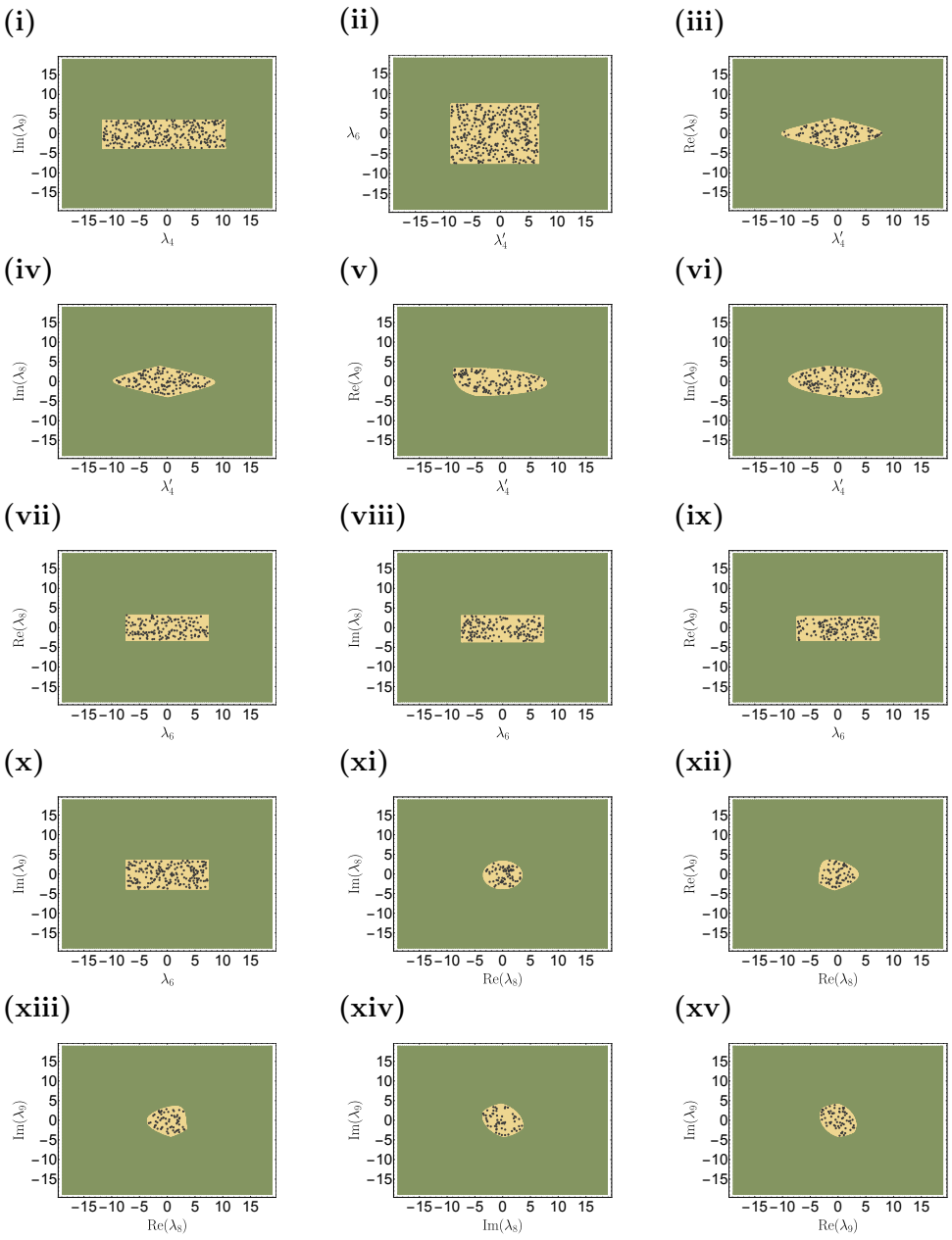

Figure B.4: Various exclusion plots for unitarity constraints in different parameter planes. The green region is excluded by the expressions in [23], the yellow region is allowed. Black points indicate valid parameter points according to a scan with PUC.

B.2 BFB

Bounded From Below (BFB) [4] is a Mathematica package written for the studies of this thesis. It is available at GitHub under `https://git.io/vFQvi`. In principle it can calculate boundedness constraints for any multi-Higgs model. The package utilizes the method outlined in Chapter 5. Unfortunately, the current implementation does not allow for the calculation of constraints for more than two Higgs doublets in a reasonable runtime. There are, however, numerous ways for improvement as has been mentioned in Section 5.7. There are currently two top level functions: GetResultant and PositivityTest .

The function GetResultant can calculate the resultant of a system of polynomial equations (see Section 5.3.4). An example of its usage is given below.

```
Get["<path-to-package>/BFB.m"];

polynomials = {a*x^3 - 2*y^3, x*z^2 + y^3, x*y*z - 3/2*z^3};
 variables  = {x, y, z};
parameters = {a};

 resultant  = GetResultant[polynomials, variables , parameters];
```

The function PositivityTest can test a given Higgs potential for boundedness. An example of its usage is given below.

```
Get["<path-to-package>/BFB.m"];

 potential  = 2*x^4 - x^2*y^2 + y^4;
 variables  = {x, y};

check =  PositivityTest [ potential ,  variables ];
```

It is important to note that currently only numerical checks are possible. Only potentials with no analytic parameters can be processed.

For analytic calculations the algorithm of Section 5.5 can be implemented in the following way:

```
Get["<path-to-package>/BFB.m"];

 potential  = a*x^4 + b*x^2*y^2 + c*y^4;
 variables  = {x, y};
parameters = {a, b, c, eig};

Q = D[potential, { variables , 4}]/4!;
polynomials = Table[Sum[Q[[i,j,k,l ]] * variables [[ j ]] * variables [[ k ]] *
     variables [[ l ]], {j ,1,2}, {k ,1,2}, {l ,1,2}] - eig* variables [[ i ]], {i ,1,2}];

```

```
resultant = GetResultant[polynomials, variables, parameters];
eigenvalues = DeleteDuplicates[eig /. Solve[resultant[["Resultant"]] == 0, eig]];
```

This will yield analytic expressions of all eigenvalues of the tensor Q if possible. They can then be tested for their property of being H-eigenvalues or not.

For instance, a numerical test of the first eigenvalue with substitution rules subrules for the parameters can be done.

```
testpolys = polynomials /. subrules /. eig -> eigenvalues[[1]];
testconditions = Apply[And, Table[testpolys[[i]] == 0, {i,1,2}]];

FindInstance[testconditions, variables, Reals, 2]
```

This will find two real solutions of the system of polynomial equations if possible. One of them will always be the trivial solution. If the resultant can be calculated analytically in a reasonable time, this test will be faster than the function PositivityTest because here the resultant is calculated only once.

Cross-checks for the implementation of BFB were performed for the IDM of Section 3.1 and several simple potential expressions as well. For reference see Section 5.6.

Bibliography

[1] Ivanov, I. P. and Silva, J. P. "CP-conserving multi-Higgs model with irremovable complex coefficients." In: *Phys. Rev.* D93.9 (2016), p. 095014. DOI: 10.1103/PhysRevD.93.095014. arXiv: 1512.09276 [hep-ph].

[2] Belyaev, A. et al. "Anatomy of the Inert Two Higgs Doublet Model in the light of the LHC and non-LHC Dark Matter Searches." In: (2016). arXiv: 1612.00511 [hep-ph].

[3] Ilnicka, A., Krawczyk, M., and Robens, T. "Inert Doublet Model in light of LHC Run I and astrophysical data." In: *Phys. Rev.* D93.5 (2016), p. 055026. DOI: 10.1103/PhysRevD.93.055026. arXiv: 1508.01671 [hep-ph].

[4] Köpke, M. *BFB, a Mathematica package for Higgs potential boundedness checks*. Available at https://git.io/vFQvi. 2017.

[5] Köpke, M. *PUC, Mathematica package to check perturbative unitarity of general Higgs potentials*. Available at https://git.io/vb2Hh. 2017.

[6] Gunion, J. F. et al. "The Higgs Hunter's Guide." In: *Front. Phys.* 80 (2000), pp. 1–404.

[7] Branco, G. C. et al. "Theory and phenomenology of two-Higgs-doublet models." In: *Phys. Rept.* 516 (2012), pp. 1–102. DOI: 10.1016/j.physrep.2012.02.002. arXiv: 1106.0034 [hep-ph].

[8] Ecker, G., Grimus, W., and Neufeld, H. "A Standard Form for Generalized CP Transformations." In: *J. Phys.* A20 (1987), p. L807. DOI: 10.1088/0305-4470/20/12/010.

[9] Ferreira, P. M., Haber, H. E., and Silva, J. P. "Generalized CP symmetries and special regions of parameter space in the two-Higgs-doublet model." In: *Phys. Rev.* D79 (2009), p. 116004. DOI: 10.1103/PhysRevD.79.116004. arXiv: 0902.1537 [hep-ph].

[10] Bernon, J. et al. "Scrutinizing the alignment limit in two-Higgs-doublet models: m_h=125 GeV." In: *Phys. Rev.* D92.7 (2015), p. 075004. DOI: 10.1103/PhysRevD.92.075004. arXiv: 1507.00933 [hep-ph].

[11] Staub, F. "SARAH." In: (2008). arXiv: 0806.0538 [hep-ph].

[12] Staub, F. "SARAH 4 : A tool for (not only SUSY) model builders." In: *Comput. Phys. Commun.* 185 (2014), pp. 1773–1790. DOI: 10.1016/j.cpc.2014.02.018. arXiv: 1309.7223 [hep-ph].

[13] Belyaev, A., Christensen, N. D., and Pukhov, A. "CalcHEP 3.4 for collider physics within and beyond the Standard Model." In: *Comput. Phys. Commun.* 184 (2013), pp. 1729–1769. DOI: 10.1016/j.cpc.2013.01.014. arXiv: 1207.6082 [hep-ph].

[14] Porod, W. "SPheno, a program for calculating supersymmetric spectra, SUSY particle decays and SUSY particle production at e+ e- colliders." In: *Comput. Phys. Commun.* 153 (2003), pp. 275–315. DOI: 10.1016/S0010-4655(03)00222-4. arXiv: hep-ph/0301101 [hep-ph].

[15] Porod, W. and Staub, F. "SPheno 3.1: Extensions including flavour, CP-phases and models beyond the MSSM." In: *Comput. Phys. Commun.* 183 (2012), pp. 2458–2469. DOI: 10.1016/j.cpc.2012.05.021. arXiv: 1104.1573 [hep-ph].

[16] Patrignani, C. et al. "Review of Particle Physics." In: *Chin. Phys.* C40.10 (2016), p. 100001. DOI: 10.1088/1674-1137/40/10/100001.

[17] Barducci, D. et al. "Collider limits on new physics within micrOMEGAs 4.3." In: *Comput. Phys. Commun.* 222 (2016), pp. 327–338. DOI: 10.1016/j.cpc.2017.08.028. arXiv: 1606.03834 [hep-ph].

[18] Staub, F. et al. "A Tool Box for Implementing Supersymmetric Models." In: *Comput. Phys. Commun.* 183 (2012), pp. 2165–2206. DOI: 10.1016/j.cpc.2012.04.013. arXiv: 1109.5147 [hep-ph].

[19] Ferreira, P. M. et al. "CP4 miracle: shaping Yukawa sector with CP symmetry of order four." In: (2017). arXiv: 1711.02042 [hep-ph].

[20] Ivanov, I. P. "Minkowski space structure of the Higgs potential in the two-Higgs-doublet model." In: *Phys. Rev. D* 75 (3 Feb. 2007), p. 035001. DOI: 10.1103/PhysRevD.75.035001.

[21] Kannike, K. "Vacuum Stability Conditions From Copositivity Criteria." In: *Eur. Phys. J.* C72 (2012), p. 2093. DOI: 10.1140/epjc/s10052-012-2093-z. arXiv: 1205.3781 [hep-ph].

[22] Deshpande, N. G. and Ma, E. "Pattern of symmetry breaking with two Higgs doublets." In: *Phys. Rev. D* 18 (7 Oct. 1978), pp. 2574–2576. DOI: 10.1103/PhysRevD.18.2574.

[23] Bento, M. P. et al. "Multi-Higgs doublet models: physical parametrization, sum rules and unitarity bounds." In: *JHEP* 11 (2017), p. 095. DOI: 10.1007/JHEP11(2017)095. arXiv: 1708.09408 [hep-ph].

[24] Gunion, J. F. and Haber, H. E. "Higgs Bosons in Supersymmetric Models. 1." In: *Nucl. Phys.* B272 (1986). [Erratum: Nucl. Phys.B402,567(1993)], p. 1. DOI: 10.1016/0550-3213(86)90340-8,10.1016/0550-3213(93)90653-7.

[25] Spira, M. and Zerwas, P. M. "Electroweak symmetry breaking and Higgs physics." In: *Lect. Notes Phys.* 512 (1998), pp. 161–225. DOI: 10.1007/BFb0106895. arXiv: hep-ph/9803257 [hep-ph].

[26] Mühlleitner, M. M. "Higgs particles in the standard model and supersymmetric theories." PhD thesis. Hamburg U., 2000. arXiv: hep-ph/0008127 [hep-ph]. URL: http://www-library.desy.de/cgi-bin/showprep.pl?desy-thesis00-033.

[27] Spira, M. "Higgs Boson Production and Decay at Hadron Colliders." In: *Prog. Part. Nucl. Phys.* 95 (2017), pp. 98–159. DOI: 10.1016/j.ppnp.2017.04.001. arXiv: 1612.07651 [hep-ph].

[28] Martin, S. P. "A Supersymmetry primer." In: (1997). [Adv. Ser. Direct. High Energy Phys.18,1(1998)]. DOI: 10.1142/9789812839657_0001,10.1142/9789814307505_0001. arXiv: hep-ph/9709356 [hep-ph].

[29] King, S. F., Mühlleitner, M. M., and Nevzorov, R. "NMSSM Higgs Benchmarks Near 125 GeV." In: *Nucl. Phys.* B860 (2012), pp. 207–244. DOI: 10.1016/j.nuclphysb.2012.02.010. arXiv: 1201.2671 [hep-ph].

[30] King, S. F. et al. "Natural NMSSM Higgs Bosons." In: *Nucl. Phys.* B870 (2013), pp. 323–352. DOI: 10.1016/j.nuclphysb.2013.01.020. arXiv: 1211.5074 [hep-ph].

[31] King, S. F. et al. "Discovery Prospects for NMSSM Higgs Bosons at the High-Energy Large Hadron Collider." In: *Phys. Rev.* D90.9 (2014), p. 095014. DOI: 10.1103/PhysRevD.90.095014. arXiv: 1408.1120 [hep-ph].

[32] Schwichtenberg, J. "Dark Matter in E_6 Grand Unification." In: (2017). arXiv: 1704.04219 [hep-ph].

[33] Mühlleitner, M. M. et al. "The N2HDM under Theoretical and Experimental Scrutiny." In: *JHEP* 03 (2017), p. 094. DOI: 10.1007/JHEP03(2017)094. arXiv: 1612.01309 [hep-ph].

[34] Klimenko, K. G. "Conditions for certain Higgs potentials to be bounded below." In: *Theoretical and Mathematical Physics* 62.1 (Jan. 1985), pp. 58–65. ISSN: 1573-9333. DOI: 10.1007/BF01034825.

[35] Mohapatra, R. N. and Senjanović, G. "Broken symmetries at high temperature." In: *Phys. Rev. D* 20 (12 Dec. 1979), pp. 3390–3398. DOI: 10.1103/PhysRevD.20.3390.

[36] Lim, L.-H. "Singular Values and Eigenvalues of Tensors: A Variational Approach." In: *ArXiv Mathematics e-prints* (July 2006). arXiv: math/0607648.

[37] Qi, L. "Eigenvalues of a real supersymmetric tensor." In: *Journal of Symbolic Computation* 40.6 (2005), pp. 1302–1324. ISSN: 0747-7171. DOI: 10.1016/j.jsc.2005.05.007.

[38] Cox, D. A., Little, J. B., and OShea, D. *Using algebraic geometry.* Graduate texts in mathematics ; 185. New York: Springer, 1998. ISBN: 0-387-98487-9; 0-387-98492-5.

[39] Grenet, B., Koiran, P., and Portier, N. "The Multivariate Resultant Is NP-hard in Any Characteristic." In: *Lecture Notes in Computer Science* 6281 (2010), p. 477. DOI: 10.1007/978-3-642-15155-2_42. arXiv: 0912.2607 [cs.CC].

[40] Macaulay, F. S. "Some Formulæ in Elimination." In: *Proceedings of the London Mathematical Society* s1-35.1 (1902), pp. 3–27. ISSN: 1460-244X. DOI: 10.1112/plms/s1-35.1.3.

[41] Qi, L. "The Spectral Theory of Tensors (Rough Version)." In: *ArXiv e-prints* (Jan. 2012). arXiv: 1201.3424 [math.SP].

[42] Qi, L. and Luo, Z. *Tensor Analysis: Spectral Theory and Special Tensors*. Other Titles in Applied Mathematics. Society for Industrial and Applied Mathematics, 2017. ISBN: 9781611974744.

[43] Wolfram Research, Inc. *Mathematica, Version 11.2*. Champaign, IL, 2017.

[44] Grayson, D. R. and Stillman, M. E. *Macaulay2, a software system for research in algebraic geometry*. Available at `http://www.math.uiuc.edu/Macaulay2/`.

[45] Maplesoft, a division of Waterloo Maple Inc. *Maple 2017*. Waterloo, Ontario, 2017.

[46] Staglianò, G. *Macaulay2 package Resultants: Resultants, discriminants, and Chow forms. Version 1.0*. Available at `http://www2.macaulay2.com/Macaulay2/doc/Macaulay2-1.10/share/doc/Macaulay2/Resultants/html/`. 2017.

[47] Zell, T. *MathOverflow - Existence of a real-valued solution to system of multivariate polynomial equations*. Available at `https://mathoverflow.net/a/66870/69288`. 2017.

[48] Faugére, J.-C. "A new efficient algorithm for computing Gröbner bases (F4)." In: *Journal of Pure and Applied Algebra* 139.1 (1999), pp. 61–88. ISSN: 0022-4049. DOI: `10.1016/S0022-4049(99)00005-5`.

[49] Faugére, J.-C. "A New Efficient Algorithm for Computing Gröbner Bases Without Reduction to Zero (F5)." In: *Proceedings of the 2002 International Symposium on Symbolic and Algebraic Computation*. ISSAC '02. Lille, France: ACM, 2002, pp. 75–83. ISBN: 1-58113-484-3. DOI: `10.1145/780506.780516`.

[50] Manocha, D. "Efficient Algorithms for MultiPolynomial Resultant." In: *The Computer Journal* 36.5 (1993), pp. 485–496. DOI: `10.1093/comjnl/36.5.485`.

[51] Manocha, D. and Canny, J. F. "MultiPolynomial Resultant Algorithms." In: *Journal of Symbolic Computation* 15.2 (1993), pp. 99–122. ISSN: 0747-7171. DOI: `10.1006/jsco.1993.1009`.

[52] Macaulay, F. S. "Note on the Resultant of a Number of Polynomials of the Same Degree." In: *Proceedings of the London Mathematical Society*

s2-21.1 (1923), pp. 14–21. ISSN: 1460-244X. DOI: 10.1112/plms/s2-21.1.14.

[53] Wallack, A., Manocha, D., and Emiris, I. *MARS, Maple/Matlab/C Resultant-based Solver*. Available at http://gamma.cs.unc.edu/MARS/. 2017.

[54] Maniatis, M., Manteuffel, A. von, and Nachtmann, O. "Determining the global minimum of Higgs potentials via Groebner bases: Applied to the NMSSM." In: *Eur. Phys. J.* C49 (2007), pp. 1067–1076. DOI: 10.1140/epjc/s10052-006-0186-2. arXiv: hep-ph/0608314 [hep-ph].

[55] Smith, C. L. "High energy behaviour and gauge symmetry." In: *Physics Letters B* 46.2 (1973), pp. 233–236. ISSN: 0370-2693. DOI: https://doi.org/10.1016/0370-2693(73)90692-8.

[56] Cornwall, J. M., Levin, D. N., and Tiktopoulos, G. "Derivation of gauge invariance from high-energy unitarity bounds on the S matrix." In: *Phys. Rev. D* 10 (4 Aug. 1974), pp. 1145–1167. DOI: 10.1103/PhysRevD.10.1145.

[57] Weldon, H. A. "Effects of multiple Higgs bosons on tree unitarity." In: *Phys. Rev. D* 30 (7 Oct. 1984), pp. 1547–1558. DOI: 10.1103/PhysRevD.30.1547.

[58] Alwall, J. et al. "The automated computation of tree-level and next-to-leading order differential cross sections, and their matching to parton shower simulations." In: *JHEP* 07 (2014), p. 079. DOI: 10.1007/JHEP07(2014)079. arXiv: 1405.0301 [hep-ph].

[59] Alloul, A. et al. "FeynRules 2.0 - A complete toolbox for tree-level phenomenology." In: *Comput. Phys. Commun.* 185 (2014), pp. 2250–2300. DOI: 10.1016/j.cpc.2014.04.012. arXiv: 1310.1921 [hep-ph].